Cloning and characterization of novel ccdc103 interactors

by

Jeffrey Gantt Daniel

A dissertation submitted to the Graduate Faculty of
Auburn University
in partial fulfillment of the
requirements for the Degree of
Doctor of Philosophy

Auburn, Alabama
August 8, 2020

Keywords: cilia, ciliopathy, ccdc103, ankef1, CRISPR

Approved by

Jennifer Panizzi, Co-chair, Associate Professor of Anatomy, Physiology, and Pharmacology
Dean Schwartz, Co-chair, Associate Professor of Anatomy, Physiology, and Pharmacology
Vinicia Biancardi, Assistant Professor of Anatomy, Physiology, and Pharmacology
Peter Panizzi, Associate Professor of Drug Discovery and Development

Abstract

Coiled-coil domain containing protein 103 is a homodimeric protein that functions as a dynein attachment factor in motile cilia. Ccdc103 defects in zebrafish (*Danio rerio*) embryos lead to paralyzed motile cilia, pronephric cysts, hydrocephalus, and a curved body axis. In humans, CCDC103 mutations cause primary ciliary dyskinesia (PCD), a genetic syndrome characterized by bronchial scarring, chronic respiratory infections, and infertility. Studies are just beginning to uncover the function of Ccdc103 in both zebrafish and humans, but, apart from *foxj1a* regulation and dynein arm attachment, little else is known about its interactors or its place in cellular pathways. We identified 14 potential interactors through a yeast-two-hybrid study using mouse Ccdc103 as bait against a mouse cDNA prey library. One of the identified interactors is ankyrin and EF-hand containing protein 1 (Ankef1), which has two paralogs (*ankef1a* and *ankef1b*) in zebrafish. Both paralogs share the same ankyrin—EF-hand—ankyrin domain structure and display conserved synteny with SNAP25 in zebrafish, frogs, mice, and humans. We first cloned *ankef1a* and *ankef1b*, then used whole-mount in situ hybridization (WISH) to identify the embryonic expression patterns of both paralogs. WISH and sectioning showed that *ankef1* is ubiquitously expressed during the first 24 hours of zebrafish development, with more restricted expression in the pharynx, swim bladder, and otic vesicles through 5 days post-fertilization (dpf). Quantitative reverse transcriptase PCR (qPCR) was used to quantify *ankef1* transcript levels in embryos and adult tissues. qPCR data showed that both transcripts are maternally contributed and increase later in development after an initial drop in expression in the first two days. *Ankef1a* was also highly expressed in the testis, which is a major site of *ANKEF1* expression in humans. We also generated knockout (KO) lines of ankef1a using CRISPR/Cas9 technology. An ankef1b KO line was

obtained from ZIRC. Future studies on mutant phenotypes will reveal potential functional overlap between Ankef1a and Ankef1b.

To Mom, Susan Daniel (God rest her soul),
who taught me the importance of Truth.

To Dad, John Daniel, and MomTwo, Amy Daniel,
who taught me how to find Truth.

And to my empathetic and patient mentor, Jennifer Panizzi,
for helping me get as close as humanly possible to scientific Truth.

Acknowledgments

I wouldn't have earned this degree without Dr. Jennifer Panizzi. As I transitioned from Research assistant to the Ph.D. program., I learned that setting up a lab was more challenging than expected. Dr. Panizzi was endlessly helpful and encouraging through our abundance of negative results at the beginning of my project. She also showed me that mistakes are inevitable, but learning as much as possible from missteps leads to better science. I may have done the bench work and writing, but I owe this degree to her drive to push me through my constant depression.

I also appreciate my committee members, Drs. Dean Schwartz, Vinicia Biancardi, and Peter Panizzi for not letting me off the hook and challenging me when I (pretty much continually) needed it. Dr. Schwartz, my co-chair, also kindly allowed me to rotate through his lab. I also thank his RA, Cristine Camp, for taking so much time to teach me their techniques. Dr. Schwartz also generously allowed me to run Veterinary Physiology review sessions and then deliver four lectures as instructor-of-record in the physiology course. I thank Dr. Biancardi for her thorough and helpful critiques of my writings, and for giving me a kind ear when I needed advice. Dr. Panizzi (Pete) always gave helpful suggestions in committee meetings and provided welcome humor to break the occasional tension. Finally, I'd like to thank my outside reader, Dr. Emily Graff, for her challenging yet fair questions during my oral exams and always being there when I/we needed to empathize or grumble about politics.

Drs. Chad Foradori and Juming Zhong also unselfishly provided me time and resources during my first semester rotations. Their RAs Melaney Jones and Dori Miller patiently taught me techniques and humored my incessant questions. Dr. Vitaly Vodyanoy was a pleasure to converse with, and his wisdom helped me become a better scientist. Similarly, the retired chair, Dr. Ed Morrison, always had an open door and gave abundant wisdom and encouragement. I have to thank Dr. Foradori for letting me visit to get things off my chest, or just plain have a good cry in his office. The whole department is best among the places I've worked and studied.

My Ph.D. was both a time of learning and a time of mourning. Five of my family members died, one in each year. My mother was a kind soul with a golden heart, and I still think of her daily, even after three years. She taught me to stand up for myself, and to show love as abundantly as possible—a tall order for an old grump like me. My granddad (granddaddy, a UA grad) died last year, and I will miss his stoic attitude. His best joke was, "Jeff, I'm glad Auburn is paying you to go to school; it's just a shame you won't get an education." My sweet "step"-grandmother Me-Me always treated me like one of her own grandchildren. Grannie died the year before mom, and if a stronger person exists, I'd love to meet them. She was thrice widowed, survived breast cancer, and lost a daughter and son-in-law in 2004. Yet, she would never miss cooking Thanksgiving and Christmas dinners. She would always say, "If I didn't pick on you, you'd think I was mad at you!" Finally, I didn't spend enough time getting to know Kelly's granddad, but he was an extremely generous man with a good heart. And tough as nails. The European theatre in WWII has that effect on people, I imagine. All of these people contributed to who I am today.

Finally, my wife and soulmate Kelly. She is the sweetest and most caring person I know. My parents-in-law are also warm and loving, charitable and sympathetic. Even after eight years, each day is better than the last. Her support toward my Ph.D. was superhuman, especially with an ol' grumpy husband. I love you, dearest.

Table of Contents

List of Tables

List of Figures

List of Abbreviations

Airway multiciliated cells (aMCC)

Ankyrin and EF-hand containing protein 1 (Ankef1)

Autosomal dominant polycystic kidney disease (ADPKD)

Autosomal recessive polycystic kidney disease (ARPKD)

Bardet-Biedl syndrome (BBS)

Basal body (BB)

Bitter taste receptor (T2R)

Centrosomal protein (CEP)

Cerebrospinal fluid (CSF)

Ciliary vesicle (CV)

Clustered regularly interspaced short palindromic repeat (CRISPR)

Coiled-coil domain-containing protein 103 (Ccdc103)

Cone-rod dystrophy (CRD)

Days post-fertilization (dpf)

DNA-binding domain (DBD)

Dorsal forerunner cells (DFC)

Dorsal marginal zone (DMZ)

Double-strand break (DSB)

Elongation factor 1α (Ef1α)

Ethylnitrosourea (ENU)

G-protein coupled receptor (GPCR)

Gene of interest (GOI)

Hedgehog (Hh)

Homology-directed repair (HDR)

Hours post-fertilization (hpf)

Intraflagellar transport (IFT)

Iterative Threading Assembly Refinement (I-TASSER)

Joubert syndrome (JBTS)

Knockdown (KD)

Knockout (KO)

Kupffer's vesicle (KV)

Lateral plate mesoderm (LPM)

Leber congenital amaurosis (LCA)

Loss-of-function (LoF)

Meckel syndrome (MKS)

Morpholino oligonucleotide (MO)

Multiciliated cells (MCC)

Nephronophthiasis (NPHP)

Next-generation sequencing (NGS)

Nitric oxide (NO)

Nonhomologous end-joining (NHEJ)

NRARP (Notch-regulated ankyrin repeat-containing protein)

Oak Ridge Polycystic Kidney (ORPK)

Ocular developmental anomaly (ODAn)

Orofaciodigital syndrome (OFD)

Outer dynein arm (ODA)

Patched (Ptch)

Planar cell polarity (PCP)

Polycystic kidney disease (PKD)

Polycystin-1 (PKD1)

Primary ciliary dyskinesia (PCD)

Protospacer adjacent motif (PAM)

Reduced generation of multiple motile cilia (RGMC)

Retinitis pigmentosa (RP)

Retinitis pigmentosa GTPase regulator (RPGR)

Schmalhans (smh) ccdc103 zebrafish mutant

Senior-Løken syndrome (SLSN)

Single guide RNA (sgRNA)

Smoothened (Smo)

Transcription activator-like effector nuclease (TALEN)

Urinary tract infection (UTI)

World Health Organization (WHO)

Zinc-finger domain (ZFD)

CHAPTER 1

REVIEW OF THE LITERATURE

INTRODUCTION

Inherited monogenic human genetic diseases have a global incidence of about 1-3% per generation (Lynch, 2010), with World Health Organization (WHO) estimates a monogenic disease prevalence of 1% of the total world population (WHO, 2019). Interestingly, even healthy individuals carry between 200 and 400 loss-of-function variants (Abecasis *et al.*, 2010; MacArthur and Tyler-Smith, 2010; Ng *et al.*, 2008; Pelak *et al.*, 2010). More precise genetic data on causative mutations could lead to more effective precision treatment and increase the overall cost-effectiveness of care (Gavan *et al.*, 2018). Thus, genetic research is indispensable in honing effective care using syndrome modeling in non-human animals.

The tropical zebrafish (*Danio rerio*) has become a prominent vertebrate model organism for genetic diseases in the last 40 years. As with most teleosts, zebrafish can quickly reproduce and are inexpensive to house and maintain. Zebrafish lay transparent eggs, which are optimal for viewing the developmental effects of both genetic lesions and drugs or suspected toxins on embryos. The zebrafish whole genome is available, along with several genetic tools to manipulate RNA expression and DNA sequences directly. More specifically, the concept of "precision medicine" can be modeled in zebrafish by creating lesions associated with human disease-causing genes (Baxendale *et al.*, 2017) in fish embryos. Various CRISPR/Cas (Clustered Regularly Interspaced Short Palindromic Repeat; CRISPR-associated protein) systems have been developed to modify both genomic DNA and RNA *in vivo* directly. CRISPR/Cas has already been used to model genetic disease in zebrafish, including genetic targets related to cilia structure and function.

Ideally, genetic testing for common ciliary markers should be done in all individuals but doing so is not economically viable with current technology. In this review, we summarize both the zebrafish ciliopathy genes that have been targeted by CRISPR technology, as well as CRISPR methods that have been used in zebrafish.

CILIA STRUCTURE AND FUNCTION

The cilium is a hair-like extension of the cell membrane that is present on nearly every cell in the human body. Researchers typically classify cilia into two groups: motile and nonmotile, also called primary/sensory, cilia. Early electron microscopy by Björn Afzelius revealed that the ultrastructure (the axoneme plus accessory proteins) of eukaryotic flagella and motile cilia are indistinguishable (Afzelius, 1976), as both have the prototypical 9+2 arrangement—nine outer microtubules and two inner microtubules. In contrast, nonmotile cilia typically have a 9+0 arrangement (Fig. 1.1). Both motile and nonmotile cilia are also present in the developing vertebrate embryo. Exceptions to the motile/nonmotile delineation do exist, including the motile 9+0 nodal cilia and the 9+2 nonmotile kinocilia in both immature mammalian hair cells and mature fish hair cells (Hudspeth and Corey, 1977; Jaeger *et al.*, 1994). Ciliated tissues and cells in mammals include dorsal root ganglia neurons (Tan *et al.*, 2007), kidney cells (Katz and Morgan, 1984), mature sperm (Blum, 1971; Holwill, 1977), fallopian tubes (Clyman, 1966; Patek and Nilsson, 1973), ependymal cells in the spinal canal (Worthington and Cathcart, 1963), and the mouse embryonic node (Hashimoto *et al.*, 2010) (Kupffer's vesicle in zebrafish (Kimmel *et al.*, 1995)). Furthermore, cilia are present on the skin of *Xenopus laevis* (Steinman, 1968, 1970) and in the pronephros of zebrafish embryos (Kramer-Zucker *et al.*, 2005). Researchers long believed cilia to be vestigial (Dahl, 1967; Garant *et al.*, 1968); however, evidence suggesting their functional

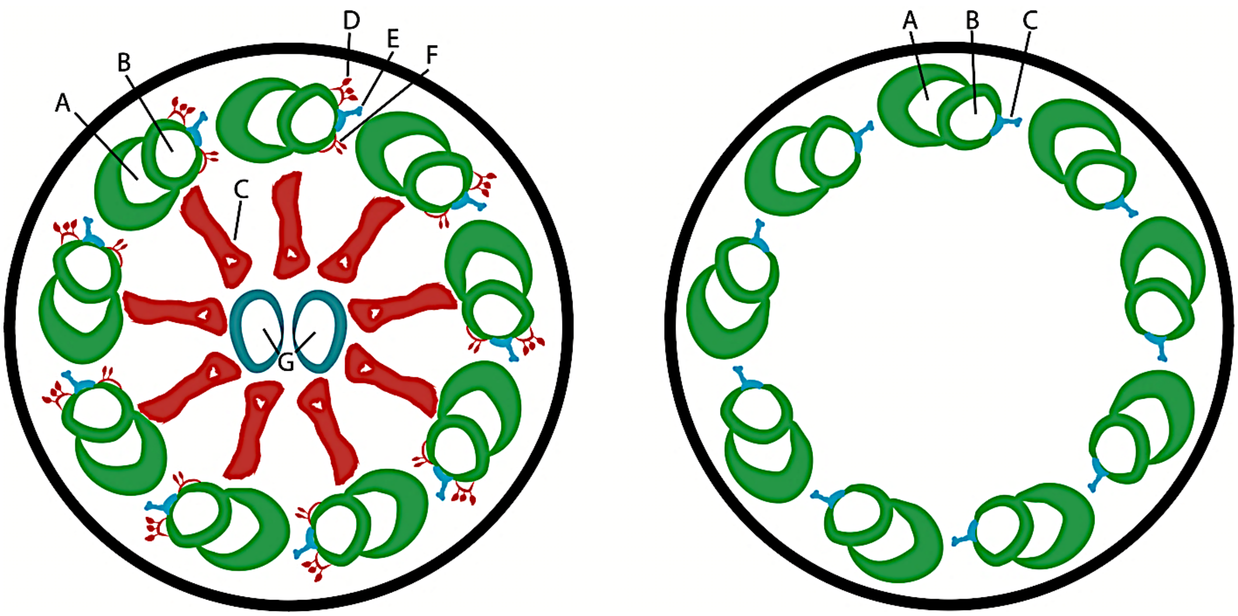

Figure 1.1: Cross section of motile cilia (left) and nonmotile cilia (right). Motile cilia parts: A, β-tubule; B, α-tubule; C, radial spoke; D, outer dynein arm; E, nexin linkage; F, inner dynein arm. Nonmotile cilia parts: A, β-tubule; B, α-tubule; C nexin linkage.

roles began accumulating in the mid-20th century (Barnes, 1961; Federman and Nichols, 1974; Milton, 1959; Munger, 1958; Satir, 1965). For example, motile cilia in Kupffer's vesicle mediate left-right asymmetry through the Nodal signaling cascade, cilium-mediated cerebrospinal fluid (CSF) flow is required for proper brain ventricle development (Essner *et al.*, 2005; Kramer-Zucker *et al.*, 2005), and nonmotile cilia mediate Leydig cell differentiation through Wnt signaling in mammals.

Cilium formation (ciliogenesis) occurs during interphase and requires centrioles, cilium-specific protein targeting, and transport of proteins up the elongating cilium. Cilia begin their formation in the cytoplasm, in which a ciliary vesicle (CV) attached to the mother centriole is moved toward the site of cilia establishment and elongation. Mother centrioles become basal bodies (BBs), which are required for cilium growth and maturation. Basal bodies have a circular array of microtubule triplets consisting of an A-, B-, and C-tubule. Many hundreds of centrioles are formed in multiciliated cells (MCCs) and become basal bodies for each cilium. The cilium axoneme is an extension of the mother centriole portion of the basal body, from which the A and B tubules extend up through the cilium. As the new cilium moves through the cytoplasm, the CV accumulates secondary vesicles. The transition zone begins to form as the CV expands and intraflagellar transport (IFT) proteins begin to attach to the centriolar microtubules. IFT involves the transport of cargo (i.e., proteins) from the cilium base to the tip (anterograde) by kinesins or from the tip to the base by cytoplasmic dyneins (retrograde) not firmly attached to the axoneme. After cilium docking and fusion with the cell membrane, the so-called "ciliary gate" completes, and cilium growth occurs via soluble molecular motors moving up and down the microtubule tracks. The ciliary gate is responsible for regulating protein entry into the "cilioplasm" (i.e. the protein milieu in the ciliary compartment). IFT is critical for the development and maintenance of somatic cell ciliary structure and function (both nonmotile and motile), but not the maintenance of sperm flagella (Damerla *et al.*, 2015). Interestingly, IFT components are not present in mature sperm, which reflects its almost complete lack of cytoplasm and absence of turnover of flagellar proteins(San Agustin *et al.*, 2015). Furthermore, molecular signals that do move between the sperm head and flagella are thought to be ions or small molecules. Dysfunctional IFT proteins lead to shortened or absent cilia and can lead to a number of developmental defects, and diseases such as polycystic kidney disease (PKD) or primary ciliary dyskinesia (PCD), due to dysfunctional nonmotile and motile cilia, respectively (Pazour *et al.*, 2000).

Nonmotile cilia function

Nonmotile cilia typically have the 9+0 structure, which lacks the dynein arms and central pair that define motile cilia. The nonmotile cilium acts as a cellular antenna and is thus the site of origin for specific signaling processes that are unique to the ciliary compartment. Various types of channels and receptors localize to nonmotile cilia and mediate sensory processes. For example, G-protein coupled receptors (GPCR) are localized to nonmotile olfactory cilia and convey odorant signals to the brain (Shibuya and Takagi, 1963). Photoreceptors—rods and cones—are modified cilia that transduce light signals to the optic nerve and beyond (Greiner *et al.*, 1983; Hinds and Hinds, 1979).

Nonmotile cilia also play a role in invertebrate and vertebrate development. Hedgehog (Hh) signaling components localize to nonmotile cilia (Fig. 1.2) and are required for normal vertebrate embryogenesis (Huang and Schier, 2009; Huangfu *et al.*, 2003; Philipp *et al.*, 2008; Ruat *et al.*, 2014). Defects in Hh genes active during early vertebrate development cause midline defects (e.g., lack of floor plate in the neural tube), while mutations in later genes can lead to a lack of eye separation (cyclopia) or distal limb truncation (Chiang *et al.*, 1996). Hh proteins were first

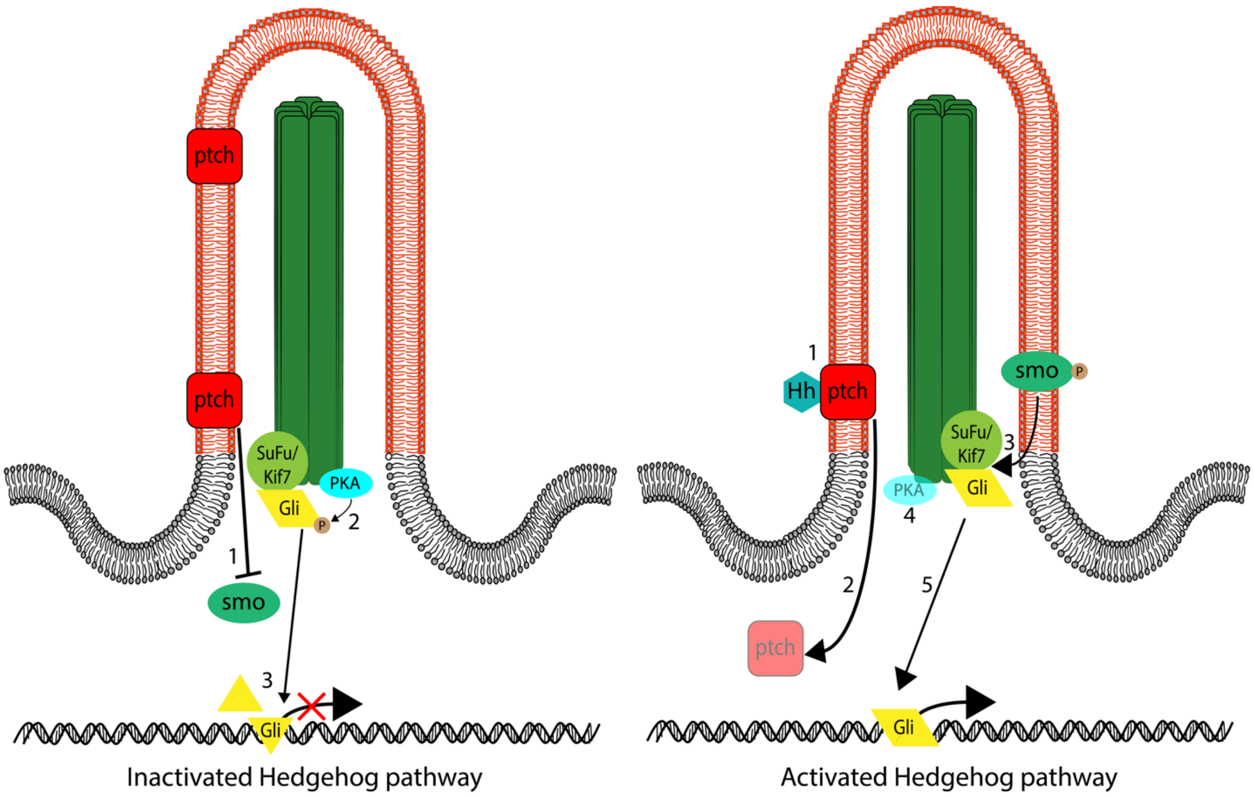

Figure 1.2: Diagram of inactivated and activated hedgehog pathways. Without the hedgehog ligand bound to patched, (1) patched inhibits smoothened (smo) localization to the ciliary membrane, (2) PKA cleaves Gli into a repressor for Hh-responsive genes. When (1) Hh binds to Patched (Ptch), Ptch is degraded (2) and the inhibition of smo is removed. (3) Smo increases the Gli activator form and (4) inactivates PKA. (5) Gli migrates to the nucleus and Hh-responsive genes are upregulated. The red phospholipids denote the ciliary compartment.

identified in *Drosophila* (Nusslein-Volhard and Wieschaus, 1980), with several classes of homologous proteins also present in vertebrates (sonic hedgehog, Shh; desert hedgehog, Dhh; Indian hedgehog, Ihh). Most vertebrates express at least one type of Hh gene (Bitgood and McMahon, 1995; Bitgood *et al.*, 1996; Hammerschmidt *et al.*, 1996a), and zebrafish have at least five Hh genes, including at least one from each class. Hh proteins are secreted as monomeric or multimeric lipoproteins, as both arrangements require the attachment of a palmitic acid and a cholesterol for proper diffusion rates and concentration gradients (Grover *et al.*, 2011; Li *et al.*, 2006). Unstimulated Hh receptors (i.e., *patched*, *ptch;* a 12-pass transmembrane receptor) primarily localize to the ciliary membrane (Fig. 1.2) and prevent downstream transcription of Hh-related genes via the *Gli* repressor (Buttitta *et al.*, 2003; Kinzler *et al.*, 1988). *Ptch* stimulation allows *Smoothened* (*smo*, a GPCR (Ruiz-Gomez *et al.*, 2007)) to enter the cilium, which then releases the *Gli* activator (Buttitta *et al.*, 2003; Rohatgi *et al.*, 2007). Downstream transcription targets of *Gli* include *foxa2*/*nkx2.2*/*nkx6.1* in the developing neural tube (Motoyama *et al.*, 2003; Taylor *et al.*, 2004) and *pax9* in the murine anterior limb bud (Vokes *et al.*, 2008). *Gli2*$^{-/-}$*Gli3*$^{-/-}$ mouse embryos showed reduced *pax9* expression and, thus, errors in sclerotome induction (Buttitta *et al.*, 2003). Morpholino oligonucleotide (MO)-induced errors in downstream signaling activation, such as *nkx2.2* in the neural tube, lead to stunted perineural glia exit from the spinal cord in developing zebrafish embryos (Kucenas *et al.*, 2008).

Motile cilia function

Embryonic and adult physiological processes (Praetorius and Spring, 2005; Rawlins and Hogan, 2008) require motile cilia for maintaining homeostasis. Motile cilia are involved in processes requiring movement of fluids or particles, such as CSF flow and airway mucus clearance. Furthermore, similarly structured sperm flagella (motile cilia) generate propulsive force perpendicular to the plane running between the central pair. Thus, the central pair gives a motile cilium its directional movement. Motility itself is generated by dynein-mediated sliding action between microtubules. Motile cilia are most commonly found with the 9+2 configuration, whereby nine doublets surround a central pair. For example, the waveform of 9+2 cilia in the respiratory tract involves an oar-like (Arsov *et al.*, 2006) active stroke followed by a recovery stroke. Motility can also proceed in a corkscrew manner, as seen in 9+0 nodal cilia (Hashimoto *et al.*, 2010), rather than rotation at the base as in the bacterial flagellar rotary motor (Satir, 1963). Microtubules, which are polymers of tubulin, typically act as structural supports for the cilium and as tracks for the movement of motor proteins (Moss *et al.*, 1992; Rosenbaum and Witman, 2002; Sale and Satir, 1977; Satir, 1980). Dynein arms attached along the length of ciliary microtubules mediate ciliary bending (Satir, 1980) through an axonemal sliding mechanism. The inner and outer dynein arms are firmly attached to one microtubule and, upon the presence of ATP, "walk" on an adjacent microtubule, producing sliding between the tubules (Shah *et al.*, 2009).

Although the motile/nonmotile classifications appear to be mutually exclusive, more recent evidence suggests that the motile and nonmotile delineations only represent the extremes of cilium function. Motile cilia in the human airway also show chemosensation in addition to motility (Shah *et al.*, 2009). Bitter taste receptors (T2R) localize to the cilia present on airway multiciliated cells (aMCC). Ciliary beat frequency on aMCC significantly increased upon stimulation with denatonium, a T2R ligand (Shah *et al.*, 2009), indicating chemosensory function in these cells. A more recent study (Mao *et al.*, 2018) showed that Hh signaling components localize to multiciliated cells in the human airway epithelium, raising the possibility of extracellular signal transduction originating in the motile cilium. Therefore, the latter study reinforces the notion that the motile cilium may transduce signals to downstream extracellular sources. As such, proteins involved in shuttling motility-related factors may also participate in localizing signaling proteins to the motile cilium.

Motile cilia also mediate essential processes in embryonic development. Motile cilia in the mouse node and zebrafish Kupffer's vesicle generate a morphogen gradient through cilia-mediated clockwise flow (Nonaka *et al.*, 1998). Zebrafish embryos form an analogous structure at the end of gastrulation called Kupffer's vesicle (Kimmel *et al.*, 1995), which is preceded by the dorsal forerunner cells (DFC) (Essner *et al.*, 2002). Cilia-driven clockwise fluid flow in the vesicle induces asymmetric activation of the Nodal signaling cascade in the lateral plate mesoderm (LPM), which leads to organ laterality. The motile cilium protein milieu is abundant with various motor proteins, adapters, receptors, and structural proteins (Figs. 1.1 and 1.2). For example, coiled-coil domain-containing protein 103 (Ccdc103) is a critical component for outer dynein arm (ODAs) attachment to the microtubule structure of the motile cilium (King and Patel-King, 2015; Panizzi *et al.*, 2012).

CILIOPATHIES

Ciliopathies, a term first used by Cornillie *et al.* (Cornillie *et al.*, 1984), are a subclass of inherited genetic diseases that lead to alterations in the structure and function of cilia. Individual ciliopathy diseases are usually rare on their own, but ciliopathy incidences range from 1 in 400 live births in ADPKD to 1:20,000 in ARPKD (Waters and Beales, 2011). Ciliopathies are associated with several human syndromes (Waters and Beales, 2011), including PCD, PKD, retinitis pigmentosa (RP), and infertility, as well as rarer disorders including Bardet-Biedl syndrome, Joubert syndrome, Leber's congenital amaurosis, nephronophthisis, Senior-Løken syndrome, and Meckel-Gruber syndrome (Table 1.1). The first direct evidence of human ciliopathy appeared in patients with immotile sperm (Afzelius, 1976). These infertile patients had several disease phenotypes, including missing inner or outer dynein arms on their sperm axonemes. Because of the missing dynein arms, the patients had paralyzed motile cilia, resulting in chronic respiratory and auditory infections, as well as male and female infertility (Papon *et al.*, 2010). Ciliopathies arise in both human and veterinary medicine, with some of the first records of a veterinary ciliopathy were noted in two English sheepdogs (Randolph and Castleman, 1984). Although Manes Kartagener (Kartagener, 1933) connected an array of symptoms—reversed organ laterality (situs inversus), chronic sinusitis, and thickened bronchial walls (bronchiectasis)—to a common etiology, A.W. Siewert was the first to publish a ciliopathy case (Siewert, 1904). Kartagener's syndrome is a form of PCD (Tadesse *et al.*, 2018), a disease in which motile cilia are unable to beat (Afzelius, 1976; Popper and Jakse, 1982; Popper *et al.*, 1985). Thirty-five distinct ciliopathies have been identified, involving 187 cilium-related genes with another 241 candidate ciliopathy-related genes (Reiter and Leroux, 2017). The 35 ciliopathies share a wide array of morbidities and comorbidities requiring a precise determination of the root genetic cause. Ciliopathy incidences vary among discrete gene pools, depending upon the degree of gene flow among, into, and out of the population.

Errors in motile cilia

Accurate diagnosis of PCD is difficult due to its genetically heterogeneous nature. Incidence has been estimated at 1 in 3,000 to 1 in 40,000, but PCD may be underdiagnosed (Kuehni *et al.*, 2010). Underdiagnosis can be due patients residing in countries with poor health expenditures, unrecognized symptoms early in life, or misdiagnosis of other conditions like asthma or recurrent bronchitis (Lucas *et al.*, 2014). Defects in motility-related proteins lead to paralyzed (immotile) cilia, or abnormal cilia beat frequencies. Accumulated fluid in brain ventricles

Ciliopathy(Reiter and Leroux, 2017**)**	**Associated genes(**Reiter and Leroux, 2017**)**	**Zebrafish models**
ADPKD	Pkd1, pkd2	None in zebrafish.
Alström syndrome	Alms1	Alms1(Lodh *et al.*, 2016; Nesmith *et al.*, 2019)
ARPKD	Pkhd1, dzip1l	Dzip1l(Lu *et al.*, 2017)
BBS	Bbs1, bbs2, bbs4, bbs5, bbs6, bbs7, bbs9, bbs10, bbs12, bbip1, ift27, lztfl1, trim32, wdpcp, ccdc28b, mks1, arl6, ttc8, ift172, sdccag8, ift74	Mks1(Stawicki *et al.*, 2016), ift74(Lindstrand *et al.*, 2016), bbs1(Lodh *et al.*, 2016), bbs4(Lodh *et al.*, 2016; Tsai *et al.*, 2019), ccdc28b(Novas *et al.*, 2018), bbs6
RP	Arl6, bbs2, ttc8, ift172, rpgr, spata7, pomgnt1, arl2bp, c20orf71, cnga1, cngb1, fam161a, mak, rp1, rp2, topors, nek2, arl3, tulp1, pik3r4, c8orf37, ofd1, rp1L1, ift140, wdr19	rp1l1(Liu *et al.*, 2017)
OFD	C2cd3, ddx59, sclt1, tmem17, ift57, tmem231, tbc1d32, ofd1, nek1, wdpcp, tmem138, mnr/ofip/kiaa0753, tmem107, c5orf42, tmem216, tctn3	None in zebrafish.
NPHP	Ift172, sdccag8, iqcb1, tmem67, tctn2, anks6, cep164, xpnpep3, glis2, cep83, znf423, nphp1, atxn10, nphp3, dcdc2, ift81, nek8, ttc21b, nphp4, invs, pik3r4, wdr19, nme3	Nme3(Hoff *et al.*, 2018)
Jeune syndrome	Ift172	None in zebrafish.
Short-rib thoracic dysplasia	Wdr35, cspp1, ttc21b, cep120, dync2h1, ift80, intu, tctex1d2, wdr34, wdr60, nek9, nek1, 1ft140, dync2li1, wdr19	None in zebrafish.
SLSN	Sdccag8, iqcb1, cep290, cep164, nphp1, nphp4, invs, traf3ip1, wdr19	None in zebrafish.
Complex lethal osteochondrodysplasia	Tapt1	Tapt1b(Symoens *et al.*, 2015)
Cranioectodermal dysplasia	Ift122, ift43, ift52, wdr35	Ift52(Dupont *et al.*, 2019)
CRD	Kiz, rab28, ttll5, unc119, c21orf2, cep78, rpgrip1, poc1b, rpgr, crx, c8orf37,	None in zebrafish.
LCA	Rpgrip1, poc1b, cluap1, lca5, crx, spata7, iqcb1, cep290, tulp1, ift40	None in zebrafish.
JBTS	Mks1, poc1b, kif7, hyls1, cnga2, ahi1, cep104, kiaa0556, pde6d, pibf1, tctn1, arl13b, cep41, kiaa0586, tmem237, inpp5e, tmem138, mnr/ofip/kiaa0753, tmem107, c5orf42, cep290, b9d1, b9d2, cc2d2a, rpgrip1l, tmem67, tmem216, cspp1, tctn2, tctn3, znf423, nphp1, atxn10, tmem231, ofd1, wdr60	Mks1(Stawicki *et al.*, 2016), inpp5e(Xu *et al.*, 2017), ahi1(Zhu *et al.*, 2019)
Spinocerebellar ataxia	Atxn10, ttbk2, atxn7	Atxn7(Carrillo-Rosas *et al.*, 2019)
MKS	Mks1, tmem237, tmem107, cep290, b9d1, b9d2, cc2d2a, rpgrip1l, tmem67, tmem216, cspp1, tctn2, nphp3, tmem231, cep164	Mks1(Stawicki *et al.*, 2016)
PCD	Rpgr, ak7, armc4, c21orf59, ccdc103, ccdc114, ccdc151, ccdc39, ccdc40, ccdc65, ccno, dnaaf3, heatr2, dnaaf2, dnaaf5, dnaah11, dnah5, dnai1, dnai2, dnal1, drc1,	None in zebrafish.

	dyx1c1, gas8, hydin, lrrc6, mcidas, nme8, pih1d3, rsph3, rsph1, rsph4a, rrph9, spag1, ttc25, zmynd10, dnah6, dnajb13, dnaaf1, ofd1	
Cranioectodermal dysplasia	Ift122, ift43, ift52, wdr35, wdr19	Ift52(Dupont *et al.*, 2019)
Basal cell carcinoma, medulloblastoma, meningioma	sufu	None in zebrafish.
Hydrolethalus syndrome	Usp8, kif7, hyls1, kiaa0586	Usp8(Kasahara *et al.*, 2018)
Congenital anosmia	Cnga2	Cng2a/cng2b(Blechman *et al.*, 2018)
Holoprosencephaly	Zic2, ptch1, gli2	Ptch1(Burns *et al.*, 2018; Chassaing *et al.*, 2016), zic2b(Sedykh *et al.*, 2017)
Heterotaxy	Cfap53, galnt11, pkd1L1, nodal, znfl1s, ccdc11, dnah10, rnf115, klf8	Znfl1s(Li *et al.*, 2019), dnah10(Liu *et al.*, 2018), rnf115(Liu *et al.*, 2018), ccdc11(Gur *et al.*, 2017), klf8(Lin *et al.*, 2017)
Chondrodysplasia	Nomo	Nomo(Cao *et al.*, 2018)
Retinal dysplasia	Tub, C21ORF2, arl13b, cep164, c2orf71l, rp1l1	rp1l1(Liu *et al.*, 2017), c2orf71l(Liu *et al.*, 2017)

Table 1.1: Ciliopathies with associated genes and their CRISPR-mediated modelling in zebrafish.

(hydrocephalus) results from either the inability of paralyzed motile cilia to induce ependymal flow (Fliegauf *et al.*, 2007) or improper alignment of ciliary beat direction via the planar cell polarity pathway (Guirao *et al.*, 2010). Immotile cilia in fallopian tubes are associated with ectopic pregnancies (Blyth and Wellesley, 2008). Other clinical signs of PCD include (Sha *et al.*, 2014) chronic cough, respiratory congestion and infections, situs inversus, infertility (due to sperm abnormal motility), and airway bleeding (hemoptysis). Motile cilia also play an essential role during development. A nonsense mutation in Dnaaf2, which is involved in dynein assembly, is embryonic lethal in mice and affected embryos arrest during organogenesis (Cheong *et al.*, 2019). As noted above, a variety of embryo defects may result from functional disorders ranging from mild nonpathological phenotypes to lethality.

The diagnosis of PCD requires a combination of several tests (Leigh *et al.*, 2009a; Leigh *et al.*, 2009b). Clinical imaging can be employed to assess the reversal of the heart loop (situs inversus due to the inability to move fluid in the embryonic node). The motility and ultrastructure of ciliated respiratory epithelial cells can be assessed with nasal biopsies, followed by culture and imaging. Bronchiectasis is another important clinical indicator of the condition and helps in distinguishing PCD from pneumonia or other respiratory infections. Furthermore, patients diagnosed with PCD may also have their fallopian tubes or sperm analyzed before making a diagnosis of infertility (Greenstone *et al.*, 1988). Interestingly, not all patients with PCD are infertile (Munro *et al.*, 1994), indicating a complicated interaction of PCD genes. In this published study, one patient's spermatozoa lacked dynein arms, but the same patient still had structurally and functionally normal nasal cilia, perhaps indicating that different genotypes in the same organism (mosaicism) are possible or that functionally similar protein forms (isoforms) exist in different cell types.

Fortunately, outcomes for PCD patients are good (Bush *et al.*, 1998), with a healthy life expectancy for affected individuals undergoing effective management of the disorder, often including chest physical therapy, antibiotics for lung infections, bronchodilators, or anti-inflammatory drugs (https://www.nhlbi.nih.gov/health-topics/primary-ciliary-dyskinesia). Studies in the zebrafish system have identified or characterized many other PCD or ciliary genes implicated in human disease. *Ccdc103* is an example of a motility-related gene whose defects have been shown in humans and zebrafish to cause PCD, which results from the loss of outer dynein arms. PCD morbidities associated with *ccdc103* defects in zebrafish include a curved body along the dorsoventral axis, kidney cysts, and hydrocephalus.

Errors in nonmotile cilia

Diseases associated with nonmotile cilia are typically due to mutations in proteins associated with cellular signaling pathways that are mediated by the cilium. Given that Hh signaling is required for many developmental processes, including vertebrate limb morphogenesis and neural cell differentiation (Bitgood and McMahon, 1995; Bitgood *et al.*, 1996; Lewis *et al.*, 1999; Qu *et al.*, 1997), the finding that vertebrate nonmotile cilia mediate Hh signaling raised the questions of what other developmental pathways signal through cilium-localized receptors and what advantages are conferred by signaling through cilia (Goetz and Anderson, 2010). The Hh receptor Ptch1 localizes to nonmotile cilia and is involved in murine embryonic patterning and survival (Huangfu *et al.*, 2003). Interestingly, nonmotile cilium-mediated Hh signaling has also been associated with increased tumorigenesis (Han and Alvarez-Buylla, 2010; Han *et al.*, 2009; Wong *et al.*, 2009a).

PKD is a disorder that follows both autosomal dominant (ADPKD) and autosomal recessive (ARPKD) inheritance patterns (Ibraghimov-Beskrovnaya *et al.*, 2000; Okada *et al.*, 1999; Qin *et al.*, 2001). Evidence suggests that renal tubular cells with shortened or absent cilia due to polycystin mutations rapidly proliferate and incompletely differentiate (Somlo and Ehrlich, 2001). ADPKD constitutes a vast majority of PKD cases with an incidence of roughly 1:400, with ARPKD being much less common (Armstrong and Thomas, 2019; Douguet *et al.*, 2019; Stayner *et al.*, 2019; Xue and Mei, 2019). Symptoms of PKD include fluid-filled renal cysts, blood in the urine (hematuria), chronic fatigue, pale skin color, and urinary tract infections (UTI). Renal epithelial cells typically have one nonmotile cilium that protrudes into the nephron tubular lumen and can act as an extracellular flow rate transducer or as a cellular mediator of fibronectin signaling (Praetorius *et al.*, 2004). Defects in polycystin-1 (PKD1) or PKD2, which mediate ciliary calcium signaling, contribute to kidney cyst formation by disrupting downstream cell proliferation/differentiation signaling (Ma *et al.*, 2017; Pazour and Rosenbaum, 2002). Interestingly, the absence of polycystins along with the absence of cilia can abrogate ADPKD (Ma *et al.*, 2017).

Photoreceptor cells have another type of nonmotile cilia and express various light-transducing proteins. The human retina, consisting of rods and cones, constitutes part of the vertebrate inner wall tissue of the eye and is active in transducing light signals into nerve impulses (Stojanovic and Hwa, 2002). These cells express rhodopsin, which localizes to the modified cilium region of the photoreceptor (Macke *et al.*, 1993; Sung *et al.*, 1991). Briefly, rhodopsin is constitutively active in the flattened disks of the rod cell, and photons reduce the amount of cGMP that is present in the rod (Baxter and Morse, 1992; Deretic *et al.*, 1995; Wald *et al.*, 1950). Light induces a decrease in cGMP, causing ion channels to close and hyperpolarize the rod cell. In cone cells, three types of photopsins (erythrolabe, chlorolabe, and cyanolabe), each detecting a specific wavelength range, act similarly to rhodopsin in rod cells. Errors in photoreceptor proteins or their downstream targets typically lead to RP, a genetic illness that affects about 1 in 5000 individuals worldwide (Araki *et al.*, 1984; Kachi *et al.*, 1999). Although rods are initially and primarily affected, cone function is disrupted as the disease progresses. Several inheritance patterns characterize retinitis pigmentosa, including autosomal dominant/recessive and X-linked recessive. Mutations in rhodopsin have been shown to cause autosomal dominant retinitis pigmentosa (Sohocki *et al.*, 2001). Mutations in RP2 or RPGR (retinitis pigmentosa GTPase regulator) were found in most of the families in a North American cohort and therefore may account for a majority of worldwide X-linked retinitis pigmentosa cases (Breuer *et al.*, 2002). In addition to photoreceptor defects, downstream signaling can be affected. A nonsense mutation in the γ subunit of the cone cyclic guanosine monophosphate phosphodiesterase, which lowers cGMP levels and thus transduces the photonic signal further downstream in the photoreceptor (Kohl *et al.*, 2012), leads to achromotopsia, a retinal dystrophy showing color blindness, photophobia, involuntary eye movements (nystagmus), and severely reduced visual acuity (Sampangi *et al.*, 2005; Tsang and Sharma, 2018).

As multiple diseases are linked to defects in ciliary formation or function, further characterization of deleterious molecular lesions is necessary to expand diagnostic and treatment options. As such, more accurate gene targeting tools are necessary to precisely reproduce naturally occurring mutations and their associated phenotypes. Model organisms such as zebrafish can significantly contribute to our understanding of disease etiology and progression.

ZEBRAFISH AS A MODEL SYSTEM FOR HUMAN PATHOLOGY

The molecular structure of cilia is highly conserved, from simple organisms like *Chlamydomonas* (Afzelius, 1961; Ringo, 1967) to mice and humans (Afzelius, 1976). The Oak Ridge Polycystic Kidney (ORPK; IFT88$^{-/-}$) mouse was the first organism used to model the role of defective IFT proteins in ciliopathies (Lehman *et al.*, 2008). Correct ciliogenesis requires IFT88 (Polaris), and the hypomorphic allele present in ORPK mice leads to shortened and malformed cilia (Robert *et al.*, 2007). Nonmammal vertebrate organisms have been successfully used to model mutant phenotypes mimicking those in humans, including many ciliary diseases. The zebrafish (*Danio rerio*) has become a noted model organism for studying physiological and developmental processes. Zebrafish maintenance and care are relatively inexpensive, and large numbers (up to 200-300) of zebrafish embryos can be generated each week by just a single breeding pair. Embryos develop very quickly, completing organogenesis by day two and enter their larval stage at day seven (Kimmel *et al.*, 1995). Therefore, developmental issues that may arise from genetic lesions or drug treatment are often seen within the seven-day developmental window. Motile cilia on the olfactory placode can easily be imaged by light or confocal microscopy to ascertain cilium structure quickly. Furthermore, the presence of functional cilia in the embryonic ependymal cells and pronephros can be easily viewed (Drummond, 2009; Drummond and Davidson, 2016). Zebrafish offer many genetic advantages as a model organism. In addition to the full genome sequence availability, 71.4% of human proteins have a zebrafish orthologue (Howe *et al.*, 2013). One-cell embryos can tolerate injections of up to around 6-8 nL of fluid (i.e., solutions of MOs, Cas9/sgRNA, or synthetic mRNA), allowing for genetic manipulation.

GENETIC METHODS USED IN ZEBRAFISH

Non-CRISPR genetic methods

Genetic methods for zebrafish are well established, with the full zebrafish genome freely available for download. Zebrafish embryos are well-suited for studying developmental mechanisms and drug effects on embryonic development. The first large-scale screen for genetic lesions with zebrafish culminated in a 1996 issue of *Development* (vol. 123, issue 1), which identified several mutant classes, including some now known to be cilium-related mutants. Males were treated with ethylnitrosourea (ENU), a potent mutagen, to induce point mutations in germ cells, and then crossed with wild-type females. The F1 generation was outcrossed with wild-type fish. Finally, the F2 generation, half of which should be heterozygous for ENU-induced mutations, was grown to breeding age and in-crossed. The F3 generation was analyzed for any abnormal developmental phenotypes. Forward genetic methods were then used to isolate the mutant gene responsible for each developmental defect through positional cloning. Although laborious and time-consuming, the ENU screening method is a nonbiased method for uncovering a wide range of developmental mutants for use in downstream functional and genetic studies.

In terms of targeted genetic manipulation, several methods existed before the appearance of CRISPR technology. MOs are still considered a crucial tool to block pre-mRNA splice sites or start codons (Flynt *et al.*, 2017; Huang *et al.*, 2012; Nasevicius and Ekker, 2000; Stainier *et al.*, 2017). Briefly, injection of embryos up to the 8-cell stage is essential for full embryo knockdown, as later injections do not diffuse throughout the blastula. The MO is a ~25 bp modified oligonucleotide that is designed to sterically hinder either pre-mRNA splice sites or the mature RNA start codon and can usually block the associated processes before MO degradation in roughly two to three days (Nasevicius and Ekker, 2000). MOs are useful tools for targeted gene disruption but are not as amenable to large-scale screens. Furthermore, genes that are active later in zebrafish development (4-5 dpf) may not be targetable by MOs due to diffusion effects.

Direct modification of zebrafish genome targets via insertional mutagenesis became available in 1994 with the use of retroviruses, and further refinement occurring in the following decade. Embryos at the 1k-cell stage are injected with a retrovirus, which introduces heritable exogenous DNA with a known sequence into the genome (Amsterdam *et al.*, 1999; Lin *et al.*, 1994). Determination of the affected region is facilitated by studying the sequence on either side of the known region. Researchers later took advantage of transposable elements by developing an insertional method using a *Tol2* transposon vector (Kawakami *et al.*, 2000; Kawakami *et al.*, 2004). Messenger RNA encoding a transposase, along with the transposon vector, is injected into one-cell embryos. The transposon can then be inserted into genomic sites with a TA sequence. In-house usage of both retroviruses and transposon methods require screening large amounts of F_1 progeny, although the drawback can be overcome by ordering modified fish bred and screened by labs or companies if the modified gene of interest (GOI) can be found.

Zinc finger nucleases (ZFNs) were the first proteins capable of directed mutagenesis in zebrafish. ZFNs are engineered proteins containing both a DNA-binding zinc-finger domain (ZFD) and a modified *Fok1* cleavage domain (Doyon *et al.*, 2008; Meng *et al.*, 2008). The ZFD is engineered to recognize a specific target sequence within a GOI, and the targeted cleavage results in repair via either the nonhomologous end-joining (NHEJ) or homology-directed repair (HDR) pathway. NHEJ relies on endogenous cellular repair mechanisms, which do not always accurately restore the original sequence. Insertions-deletions (indels) may result from the low repair accuracy and frequently introduce missense mutations or even early stop codons. HDR uses an exogenous DNA template to repair the DSB, typically an engineered sequence flanked by sequences homologous to the target. HDR pathways can use an injected DNA template and thus allow for more user control over the resultant sequence; however, HDR is much less efficient than NHEJ, so the likelihood of mosaic embryos is much higher. ZFNs are quite expensive to produce and are very difficult to synthesize in-house.

Transcription activator-like effector nucleases (TALENs) are another class of engineered proteins capable of targeted gene disruption. The TALEN protein contains a DNA-binding (DBD) and nuclease dimer structure similar to ZFNs but is much cheaper to produce. TALENs have an advantage over ZFNs in their simpler and more predictable target binding mechanism; however, the larger size of TALENs makes delivery less efficient than ZFNs. Furthermore, investigator-generated TALENs require a significant time investment in the design and production of the final protein product. Both ZFN and TALEN proteins can be expressed through transgenesis, which allows for promotor control, or through overexpression by injected mRNA (Gaj *et al.*, 2013; Ma and Liu, 2015). Although both methods allow for target-specific cleavage, their disadvantages compared to CRISPR/Cas systems make CRISPRs an attractive method toward targeted gene disruption.

CRISPR/Cas9 methods

Evidence toward clarifying the CRISPR/Cas bacterial immunity system has its roots in the 1980s through the 2000s (Barrangou *et al.*, 2007; Bolotin *et al.*, 2005; Ishino *et al.*, 1987; Mojica *et al.*, 2005; Mojica *et al.*, 1995; Pourcel *et al.*, 2005). Bacteria and archaea both express CRISPR associated proteins (cas), which bind to a target sequence via a guide RNA (gRNA) and cleave foreign DNA introduced by bacteriophages. The first papers on the biomedical use of CRISPR technology were published within the last decade (Cong *et al.*, 2013; Hwang *et al.*, 2013; Jinek *et al.*, 2012; Mali *et al.*, 2013). Since then, CRISPR methods have become a versatile tool for disease modeling in biomedical science. Briefly, the single guide RNA (sgRNA) contains a gene-specific segment (~20 nucleotides; tracrRNA) and a scaffold (crRNA), which binds to Cas9. The enzyme scans the genome for any PAM sites (e.g., sequences with the NGG nucleotide pattern), which then cues the Cas9 enzyme to interrogate the adjacent sequence for a match with its gene-specific sgRNA. If the genomic sequence matches the sgRNA, Cas9 then creates a double-strand break (DSB), usually three nucleotides upstream of the PAM site. The cellular repair mechanism restores the original sequence with low fidelity, so indels are introduced into the sequence via NHEJ and can disrupt pre-mRNA splicing or protein translation.

Direct DNA editing creates a permanent change to a cell's genetic makeup, rather than the transient knockdown created by MOs. Despite the permanent change, a caveat exists, in that the sequence repair is not usually the same between affected alleles and can vary from cell to cell (Auer and Del Bene, 2014). Thus, even injection into a one-cell zebrafish embryo will almost certainly result in a genetically mosaic organism. Additionally, Cas9 is known to have off-target effects despite the predictive algorithms used on CRISPR design sites. Even without off-target effects, the NHEJ repair mechanism is not predictable, so crispants (CRISPR-created mutants) will likely be mosaic or the repair may result in a non-deleterious sequence (Burger *et al.*, 2016). Several methods have been developed to overcome CRISPR-induced mosaicism. A researcher may use the cell's HDR mechanism to introduce a known sequence into the break site by coinjection with a donor strand containing the desired edit, flanked by regions homologous to the break site. One method of HDR template design introduces a stop codon into all three reading frames (Gagnon *et al.*, 2014), thus overcoming the mosaicism effect if the knock-in is efficient. HDR can overcome some of the unpredictable NHEJ repairs by inserting a known sequence into the cleavage site. However, due to low HDR efficiency, Cas9-mediated HDR may be better suited for germline editing in zebrafish, in which one can enrich for the desired genetic lesion, unless higher template incorporation efficiencies can be achieved.

Perhaps the most straightforward way of using the CRISPR/Cas system is by microinjection of the Cas9 protein or mRNA encoding Cas9 under control of the β-globin promoter

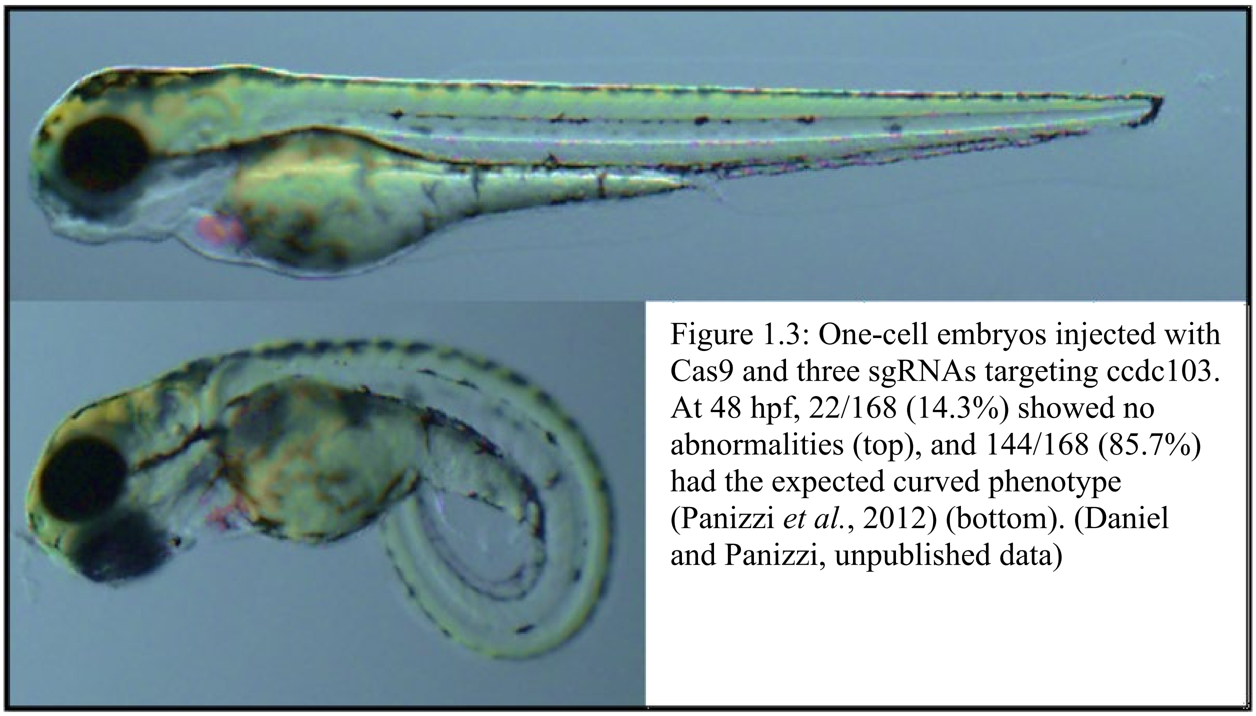

Figure 1.3: One-cell embryos injected with Cas9 and three sgRNAs targeting ccdc103. At 48 hpf, 22/168 (14.3%) showed no abnormalities (top), and 144/168 (85.7%) had the expected curved phenotype (Panizzi *et al.*, 2012) (bottom). (Daniel and Panizzi, unpublished data)

along with sgRNA(s) specific to the gene of interest. Several online resources exist for sgRNA design (Cui *et al.*, 2018), and multiple candidate sgRNA templates are typically generated to maximize the chance of knocking out a GOI. Figure 1.4 depicts WT embryos injected with three sgRNAs specific to *ccdc103* along with the Cas9 protein, producing the expected curled phenotype seen in *smh* mutants (Brand *et al.*, 1996; Panizzi *et al.*, 2012). To confirm target gene was edited, myc-ccdc103 mRNA rescue was successful (Figs. 1.3, 1.4). A successful mRNA rescue experiment is strong proof that the CRISPR-mediated lesion reproduces a disease phenotype (Stainier *et al.*, 2017). Even with high predicted efficiencies, an effective knockout usually requires multiple sgRNAs targeted to a single gene (Moreno-Mateos *et al.*, 2015; Vejnar *et al.*, 2016a).

CRISPR/Cas technology also provides an efficient method for creating a stable germline mutation, whereby a Cas9 mRNA construct under the control of the *nanos* 3' UTR is injected in order to restrict Cas9 expression to germ cells (Vejnar *et al.*, 2016b). Briefly, embryos are injected with an mRNA construct containing Cas9-*nanos*-3'UTR along with sgRNA(s) targeting the gene one wishes to propagate. Injected fish (F_0) are then grown to sexual maturity and outcrossed with a wild type line to generate heterozygous mutants (F_1). At this point, the mutant pool may contain one or several genetic lesions at the sgRNA sites. The GOI can be amplified and sequenced in several F_1 embryos to assess whether the germline edits were successful. Primers can be designed to amplify a region of genomic DNA with an ~100-200bp amplicon centered on the putative cleavage sites. After successful edits are confirmed, the F_1 embryos are grown to sexual maturity and genotyped to uncover the specific mutant allele that is present in the F_2 founder fish.

Recent CRISPR method refinement

The CRISPR/Cas9 system is undoubtedly a powerful tool for specific genetic modification, but more recent Cas enzyme developments address the drawbacks of using Cas9 enzyme-based

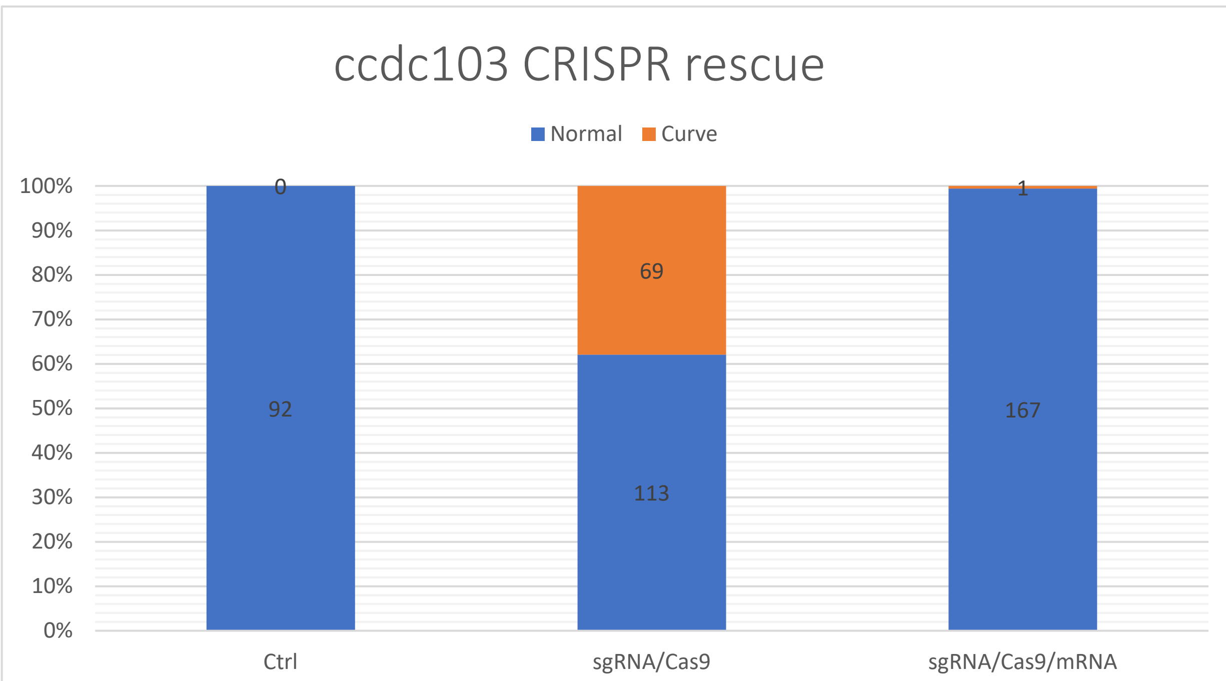

Figure 1.4: mRNA rescue of CRISPR-mediated genomic lesions. The group injected with the Cas9 enzyme and ccdc103-specific sgRNA displayed the expected curved phenotype, which was fully rescued with the mRNA rescue.

genetic modifications and have expanded the CRISPR toolbox (Table 1.2). Single-base editing can be achieved with a fusion of catalytically inactive Cas9 (dCas9) to either a cytidine deaminase (cytosine to thymine) or an adenine deaminase (adenine to inosine, treated as a guanine base). Cpf1/Cas12 is a smaller endonuclease with different PAM sequences and cutting sites. Whereas the Cas9 enzyme creates blunt ends, a Cpf1 DSB results in 4-5 nucleotide sticky ends. Sticky ends can potentially increase the efficiency of exogenous template insertion, such as a specific sequence with a disease-causing lesion, a stop cassette, or sequences encoding a fluorescent protein. Other Cas9-based methods exist for transcriptional control rather than base editing. A catalytically inactive Cas9 (dCas9) is injected along with a sgRNA designed to activate (CRISPRa) or inhibit (CRISPRi) GOI transcription (Gilbert *et al.*, 2013; Prykhozhij *et al.*, 2017; Qi *et al.*, 2013).

CILIOPATHY MODELING IN ZEBRAFISH

As mentioned above, a wide variety of genetic modalities can easily manipulate zebrafish developmental mechanisms, and many online genetic databases are available for use with CRISPR technology. Also, researchers can choose and order from the more than 40,000 potential mutant lines maintained by ZIRC, including alleles of many of the cilium-related genes. CRISPR technology may be used to generate germline mutants as described above if no mutant line exists for a gene of interest. CRISPR technology is inexpensive to implement. As such, one may also simultaneously attempt to knock out the GOI using the Cas9 enzyme to introduce indels through NHEJ or using a stop cassette introduced via the HDR pathway. For a full listing of ciliopathy models in zebrafish using CRISPR/Cas systems, see Table 1.1. Likewise, see Table 1.2 for a summary of CRISPR/Cas systems mentioned here, as well as design tools and references for protocols.

CRISPR models

The aforementioned targeted screening methods, which were only recently made available, are useful in clarifying the interplay between biological pathway components. Targeted gene editing with CRISPRs allows for permanent sequence-specific changes in nucleic acids. Interestingly, the *Shh* pathway has been screened in cell lines using CRISPR technology (Pusapati *et al.*, 2018), and one study used a CRISPR screen to uncover both novel ciliopathy genes and new roles for proteins involved in centriole stability (Breslow *et al.*, 2018). A recent zebrafish CRISPR screen for novel retinal protein functions used guide RNAs for 54 putative cilia-associated genes and uncovered three proteins required for normal retinal development (Hu *et al.*, 2019). The germline mutants used in the study overcame two scenarios common to direct editing of embryos: 1) the likelihood of mosaic somatic mutations that could be induced by Cas9 with a resultant WT phenotype and 2) the possibility that normal phenotypes still occur in offspring due to maternally contributed mRNA compensation.

Gene function can be directly knocked out by the CRISPR/Cas9 system in order to model disease processes during development. One study (Chassaing *et al.*, 2016) sequenced ocular developmental anomaly (ODAn) patients and identified *patched1* (*ptch1;* a 12-pass transmembrane receptor (Ingham *et al.*, 1991) as a causative gene in ODAn. Chassaing *et al*. injected one-cell stage zebrafish embryos with the cas9 protein along with a ptch1-targeted gRNA. Due to the random repair mechanism of NHEJ, genetic mosaicism was estimated to be between 10-65% within the group of crispants; however, 70% of the crispants displayed the expected microphthalmia, which is characteristic of ODAn. Other groups have modeled ciliopathies in zebrafish (Table 1.1) with the cas9/sgRNA system targeted to *dnah10/rnf115* (Liu *et al.*, 2018), *ncapg* (Khan *et al.*, 2019), *elmo1* (Sharma *et al.*, 2016), and *ahi1* (Zhu *et al.*, 2019).

CRISPR modality	**Mechanism summary**	**Target design**	**Zebrafish protocol reference**
Cas3	Creates up to 100kb deletions, starting at the sgRNA recognition site.	None. See refs (Cooper *et al.*, 2018; Leenay *et al.*, 2016; Morisaka *et al.*, 2019).	None. See refs (Csörgő *et al.*, 2019; Hochstrasser *et al.*, 2014).
Cas9	Creates blunt-end DSB four nucleotides upstream of the PAM site. NHEJ or HDR repair then occurs.	CRISPRScan, CHOPCHOP, ccTop, Cas-Designer	(Vejnar *et al.*, 2016b)
CRISPRa/CRISPRi	Catalytically active dCas9 binds to transcriptional regulation sites for activation or repression.	CRISPR-ERA, CHOPCHOP	(Long *et al.*, 2015)
Cas12a/Cpf1	Adenosine deaminase changes A>G, cytidine deaminase changes C>T.	CRISPRScan, CHOPCHOP, ccTop, Cas-Designer	(Liu *et al.*, 2019; Wierson *et al.*, 2019)
Cas13	RNA cleavage. Can be used for RNA single base editing(Katrekar *et al.*, 2019), transcript imaging(Abudayyeh *et al.*, 2017), or knockdown(Cox *et al.*, 2017).	CHOPCHOP	None. See refs under Cas13 `mechanism summary.

Table 1.2: Summary of CRISPR methods and accompanying protocol references. Others can be found at https://zlab.bio/guide-design-resources (Accessed 1/4/2020).

The previous ptch1 study (Chassaing *et al.*, 2016) did not target a specific cell or tissue, but the Cas9/sgRNA system can also be used for cell-specific disruption using regulation elements that are only active in specific tissues. Targeted knockout of ptch1 in T-cells was obtained by a T-cell-specific (*rag2*) promoter expression cassette (Cas9-T2A-GFP under *rag2* control) rather than an injected Cas9 protein (Burns *et al.*, 2018). The authors found that indels in *ptch1* led to the onset of T-cell acute lymphoblastic leukemia. This approach is advantageous when embryo-wide knockouts are be developmentally lethal, allowing for tissue-specific loss-of-function studies (Ablain *et al.*, 2015; Ablain and Zon, 2016).

Ciliopathy-associated mutation correction with CRISPR/Cas

Mutant phenotype correction is the next step in the application of CRISPR technology. Some of the symptoms of ciliopathies are relatively benign (i.e., extra digits—polydactyly), but a majority of symptoms cause detrimental morbidities. Treatments can ameliorate symptoms caused by genetic lesions, but the underlying cause is never corrected. For example, treatment for polycystic kidney disease is more about managing kidney function, high blood pressure, pain, and infection. Cases of retinitis pigmentosa may be treated with low vision aids or daily vitamin A to slow the progression. Notably, a group recently showed that eupatilin, a drug developed in Korea for the treatment of gastritis and peptic ulcers (Choi *et al.*, 2017; Ryoo *et al.*, 2014; Seol *et al.*, 2004), could rescue primary ciliogenesis in a CEP290$^{-/-}$ RPE1 (retinal pigmented epithelium) human cell line by blocking calmodulin binding to NHPH5 (Kim *et al.*, 2018), but no drugs have thus far been FDA-approved for the treatment of ciliopathies.

Several potentially applicable approaches for gene therapy are undergoing preliminary testing in various eukaryotic models (Kim and Kim, 2019), including CRISPR/Cas9 correction of retinitis pigmentosa GTPase regulator (RPGR) in human-derived retinal organoids (Deng *et al.*,

2018) and in a mouse model (Ruan *et al.*, 2017) via subretinal injection of AAV-sgRNA/Cas9. The previous study corrected three patient-derived RPGR mutations in organoids created from iPSC (induced pluripotent stem cells). To our knowledge, stable *in vivo* corrections of ciliopathy protein defects in zebrafish have not been published; however, spCas9-expressing adult zebrafish retinas were injected with a sgRNA directed to achaete-scute family bHLH transcription factor a (*ascl1a*) and electroporated to move the sgRNA into retinal cells (Yin *et al.*, 2015), showing that adult *in vivo* gene editing via the CRISPR/Cas9 system is possible.

CILIOPATHY PROGRESS AND FUTURE CHALLENGES

Cilia play diverse roles in the development and physiology of vertebrates. Defects in both classes of cilia contribute to a wide range of ciliopathies, and researchers are finding additional ciliopathy-related genes every year. Forward and reverse genetic methods have significantly contributed to our understanding of ciliopathies, with CRISPRs adding an invaluable tool to our methods repertoire. As such, ciliopathy modeling in vertebrate organisms can be performed with CRISPR screening methods as well as targeted methods described above. In the last four decades, the zebrafish has quickly become a popular model system and is well-adapted for modeling genetic perturbations during development (e.g., morphogenetic movements, patterning, morphogenesis) and adult physiology (e.g., ependymal flow). Adult zebrafish are also useful for determining how genetic defects can affect the physiology of cilia. The goal of modeling genetic disease in nonmammalian vertebrates is to translate that knowledge into human therapies. Current gene therapy modalities either require modified virions to deliver functional genes to the nucleus or removal of a specific cell type to be modified and returned to the patient. The CRISPR/Cas systems mentioned above offer a wide variety of methods toward knocking down or knocking out genes and gene products. Precision medicine is an essential goal of CRISPR/Cas development, but several roadblocks are in place before they make it to the bedside. Cas9 engineering has increased the specificity and efficiency of the enzyme, but off-target effects can persist and could cause new pathologies even if the existing genetic lesion was repaired. Consistent delivery of Cas9/sgRNAs to specific adult tissues, particularly the CNS, remains challenging. As targeted genetic approaches are continually refined in their ability to make more specific edits, modeling ciliopathies and other genetic diseases in vertebrate organisms will significantly benefit from the CRISPR systems.

Chapter 2

Coiled-coil domain containing protein 103 (ccdc103) interactome analysis using a yeast two-hybrid method

Abstract

Proper motile cilia function is required for an array of physiological processes, including correct organ laterality, sperm motility, and mucus clearance. Errors in motile cilia structural organization or functional pathways can lead to primary ciliary dyskinesia (PCD), a genetic disease characterized by immotile cilia. Axonemal dyneins are a group of motor proteins that is required for ciliary movement. Coiled-coil domain containing protein 103 (Ccdc103) is a homodimeric dynein attachment factor that is closely associated with cilium motility, as it is required for proper dynein arm assembly. Although recent studies have begun to uncover the molecular role of Ccdc103 in dynein attachment, little is known about the proteins involved in dynein assembly through Ccdc103, or the pathways involved in regulating dynein attachment. In this study, we uncovered 14 putative Ccdc103 interactors through a yeast two-hybrid screen. Further results showed that 13 of the interactors have human orthologs, and nine of those 13 have shared synteny between humans, mice, and zebrafish. Our results reveal 14 proteins that could interact with Ccdc103 in the proper cellular context and thus play a role in motile ciliogenesis.

1. Introduction

The motile cilium is a whiplike, highly conserved organelle that is present in a diverse range of organisms (e.g., *Chlamydomonas*, *Paramecium*, zebrafish, and humans). A circular array of nine microtubule doublets, along with a central pair of microtubule singlets, constitute the cytoskeletal scaffolding of cilia (Afzelius, 1961; Afzelius *et al.*, 1975). The “9+2” makeup is found in a majority of motile cilia, with the exception of 9+0 motile cilia lining the transient, spherical Kupffer’s vesicle (KV; analogous to the mouse node) during zebrafish embryonic development (Essner *et al.*, 2005). Organisms can also create 3+0 and 6+0 cilia arrangements (Gibbons, 1981; Goldstein *et al.*, 1979; Prensier *et al.*, 1980), illustrating the wide diversity of motile cilium structure and thus a variety of assembly and maintenance mechanisms.

The process of cilium formation (ciliogenesis) in vertebrate cells begins during the G_1 phase of the cell cycle, resulting in a fully-formed cilium that persists throughout the G_0 phase (Kalnins and Porter, 1969; Sorokin, 1968; Steinman, 1968). Notably, mother centrioles duplicate during S phase and cilia are resorbed prior to mitosis. Increased levels of centrosomal proteins (CEP) at the mother centriole induce ciliogenesis (Kalnins and Porter, 1969; Sorokin, 1968; Steinman, 1968). Increased levels of centrosomal proteins (CEP) at the mother centriole, which constitutes part of the centrosome along with a daughter centriole, induce ciliogenesis. The deuterosome is a recently discovered organelle responsible for anchoring duplicated centrioles prior to migration to the cell membrane (Shahid and Singh, 2018). Vesicles associated with the small GTPase Rab8 are recruited to the mother centriole (older centriole) and begin to form the ciliary vesicle (CV) around the distal end (Kim *et al.*, 2008). The CV elongates as more vesicles are recruited, and microtubules extend from the distal end of the mother centriole into the vesicular compartment (Dawe *et al.*, 2007). The mother centriole constitutes the basal body (BB) and serves as the foundation of the fully formed cilium. Actin mediates mother centriole attachment to the cell cortex (Lemullois *et al.*, 1988). Multiciliated cells (MCC) form hundreds of motile cilia, so centrioles are rapidly duplicated in G_0 cells to meet the cellular demand for cilia nucleation by basal bodies.

Axonemal assembly is a highly orchestrated process involving microtubule elongation and stabilization, receptor localization, and multi-subunit inner- and outer dynein arm (IDA/ODA) attachment to the microtubule doublets (Cole *et al.*, 1998). After the cilium foundation is established at the cell membrane, ciliary elongation continues via intraflagellar transport (IFT) mechanisms (Cole *et al.*, 1998). New tubulin is added to the tip until the cilium reaches its proper length, which varies between different cell types (Stephens, 1999). Evidence suggests that the cilium is loaded with a finite number of IFT complexes, and the rate of axonemal assembly balances with the rate of disassembly (Avasthi and Marshall, 2012). Axonemal dynein heavy chain (HC) motor domains resemble AAA proteins (ATPase Associated with diverse cellular activities) in their doughnut-shaped structure. The HC has a "stalk" that tightly binds to the microtubule and a "stem", which performs the walking action on the neighboring microtubule (Roberts *et al.*, 2009). Axonemal dyneins are also made up of intermediate chains (IC) and light chains (LC) (Horvath *et al.*, 2005; Lo *et al.*, 2006; Loges *et al.*, 2008). LCs have been shown to play a role in beat regulation by decreasing the microtubule binding affinity of dynein, whereas IC may play a role in mediating motor unit attachment to microtubules. The plasma membrane enwraps the axoneme and thus the ciliary compartment has a different protein composition (the ciliome) than other parts of the cell. The axoneme spiral repeats every 96 nm, with four outer dynein arms constituting each repeat in zebrafish (Ishikawa, 2015, 2017). Cilia beating in 9+2 cilia occurs in a plane parallel to an imaginary line running between the central pair. Basal bodies provide proper alignment of motile cilia (Boisvieux-Ulrich *et al.*, 1985) in response to feedback between planar cell polarity (PCP) and flow sensing, such that all cilia beat in the same direction on multiciliated cells or within an enclosed space (i.e., tubular lumen or KV).

Motile cilia in the airways, oviducts, and central nervous system (CNS) create flow via an oar-like motion, with a rolling recovery stroke back to the start position (Satir, 1963; Satir, 1965). Multiciliated cells lining vertebrate brain ventricles generate unidirectional flow to eliminate mucus and particles from airways, transport ova through oviducts, and move CSF through ventricles. The 9+0 cilia in KV move in a corkscrew manner and create a counterclockwise directional fluid flow (Essner *et al.*, 2002). Flow within KV leads to asymmetric distribution of laterality signaling components (e.g., Nodal, Lefty, Pitx2), which leads to proper organ orientation (Karcher *et al.*, 2005; Nonaka *et al.*, 1998; Yamauchi *et al.*, 2009). Reversed organ laterality (situs inversus) results from reversed KV ciliary motion and paralyzed (immotile) KV cilia lead to randomized organ laterality.

Dysfunction in motile cilia leads to primary ciliary dyskinesia (PCD), an autosomal recessive genetic disease that affects about 1:15000 live births, or around 500,000 people worldwide (Goutaki *et al.*, 2019; Shapiro *et al.*, 2018). Around 90% of PCD patients have defects in IDAs or ODAs, and, of those, roughly 40% of those have deleterious mutations in two outer dynein arm genes, DNAI1 and DNAH5. IDA dysfunction alters the typical cilium waveform, whereas ODA dysfunction leads to a reduction in beat frequency. PCD symptoms include laterality defects (situs inversus or situs ambiguus), kidney cysts, infertility, chronic ear inflammation (otitis media), thickened bronchi (bronchiectasis), and chronic sinusitis (Zariwala *et al.*, 1993). Around 50% of PCD patients have situs inversus, due to the randomized laterality caused by immotile cilia in the embryonic node. Diagnosis is difficult with our current knowledge, although low exhaled nitric oxide (NO) has been associated with PCD (Shapiro *et al.*, 2018). Testing for NO levels has a low rate of false negatives and false positives but should still be used in conjunction with other tests. Likewise, x-rays to assess organ laterality can contribute to a PCD diagnosis, with the caveat that not all PCD patients display situs defects. Biopsies of ciliated tissues with subsequent ultrastructural analysis with electron microscopy is the current gold standard; however, sample preparation, shipping, and analysis are laborious (Shapiro *et al.*, 2018). Genetic testing is a strong diagnostic tool toward diagnosing PCD. As the known gene complement of PCD increases, the diagnostic strength of genetic testing increases. In fact, with current knowledge, a PCD genetic panel is diagnostic in at least 70% of cases (Shapiro *et al.*, 2018), although variants of unknown pathogenic significance can confound diagnosis (Horani and Ferkol, 2018). Improved knowledge of motility-associated genes and their role in cilia function will increase our ability to accurately diagnose PCD.

The coiled-coil domain containing 103 (Ccdc103) protein in zebrafish is a 247-residue protein encoded by the *ccdc103* gene and is expressed from a 2291 bp transcript (Panizzi *et al.*, 2012). Zebrafish embryos with the *schmalhan*s (*smh*) mutation (Brand *et al.*, 1996) display pronephric cysts and reversed organ orientation (situs inversus), due to missing dynein arms in otherwise normal motile cilia. Nonsense mutations in CCDC103 from a consanguineous Pakistani family were linked to bronchiectasis, situs defects, and cystic kidneys, all of which are classic symptoms of defective motile cilia. Ccdc103 is an outer dynein attachment factor and has been shown to associate with microtubules in vitro and to copurify with dynein (Panizzi *et al.*, 2012). Further studies suggest that Ccdc103 periodically binds to microtubules every 24 nm and may act as an adapter protein to the dynein docking complex (King and Patel-King, 2015), however, very little is known about any additional molecular processes through which ccdc103 acts in ciliated cells. Here, we sought to uncover Ccdc103 interactors through the yeast-two-hybrid system and to initially characterize the genetics of putative Ccdc103 interactors.

2. Results and discussion

The first round of Y2H screening with mouse Ccdc103 bait and the mouse cDNA prey library (Clontech, Cat. #630489) yielded 43 individual blue colonies on the QDO-X-A plates, which were then patched onto QDO/X/A (**Fig. 2.2, Table 2.1**). Colony PCR was performed, and sequences were submitted to NCBI-BLASTn, which revealed 30 positive genetic matches (**Table 2.2**), with duplicate or triplicate colony plasmid sequences for nine genes (**Table 2.2**). The HomoloGene function of NCBI was used to identify the zebrafish orthologs of the interactor genes. After second-round interactor screening via yeast cotransformation with bait and candidate prey proteins, 13 sequences were eliminated as false positives (**Table 2.3**). We were unsuccessful in subcloning two interactor genes into plasmid vectors: histone-lysine N-methyltransferase 2E (kmt2e) and structural maintenance of chromosomes protein 6 (smc6). The remaining 10 sequences, along with two paralogs (*ankef1b*, *dnajb1b*), were successfully subcloned into pCS2 destination vectors (untagged and FLAG-tagged) vectors and confirmed by Sanger sequencing. Orthologous human proteins were found for thirteen of the fourteen genuine positives. Publicly available RNA-seq expression data showed that five proteins were most highly expressed in the human testis, which is an organ rich in motile cilia as well as abundant ciliogenesis (Horowitz *et al.*, 2005; Kiselak *et al.*, 2010; Zhang *et al.*, 2017). Four of the putative Ccdc103 interactors have paralogs identified in zebrafish (**Table 2.4**), likely due to genome duplication.

RNA-seq data on four genes (*fem1c*, *etfa*, *polk*, *kmt2e*) showed widespread expression in humans and mice (Fagerberg *et al.*, 2014), and have not been specifically linked to cilia structure or function. Likewise, dnajb1a is a well-studied heat shock protein family member that mediates proper protein folding. MO knockdown of *dnajb1a* and *dnajb1b* in zebrafish produced ocular abnormalities (Khan *et al.*, 2016), consistent with the finding that Dnajb1 is a part of photoreceptor proteome (Liu *et al.*, 2007). Likewise, i*mpact*, a translational regulator during cellular stress, was

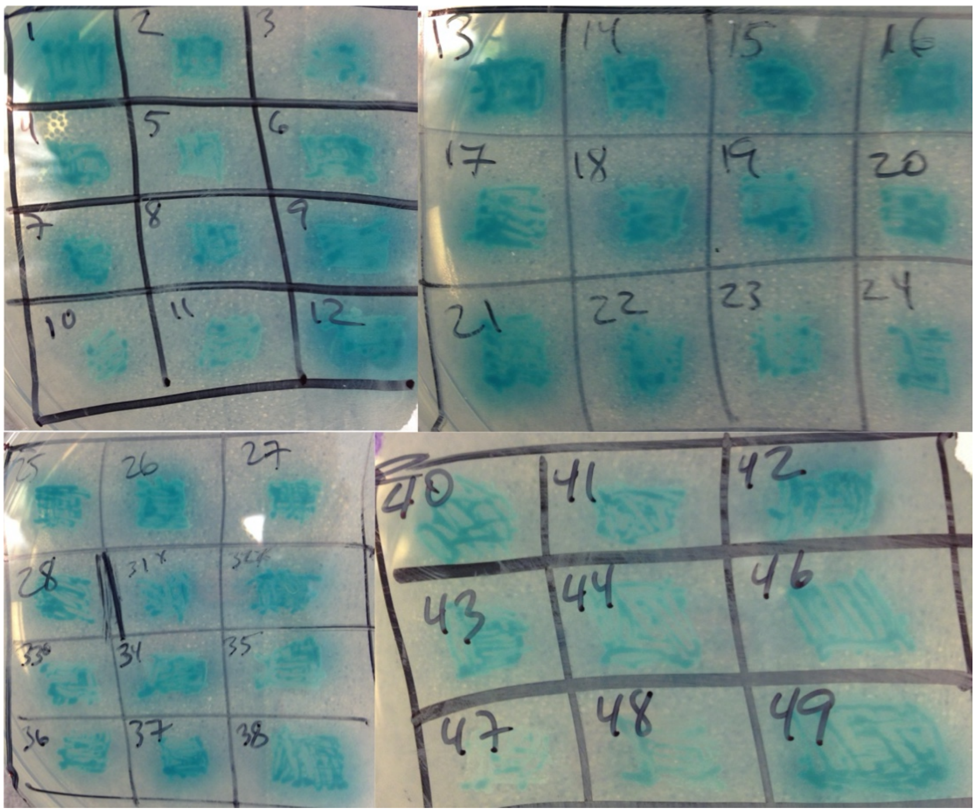

Figure 2.2: QDO/X/A plates after first round of screening. Prey plasmids were rescued from each patch and cotransformed as described in methods. Table 2.1 displays the results of the second round of screening.

First round #	***Empty pGBKT7 + candidate prey***	***Bait + candidate prey***	***Genuine positive?***
1	No colonies.	Blue colonies.	Y
2	No colonies.	Blue colonies.	Y
3	No colonies.	Blue colonies.	Y
4	Blue colonies.	Blue colonies.	N
5	Blue colonies.	Blue colonies.	N
7	No colonies.	Blue colonies.	Y
11	No colonies.	Blue colonies.	Y
13	Blue colonies.	Blue colonies.	N
14	Blue colonies.	Blue colonies.	N
17	Blue colonies.	Blue colonies.	N
18	No colonies.	Blue colonies.	Y
19	Indeterminate.	Blue colonies.	N
20	No colonies.	Blue colonies.	Y
22	No colonies.	Blue colonies.	Y
23	No colonies.	Blue colonies.	Y
24	Indeterminate.	Indeterminate.	N
25	Blue colonies.	Blue colonies.	N
27	No colonies.	Blue colonies.	Y
28	Blue colonies.	Blue colonies.	N
32	Blue colonies.	Blue colonies.	N
35	Blue colonies.	Blue colonies.	N
36	Blue colonies.	No colonies.	N
37	Blue colonies.	No colonies.	N
38	No colonies.	Blue colonies.	Y
41	Blue colonies.	Blue colonies.	N
42	No colonies.	Blue colonies.	Y
43	No colonies.	Blue colonies.	Y
44	Blue colonies.	Blue colonies.	N
46	Blue colonies.	Blue colonies.	N
49	No colonies.	Blue colonies.	Y

Table 2.1: Results of cotransformation of prey plasmid with either empty pGBKT7 vector or bait + pGBKT7.

#	Zebrafish ortholog name	Symbol	Accession	# of first-round hits
1	structural maintenance of chromosomes protein 6	*smc6*	NP_001121806.1	2
2	inhibitor of growth protein 3	*ing3*	NP_957231.1	3
3	isoaspartyl peptidase/L-asparaginase	*asrgl1*	NP_001013547.1	2
4	ankyrin repeat and EF-hand domain-containing protein 1a	*ankef1a*	NP_001020714.1	3
5	growth hormone receptor precursor	*ghra*	NP_001077047.1	2
6	protein fem-1 homolog C	*fem1c*	NP_937788.2	1
7	histone-lysine N-methyltransferase 2E isoform X2	*kmt2e*	XP_692965.5	1
8	electron transfer flavoprotein subunit α, mitochondrial	*etfa*	NP_944591.1	2
9	DNA polymerase kappa	*polk*	XP_691219.4	1
10	protein Imprinted and ancient	*impact*	NP_001005595.1	1
11	adenylate kinase 2, mitochondrial	*ak2*	NP_997761.1	1
12	V-type proton ATPase subunit D	*atp6v1d*	NP_001161426.1	1
13	DnaJ heat shock protein family (Hsp40) member B1a	*dnajb1a*	NP_001003571.1	1
14	si:dkey-76p14.2 (C20ORF96 homolog)	*c20orf96*	XP_691039.2	1

Table 2.2: List of genuine positives revealed by the first and second rounds of screening. Genes 1-14 were genuine positives, while genes 15-27 were eliminated as false positives after cotransformation with bait (ccdc103) and prey plasmids containing the above 14 prey genes. The genes selected for further study are highlighted in yellow.

#	Zebrafish ortholog name	Symbol	Accession	# of first-round hits
15	AP-3 complex subunit delta-1	*ap3d1*	NP_001038480.1	3
16	COMM domain-containing protein 4	*commd4*	NP_001307104.1	3
17	SH3GL interacting endocytic adaptor 1a	*sgip1*	XP_005165952.1	1
18	argininosuccinate synthase	*ass1*	NP_001004603.1	1
19	retinal rod rhodopsin-sensitive cGMP 3',5'-cyclic phosphodiesterase subunit delta	*pde6d*	NP_001002708.1	1
20	dolichyl-diphosphooligosaccharide--protein glycosyltransferase subunit 2 precursor	*rpn2*	NP_997913.1	1
21	polycomb complex protein BMI-1-B	*bmi1*	NP_001074220.1	1
22	citrate synthase, mitochondrial precursor	*cs*	NP_955892.1	1
23	dnaJ homolog subfamily B member 4	*dnajb4*	NP_001003455.1	1
24	40S ribosomal protein S20	*rps20*	NP_998369.1	2
25	mothers against decapentaplegic homolog 2	*smad2*	NP_571441.3	1
26	BRO1 domain-containing protein BROX	*brox*	NP_001007428.2	1
27	SGT1 homolog, MIS12 kinetochore complex assembly cochaperone	*sugt1*	NP_001007362.1	1

Table 2.3: List of false- positives revealed by the first and second rounds of screening. Genes 15-27 were eliminated as false positives after cotransformation with bait (ccdc103) and prey plasmids containing the above 13 prey genes.

Zebrafish gene (chromosome #)	**Human ortholog (chr.)**	**Zebrafish paralogs (chr.)**	**Shared synteny**
smc6 (17)	Y (2)	si:dkey-119f1.1 (2)	X.
ing3 (4)	Y (7)	None.	H, M, X.
asrgl1	Y (11)	None.	None.
ankef1a	Y (20)	*ankef1b* (17)	H, M, X.
ghra	N	*ghrb* (21)	None.
fem1c	Y (5)	None.	H, M, X.
kmt2e	Y(7)	None.	H, M, X.
etfa	Y (15)	None.	H, M, X.
Polk (5)	Y (5)	None.	H, M.
Impact (22)	Y (18)	None.	X.
ak2 (19)	Y (1)	None.	H, M, X
atp6v1d (20)	Y (14)	None.	H, M, X.
dnajb1a (3)	Y (19)	*dnajb1b* (1)	H, M, X.
C20ORF96 (11)	Y (20)	None.	H, M, X.

Table 2.4: Comparative genetics of putative ccdc103 interactors. Shared synteny was determined using the Region Comparison feature of Ensembl. H, human; M, mouse; X, *Xenopus*. Shared synteny was considered to be present if at least one gene is adjacent to our gene of interest on the same chromosome in both species. Organ expression data was adapted from NCBI, using the HomoloGene function from each Y2H genuine positive.

indeed shown to be upregulated in PCD patients (Geremek *et al.*, 2011). Upregulation in PCD is likely secondary to disease and to our knowledge no lines of evidence have shown a role for *impact* in cilia structure or function. *Ing3* was associated with ciliogenesis in mammals (Ross *et al.*, 2007); however, its expression has not been shown in classical ciliated tissue. Furthermore, *ing3* interacts with *p53* to inhibit cell growth and promote apoptosis (Kataoka *et al.*, 2003), so it is unlikely to play a functional role in motile ciliogenesis. *Smc6* is expressed in the testis (Fagerberg *et al.*, 2014) but evidence suggests it is more likely associated with its functional roles in meiosis and chromosomal maturation (Aragon, 2018; Diaz *et al.*, 2019) than with motile cilium assembly, given no studies have yet associated *smc6* with cilia-related processes. Ak2 catalyzes the interconversions of adenosine phosphates in the mitochondria and a knockdown phenotype in zebrafish revealed neutrophil dysgenesis. Interestingly, other AK isoforms have been associated with PCD (Dzeja and Terzic, 2009), but ak2 has not yet been connected to motile cilia physiology or pathology.

Two enzymes were associated with ciliogenesis and would be excellent candidates for further study, Asrgl1 and Atp6v1d. *Asrgl1* was a strong candidate due to its expression in testis and connection to ciliogenesis (Chekuri *et al.*, 2018). L-asparaginases are enzymes that hydrolyze L-asparagine to L-aspartic acid and ammonia. Biochemical data suggests that asrgl1 plays a role in repairing isoaspartyl-damaged proteins, which is a common type of nonenzymatic protein damage (Huvila *et al.*, 2018; Lv *et al.*, 2018). The isoaspartyl residue introduces a sharp turn into the protein, thus disrupting protein folding. *Asrgl1* expression was first shown in the mouse and human sperm midpiece (Bush *et al.*, 2002), with high expression later shown in the human endometrium (Biswas *et al.*, 2016). One form of autosomal recessive retinal degeneration was linked with nonfunctional asrgl1 in humans (Biswas *et al.*, 2016), with a later study showing that *asrgl1* knockdown leads to growth inhibition and apoptosis in a human cervical cancer cell line (Lv *et al.*, 2018). Despite these ciliary links, further study on Asrgl1 was not pursued. *Asrgl1* expression is not spatially restricted throughout zebrafish development (Thisse *et al.*, 2004), nor does it share synteny with frogs, mice, or humans (**Table 2.4**). Given the role of Asrgl1 in protein repair, it may play a role in protein damage control during tracheal MCC ciliogenesis, but no current evidence has provided a direct link with motile cilium structure or function. The putative Ccdc103 interactor Atp6v1d is the subunit of an autophagy-related enzyme (vacuolar-type H^+/ATPase; V-ATPase) that was connected to ciliogenesis by a large-scale screen of photoreceptor proteins (Liu *et al.*, 2007). The V-ATPase acidifies endosomes and regulates ciliogenesis by allowing Rab8a to fuse with the ciliary membrane (Chen *et al.*, 2012). Despite the connection to ciliogenesis, V-ATPases are likely part of downstream regulation of ciliogenesis, as the processes of autophagy and ciliogenesis have significant crosstalk (Pampliega *et al.*, 2013; Tang *et al.*, 2013). We sought to provide initial characterization of putative Ccdc103 interactors, and thus selected two of the genuine positive interactors for further analysis on the basis of high testis expression in both humans and mice, and evidence associating these genes with cilia-related processes (**Table 2.6**). These genes are ankyrin and EF-hand containing protein 1a (*ankef1a*) and si:dkey-76p14.2 (*c20orf96*).

Ankef1a is a 779-residue protein with an alternating ankyrin—EF-hand—ankyrin structure that was shown by RNA-seq (Fagerberg *et al.*, 2014) to be enriched in the testis in mice and humans (**Table 2.5**). Zebrafish express two ankef1 paralogs, *ankef1a* and *ankef1b*, which share overlapping expression patterns in the developing embryo (Daniel and Panizzi, 2019). Quantitative RT-PCR showed enriched expression in the adult zebrafish testis, suggesting functional conservation between humans and fish. Furthermore, *ankef1a* and *ankef1b* expression was shown

Symbol (Zfish paralog)	**Gene name**	**Major expression sites (Human)**	**Major expression sites (Mouse)**	**CilDb association (human/mouse)**
smc6 (si:dkey-119f1.1)	structural maintenance of chromosomes protein 6	Testis, lymph node	Testis, lymph node	None.
ing3	inhibitor of growth protein 3	Bone marrow	Placenta	Expression during ciliogenesis.
asrgl1	isoaspartyl peptidase/L-asparaginase	Testis, endometrium, brain, kidney	Testis	Expression during ciliogenesis.
ankef1a (ankef1b)	ankyrin repeat and EF-hand domain-containing protein 1a	Testis, thyroid	Testis	Expression in tracheal multiciliated cells.
ghra (ghrb)	growth hormone receptor precursor	Fat, liver	Subcutaneous fat pad adult	None.
fem1c	protein fem-1 homolog C	Bone marrow	Testis	None.
kmt2e	histone-lysine N-methyltransferase 2E isoform X2	Widespread	Widespread	None.
etfa	electron transfer flavoprotein subunit α, mitochondrial	Widespread	Widespread	None.
polk	DNA polymerase kappa	Widespread	Widespread	None.
impact	protein IMPACT	Testis, thyroid	Brain, placenta	Expression in PCD patients.
ak2	adenylate kinase 2, mitochondrial	Kidney	Widespread	Sperm flagellar axonemes proteome.
atp6v1d	V-type proton ATPase subunit D	Widespread	Brain, placenta	Cilium proteome.
dnajb1a (dnajb1b)	DnaJ heat shock protein family (Hsp40) member B1a	Adrenal, esophagus, gall bladder, testis	Testis	Cilium proteome.
si:dkey-76p14.2	C20ORF96 homolog	Testis, endometrium, lung, thyroid, ovary	Testis	Expression in PCD patients. Expression in tracheal MCCs. Expression in ciliated tissues.

Table 2.5: Expression data summary from genuine positives from NCBI and CilDb.

Gene name	**Primer sequence**
ak2 F	GGGGACAAGTTTGTACAAAAAAGCAGGCTCCATGGCCCCTAGCACACA
ak2 R	GGGGACCACTTTGTACAAGAAAGCTGGGTTTATTTAGACAAAATAAACGAGATCTTT
ankef1a F	GGGGACAAGTTTGTACAAAAAAGCAGGCTTCAGGTTCAAAATGTCCTGCAAACA
ankef1a R	GGGGACCACTTTGTACAAGAAAGCTGGGTTACCTGTTAGTCAGTGAGCT
ankef1b F	TGCGTGCTGATAGTTGACGA
ankef1b R	GAAGCTGGCATTGAAGCAGG
atp6v1d F	GGGGACAAGTTTGTACAAAAAAGCAGGCTCAAGAAGAAAGATGTCGGGAA
atp6v1d R	GGGGACCACTTTGTACAAGAAAGCTGGGTATCTCTCAGCGCCCGTAG
C20ORF96 F	GGGGACAAGTTTGTACAAAAAAGCAGGCTACATCATAATGATTGGTCGAGA
C20ORF96 R	GGGGACCACTTTGTACAAGAAAGCTGGGTGCAAAGGGCTACACGGGG
dnajb1a F	GGGGACAAGTTTGTACAAAAAAGCAGGCTCGAGTGTTGTGATGGGAAAAGA
dnajb1a R	GGGGACCACTTTGTACAAGAAAGCTGGGTTTCGTAGCGATCAAGGTGGC
dnajb1b F	GGGGACAAGTTTGTACAAAAAAGCAGGCTGCCTAATGGTGAAGATGGGGA
dnajb1b R	GGGGACCACTTTGTACAAGAAAGCTGGGTAGTACATGCAGCTCAAGAAG
etfa F	GGGGACAAGTTTGTACAAAAAAGCAGGCTGGACTGCTGTAATCATGCTCA
etfa R	GGGGACCACTTTGTACAAGAAAGCTGGGTGGCAAGTAAAGTCTTAGTAAAGT
fem1c F	GGGGACAAGTTTGTACAAAAAAGCAGGCTCACCCTATGCCATGGATCTGA
fem1c R	GGGGACCACTTTGTACAAGAAAGCTGGGTACACACGCAGCTCACACTAT
ghr F	GGGGACAAGTTTGTACAAAAAAGCAGGCTCAGAAGCCATGGCCCACTC
ghr R	GGGGACCACTTTGTACAAGAAAGCTGGGTGATGCTTATCTGGGTTGCGC
impact F	GGGGACAAGTTTGTACAAAAAAGCAGGCTTCATGGACAAATTAGAGGATCATG
impact R	GGGGACCACTTTGTACAAGAAAGCTGGGTAGTCCAAGTAGACTTTTACTTTG

ing3 F	<u>GGGGACAAGTTTGTACAAAAAAGC</u>AGGCTTCTCCGCCAGAATGTTGTACCT
ing3 R	<u>GGGGACCACTTTGTACAAGAAAGC</u>TGGGTGTGATCTGGCTTTCATTTGTGC
kmt2e F	<u>GGGGACAAGTTTGTACAAAAAAGC</u>AGGCTTCGCACAGAACGTCATGAGCAT
kmt2e R	<u>GGGGACCACTTTGTACAAGAAAGC</u>TGGGTGGGTTTTGGTGGGTGTGG
polk F	<u>GGGGACAAGTTTGTACAAAAAAGC</u>AGGCTCGCTGGATGAAATGAGGCAGC
polk R	<u>GGGGACCACTTTGTACAAGAAAGC</u>TGGGTTGGTCTGTGTGGATTTGTAGCA
smc6 F	<u>GGGGACAAGTTTGTACAAAAAAGC</u>AGGCTCAGAGTTGGAGATGTCGAAG
smc6 R	<u>GGGGACCACTTTGTACAAGAAAGC</u>TGGGTGGTCAGAAACATCACTCTGGG
C20ORF96 qPCR F	TGTACTCCAGATATGGACGT
C20ORF96 qPCR R	TAGTGGCTCCATTGATTTCC

Table 2.6: List of primers used in Y2H gene cloning and qPCR. Underlined sequences denote Gateway-specific primer regions. F, forward; R, reverse.

in the otic vesicle, a structure analogous to the human inner ear. Both structures are lined with motile cilia, thus strengthening the link between ankef1 and motile cilia. *Ankef1* has had only one functional study performed in frogs (Chung *et al.*, 2007), which showed a role for Ankef1 in cell adhesion and protrusion. Cultured murine tracheal MCCs showed ankef1 localization to cilia (Hoh *et al.*, 2012). *Ankef1* has also been indirectly associated with human pathology through screens of up- or down-regulated transcripts (Jin *et al.*, 2016; Nguyen *et al.*, 2017). A decreased ankef1 transcript level was linked with an increased risk of prostate cancer recurrence (Jin *et al.*, 2016). Interestingly, increased polyunsaturated fatty acid intake during murine pregnancy was also associated with significantly lower ankef1 expression in offspring and thus a higher cancer risk (Nguyen *et al.*, 2017). Due to the gap in functional knowledge, ankef1 is a good candidate for future studies seeking to further clarify its role in both embryonic development and adult physiology, although studies in zebrafish would need to account for functional redundancy with the *ankef1b* paralog.

The zebrafish C20ORF96 (also si:dkey-76p14.2) protein was shown to be a novel cilium-related (McClintock *et al.*, 2008; Vandenbrouck *et al.*, 2016) molecule (**Table 2.5**) and was predicted to be expressed in zebrafish (NCBI: XM_685947.7). Although the gene has been associated with several screens, including genome-wide methylation patterns (Hasso-Agopsowicz *et al.*, 2018), canine mast cell tumor transcriptome changes (Pulz *et al.*, 2019), chemotherapy-induced alterations in neuroblastomas (Duan *et al.*, 2018), and zebrafish transcriptome dynamics in lysine imbalance (Gomez-Requeni *et al.*, 2011), the developmental expression profile and protein function are still unknown. A human ortholog (C20ORF96) to the predicted zebrafish protein exists, along with shared synteny between the human, mouse, and zebrafish genes (**Table 2.4**). Although human organ RNA-seq data shows that C20ORF96 is most highly expressed in the testis (Fagerberg *et al.*, 2014), to our knowledge no developmental expression data exists for the gene. Our qPCR assay revealed a maternal C20ORF96 mRNA contribution (**Fig. 2.3**), with minimal expression levels until a rise beginning sometime around 4 days post-fertilization (dpf) and continuing into day 5. Due to the nature of our study, we did not continue past 5 dpf, but both the maternal mRNA and the increase in embryonic expression at 4 dpf suggests a role for zC20ORF96 in zebrafish embryonic development.

3. Conclusion

Ccdc103 is a 241-residue dynein attachment factor with high expression in the testis, with enriched expression also seen in the brain, lung, and kidney—organs known to form motile cilia. Our Y2H screen identified 14 putative ccdc103 interactors with eight directly linked to cilia (**Table 5**) and seven transcripts specifically enriched in ciliated tissues (**Table 5**). Although these 14 proteins were shown to interact with ccdc103, the cellular and histological context of each pair must also be considered. Thus, we chose to focus further studies on *ankef1* and C20ORF96, based on their lack of functional and expression data, as well as their enriched expression in the testis and a direct link to cilia through other screens. Further work must be done to confirm the interactions between Ccdc103 and these putative interactors using coimmunoprecipitation studies. Likewise, colocalization studies with Ccdc103 in ciliated cells will strengthen these two interactors' links to motile cilia. The genes identified in this study hold promise toward clarifying mechanisms of motile ciliogenesis in both humans and zebrafish.

4. Materials and methods

4.1. Zebrafish care and maintenance

Adult wild-type fish (AB line) were maintained in a circulating system (Aquarius Fish Systems) at 28.5º C on a 14h/10h light/dark cycle, with other parameters maintained as previously described (Lawrence, 2007). Embryos were collected from natural crosses and grown in 0.5x E2 media (7.5mM NaCl, 0.25mM KCl, 0.5mM $MgSO_4$, 75µM KH_2PO_4, 25µM Na_2HPO_4, 0.5mM $CaCl_2$, 0.35mM $NaHCO_3$, pH 7.2-7.6) at 28.5º C. Embryonic staging criteria was determined by standard protocols (Kimmel *et al.*, 1995). All protocols and experiments used in this paper were monitored and approved by the Auburn University Institutional Animal Care and Use Committee (IACUC).

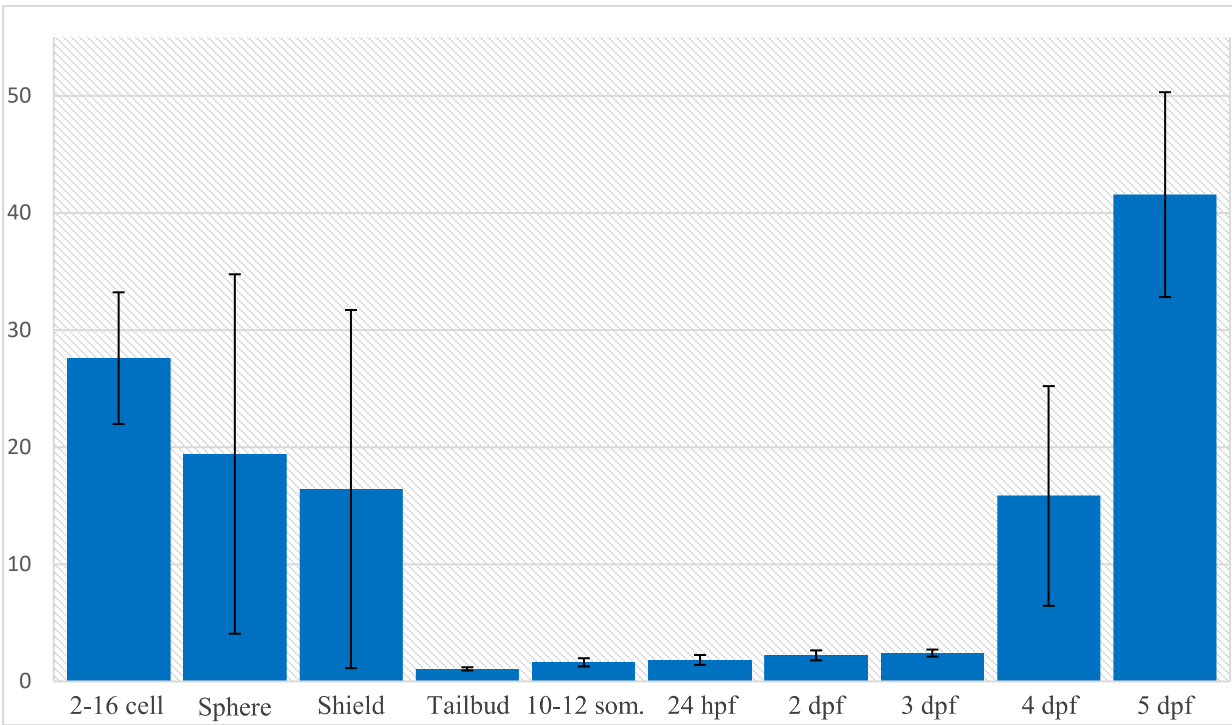

Figure 2.3: Relative normalized expression of C20ORF96 throughout zebrafish embryonic development. All stages were normalized to the tailbud stage expression level.

4.2. Yeast two-hybrid screen

Bait fusion proteins were produced from full-length mouse ccdc103 cDNA subcloned into pGBKT7 (GAL4-DBD) using the In-Fusion Advantage PCR cloning kit (see also **Fig. 2.1** flowchart). Prey constructs in pGADT7-RecAB were part of the Universal normalized mouse Mate and Plate library (Cat. # 630482). We used the Matchmaker Gold yeast two-hybrid system (Clontech) for ccdc103 interactor screening following the manufacturer protocol. Positive and negative control mating experiments were performed to check growth media and as a standard of comparison for downstream experiments. Y2H Gold competent cells were then transformed with the ccdc103-pGBKT7 construct to confirm the absence of ccdc103 autoactivation. Next, the Y2HGold + ccdc103-pGBKT7 strain was mated with Y187 + mouse library strain. Dilutions of 1/10, 1/100, 1/1000 were plated onto SD/-Trp, SD/-Leu, SD/-Trp/-Leu (DDO) media and the remainder of the mating culture was plated on SD/-Trp/-Leu/X-α-gal/Aureobasidin A (DDO/X/A) media. Mating efficiency and the number of screened clones were calculated at 3.85% and 7.8×10^6, respectively and were within recommended parameters. Blue colonies from the DDO/X/A media were then patched onto SD/-Ade/-His/-Leu/-Trp/X-α-gal/Aureobasidin A (QDO/X/A) media. Each patch with blue colonies was streaked and restreaked onto DDO/X/A plates to obtain isolated colonies. Plasmids were extracted from isolated blue colonies grown on QDO/X/A using the Yeast Plasmid Isolation Kit (Clontech, #630467). For colony PCR, *E. coli* 5α cells (Zymo Research, #T3009) were transformed with isolated yeast plasmids, following the manufacturer protocol. Cells were plated onto LB/ampicillin (amp) agar (Thermo-Fisher, #Q60120) and grown overnight at 37°C. Two mL of LB/amp broth was inoculated with well-isolated colonies from each plate and grown overnight at 37°C at 225 rpm. Plasmids were then isolated from cultures with the alkaline lysis method and submitted to Eurofins Genomics for

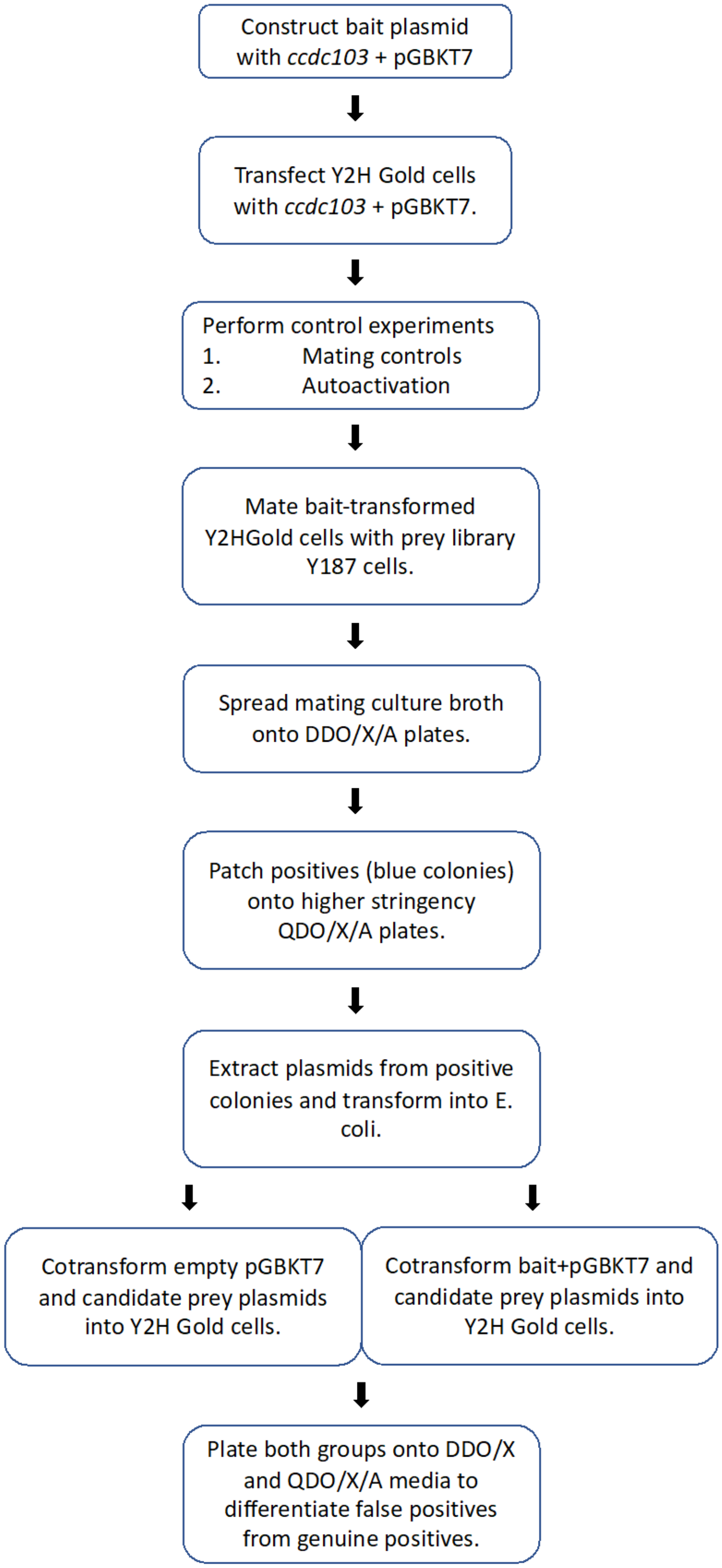

Figure 2.1: Yeast two-hybrid summary flow chart.

Sanger sequencing using the T7 promotor. Sequence identities were obtained using the BLASTn suite service provided by NCBI (Altschul *et al.*, 1990; Altschul and Lipman, 1990). One representative from each prey gene was cotransformed along with the bait + pGBKT7 or empty pGBKT7 into Y2H Gold cells in order to confirm protein interactions (**Fig. 2.1**). Cotransformed cells with prey and bait + pGBKT7 or empty pGBKT7 were plated onto DDO/X/A and QDO/X/A media to differentiate between genuine and false positives.

4.3. Cloning ccdc103 interactors

Total RNA was isolated from 14 embryonic stages from 2-cell through 5 dpf (WT, AB strain) using the TRIzol reagent (Invitrogen, #15596026). Total RNA concentration and integrity was verified on a 1.2% agarose gel stained with GelRed (Biotium, #41003). cDNA was then produced with the Superscript IV First-Strand synthesis system (Thermo Fisher Scientific, #18091200) using oligo-dT primers. Primers spanning the predicted stop and start codons of interactor genes were designed using Primer3 Plus (Untergasser *et al.*, 2012b), checked for specificity via the NCBI-BLASTn tool (Altschul *et al.*, 1990), and ordered from Eurofins Genomics (see **Table 5** for sequences). The forward primer was kept in-frame to allow for subcloning into destination vectors with N-terminal fusion proteins. 1.0 µL of cDNA from each embryonic stage was pooled, and gene-specific primers with attB1/attB2 adapter sites were used to amplify interactors, using the AccuPrime Pfx Supermix (Thermo Fisher Scientific, #12344040). In addition to standard PCR conditions recommended for Pfx, the following protocol (T100, Bio-Rad) was used, with gene-specific annealing temperatures: 52°C (*ankef1a*, *C20ORF96*), 53°C (*smc6*, *impact*), 53.5 °C (*ak2*, *etfa*, *atp6v1d*), 54.3°C (*dnajb1b*), 57.3°C (*dnajb1a*, *ing3*, *fem1c*, *kmt2e*, *polk*), 58°C (*ghr*) annealing; 5 minute extension time; 35 cycles with a 6 minute final extension stage. Amplicons were gel-purified with the QIAquick gel extraction kit (Qiagen) and used in a BP recombination reaction for insertion into the pCS2-Dest vector (Villefranc *et al.*, 2007) then transformed into NEB-10β chemically competent *E. coli* cells (New England BioLabs, #C3019I) using the manufacturer protocols. pCS2-Dest was a kind gift from Dr. Nathan Lawson (Addgene plasmid #22423). Isolated colonies were used to inoculate LB broth with ampicillin and plasmids were extracted using plasmid miniprep kit (Qiagen, #27104). Plasmid sequences were verified by Sanger sequencing (Eurofins Genomics) using the Sequencher sequence analysis software (version 5.4.6).

4.4. ***Quantitative RT-PCR***

All parameters described were checked to be in accordance with the MIQE guidelines for RT-qPCR data submission (Bustin *et al.*, 2009). Embryos from 10 developmental stages were collected from three biological replicates each containing 4-6 adult crosses per replicate, with at least 100 fertilized embryos per adult pair included in each biological replicate. Ten embryos from each stage were dechorionated and total RNA was extracted using the TRIzol reagent (Invitrogen 15596026) following the manufacturer's protocol. Total RNA purity, concentration, and integrity were checked as in 4.3, and reverse transcription was performed using the qScript system according to manufacturer protocol. The same RNA input for all samples (375 ng) was used in each 20 mL cDNA synthesis reaction. Primers for *C20ORF96* were designed as described above using Primer3Plus. The *C20ORF96* qPCR amplicon was designed to span the stop codon of the predicted coding region (see **Table 5** for primer sequences). Amplicon size (*C20ORF96* – 139 bp) was confirmed on a 1.2% agarose gel and by sequencing after PCR amplification from a cDNA mixture of all stages used in the qPCR study. Primer efficiency was checked using serial dilutions of ApaI-linearized pCRII-TOPO plasmid containing the *C20ORF96* qPCR amplicons and melt curves were checked for single peaks. The geometric mean of both *ef1α* and *β-actin* C_q values were used as the normalization factor. Several studies have indicated that *Ef1α* and *β-actin* have high stability throughout development (Casadei *et al.*, 2011; McCurley and Callard, 2008; Tang *et al.*, 2007). Reactions were set up in triplicate with total reaction volumes of 10 µL using 2X PerfeCTa SYBR green (Quanta Biosciences 95072), primer concentrations of 300 nM, and 1.0 µL of cDNA template from developmental stages. The following PCR protocol was used (CFX96, Bio-Rad) for all reactions: 1) 95° C for 3 minutes; 2) 95° C for 10 seconds; 3) 58° C for 20 seconds; 4) plate read; 5) repeat steps 2-4 39x; 6) melt curve 65° C, increase by 0.5° C every 5 seconds up to 95° C, with a plate read after each increase. CFX manager software (version 3.1, Bio-Rad) was used to analyze and display real-time data. C_q values were determined using the single-threshold method. Relative expression was calculated using the $2^{-\Delta\Delta Ct}$ method (Livak and Schmittgen, 2001).

CHAPTER 3

Spatiotemporal expression profile of embryonic and adult ankyrin repeat and EF-hand domain containing protein 1 encoding genes *ankef1a* and *ankef1b* in zebrafish

(This chapter was published in *Gene Expression Patterns*, Vol. 34, December 2019)

ABSTRACT

Recent human next-generation sequencing (NGS) studies indicate a correlation of *ANKEF1* (ankyrin repeat and EF-hand domain containing protein 1) expression and cilia formation or function. Additionally, a single study conducted in the African clawed frog (*Xenopus laevis*) has indicated *ankef1* is down-regulated after pharmacological fibroblast growth factor (FGF) inhibition and plays a role in protocadherin-mediated cell protrusion and adhesion. That study also revealed a critical role for *ankef1* in the embryonic development of the frog, with morphants exhibiting phenotypes including spina bifida and a shortened body axis. Interestingly, while little is known about ANKEF1 function in other vertebrate systems, recent proteomic data has shown ANKEF1 is enriched in ciliated cells. Likewise, publicly available EST profile databases indicate *ANKEF1* expression in multiple human tissues, including high levels in the testes. Together, these previous studies suggest an important role for ANKEF1 in ciliated tissues and during embryonic development. Here, we have cloned zebrafish (*Danio rerio*) *ankef1a*, as well as its paralog, *ankef1b*, and conducted expression analyses by whole-mount *in situ* hybridization (WISH) and quantitative polymerase chain reaction (qPCR) during embryonic development and in adult tissues. WISH revealed that both forms are ubiquitously expressed early in development, with more discrete expression of both transcripts in embryonic tissues known to precede or possess motile cilia, including dorsal forerunner cells (DFC) and the otic vesicles, respectively. Additionally, both transcripts are enriched in the developing pharynx and swim bladder. Our qPCR

results revealed enhanced expression in the testes, along with increased expression in brain. Certainly, our experiments in the zebrafish model system with *ankef1a* and *ankef1b* provide a solid foundation for future studies to uncover the molecular pathways through which Ankef1 acts in both healthy and disease states.

Introduction

Ankyrin repeat and EF-hand domain containing 1 protein (ankef1, also called ankrd5 or anr5) was identified as a participant in cell adhesion and protrusion, as well as an important component of proper gastrulation in the frog (*Xenopus laevis*) (Chung *et al.*, 2007). The ankyrin repeat motif contains helix-turn-helix domains arranged in a flexible string of repeats and is a commonly found motif involved in protein-protein interactions (Li et al., 2006). Ankyrin repeats are found in proteins involved in a wide range of cellular pathways, including NRARP (Notch-regulated ankyrin repeat-containing protein) in Notch signaling (Lamar *et al.*, 2001), as well as inversin in cilium-associated Wnt signaling (Morgan *et al.*, 2002).

Ankef1 also contains a predicted EF-hand domain with calcium (Ca^{2+}) binding regions, although little is known about the specific function of this motif. From studies with other proteins, the EF-hand motif has been identified as a Ca^{2+} sensor and typically mediates calcium-responsive conformational changes (Herzberg *et al.*, 1986; Kretsinger and Nockolds, 1973). Calmodulin, which contains two pairs of calcium-binding EF-hand motifs (Kretsinger *et al.*, 1986), is an example of a Ca^{2+}-responsive protein that participates with inversin as an intermediary in developmental signal transduction. Increased intracellular Ca^{2+} induces a conformational change in calmodulin, which then dissociates from inversin (Whittaker and Milligan, 1997). A dorsal marginal zone (DMZ) dissociation and reaggregation assay showed that knockdown of *ankef1* in the frog by morpholino oligonucleotide (MO) ablated the reaggregation upon addition of Ca^{2+} (Chung *et al.*, 2007). The same study showed that calcium-dependent dorsal marginal zone (DMZ) cell reaggregation was rescued by coinjection of *ankef1* mRNA and *ankef1* MO, indicating a role for ankef1 in cell-cell adhesion. Frog paraxial protocadherin (papc), whose zebrafish form is required for dorsal midline cell convergence during gastrulation (Yamamoto *et al.*, 1998), was also shown to physically interact with the C-terminal ankyrin repeats of ankef1 (Chung *et al.*, 2007), thus strengthening the link with cell-cell adhesion.

Although the role of *ANKEF1* remains unknown, specific tissues expressing *ANKEF1* have been identified in several vertebrate systems. Proteomic data from isolated human airway cilia (Blackburn *et al.*, 2017), as well as embryonic zebrafish kidney single-cell analyses (Tang *et al.*, 2017), have found ANKEF1 to be enriched in ciliated cells. Mouse *Ankef1* was shown to be upregulated in both vestibular and cochlear hair cells, as compared to epithelial non-hair cells (Elkon *et al.*, 2015). Hair cells are known to carry both the archetypal primary cilia (kinocilia) and actin-based stereocilia, the latter of which is distinct from primary/motile cilia and microvilli. *Ankef1* was also shown to be upregulated during multiciliated cell (MCC) differentiation in frog in an Rfx2/Foxj1-mediated pathway (Sedzinski *et al.*, 2017). Furthermore, *ANKEF1* transcripts are found at high levels in the human testes (Fagerberg *et al.*, 2014), a site producing large quantities of flagellated cells (i.e. spermatogenesis). *ANKEF1* appears to be a good candidate for future studies of genetic disease, potentially those involving ciliated epithelia.

Most post-mitotic vertebrate cell types possess at least one cilium, implying that cilia play an important role in diverse physiological processes. Interestingly, inhibition of ciliary resorption can suppress tumorigenesis (Han and Alvarez-Buylla, 2010; Han *et al.*, 2009; Wong *et al.*, 2009b). Cilia are typically classified into two groups: motile and nonmotile (or primary/sensory) cilia.

Motile cilia are involved in processes that require movement of fluids or particles, such as CSF movement and mucus clearance. Ciliated structures in humans include epithelial cells lining kidney tubules (Katz and Morgan, 1984), ependymal cells of the spinal canal (Worthington and Cathcart, 1963), and fallopian tubes (Clyman, 1966). Cilia also mediate signaling pathways through cilium-localized receptors, including fibroblast growth factor (Tang *et al.*, 2017), as well as epidermal growth factor signaling mediated by PKD2 (Ma *et al.*, 2005), a calcium-permeable cation channel (Huang *et al.*, 2007)

Experiments conducted in frog provided the first direct evidence toward determining ankef1 function, primarily reporting loss-of-function consequences on gastrulation (Chung *et al.*, 2007). *Ankef1* knockdown in frog showed both shortened and spina bifida phenotypes. Their work showed both that ankef1 is an upstream effector of Rho and that the *ankef1* knockdown phenotype could be partially rescued by coinjection of constitutively active Rho mRNA, whereas coinjection of *ankef1* MO with constitutively active Rac mRNA did not show rescue. Given that the zebrafish is a strong model system for developmental processes, and that ankef1 was shown to play a critical developmental role in frog, further study of ankef1 in zebrafish will shed further light on its physiological role.

As zebrafish are predicted to express two paralogs of *ankef1* (David *et al.*, 2003; Sreenivasan *et al.*, 2008; Udvadia, 2008), here we present cloning, sequencing, and expression data for *ankef1a* and *ankef1b* to shed light on the developmental and adult organ expression patterns of zebrafish *ankef1*. To our knowledge, the study presented here is the first to describe the spatiotemporal expression patterns of zebrafish *ankef1a* and *ankef1b* during development, as well as their distribution in adult tissues

Results

Sequence comparison of Ankef1a and Ankef1b

Whole exome sequence data from our lab was aligned to GRCz11 with Sequencher 5.4.6 and searched for both *ankef1a* and *ankef1b* transcripts using available exon sequences, which confirmed their presence in 48 hpf embryos (data not shown). The genes encoding zebrafish Ankef1a and Ankef1b are located on chromosomes 20 and 17, respectively, and these proteins show remarkable similarity to other vertebrate homologs, retaining the same ankyrin—EF-hand—ankyrin domain architecture (**Fig. 3.1A-B**). The *ankef1a* coding region is 2340 bp and contains a predicted 11 exons. Our results support NCBI bioinformatics data that Ankef1a is a 779-residue protein with a predicted molecular weight of 86.8 kDa. Ankef1a shows 49% overall identity (67% similarity) to the human ortholog (**Fig. 3.2A-B**). Sequence analyses of the ankyrin repeat alone revealed the degree of conservation is higher in the two ankyrin repeats of zAnkef1a versus hANKEF1, with 57% identity (73% similarity) between the N-terminal ankyrin repeats and 56% identity (74% similarity) between the C-terminal ankyrin repeats, while the EF-hand domain for these two proteins showed 34% identity (45% similarity).

Interestingly, sequence alignment of our cloned *ankef1b* and predicted coding sequence (*ankef1b*: ZDB-GENE-060810-68) revealed that our cloned version contained a 39-bp in-frame insertion at the end of predicted exon 5, which was spliced into the transcript from the beginning of intron 5-6. As a result, our cloned coding region is 2031 bp, instead of 1992 bp. Our data suggests that Ankef1b is a 676-residue protein and has a predicted molecular weight of 74.9 kDa, with approximately the same predicted ankyrin—EF-hand—ankyrin arrangement as Ankef1a. The full-length zAnkef1b and hANKEF1 amino acid sequences are 48% identical (66% similarity), excluding the truncated C-terminal end of Ankef1b (**Fig. 3.2A-B**). Comparison of the N- and C-

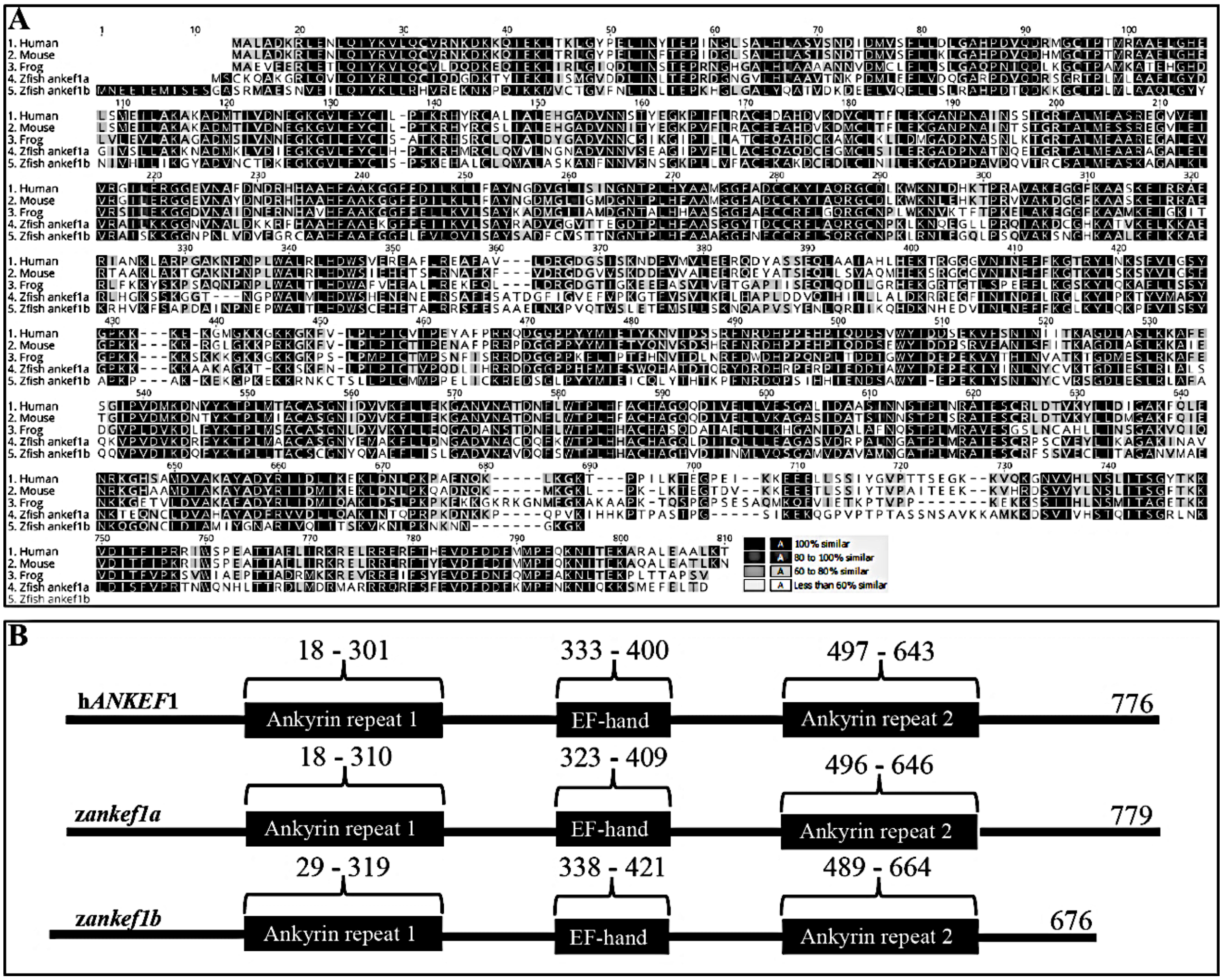

Figure 3.1: **A**. Alignment of ANKEF1 protein sequence with other common vertebrate model organisms. *Homo sapiens*, **human** - NP_071379.3; *Mus musculus*, **mouse** - NP_783598.1; *Xenopus laevis*, **frog** - NP_001085241.1; *Danio rerio,* **zebrafish Ankef1a** – reported here (Supplemental); *Danio rerio*, **zebrafish Ankef1b** – reported here (Supplemental). Black boxes indicate 100% similarity; dark gray boxes indicate 80-100% similarity; light gray boxes indicate 60-80% similarity; white boxes indicate less than 60% similarity. **B**. Schematic of Ankef1a, Ankef1b, and hANKEF1 domain architecture. Amino acid sequence ranges indicated for each domain.

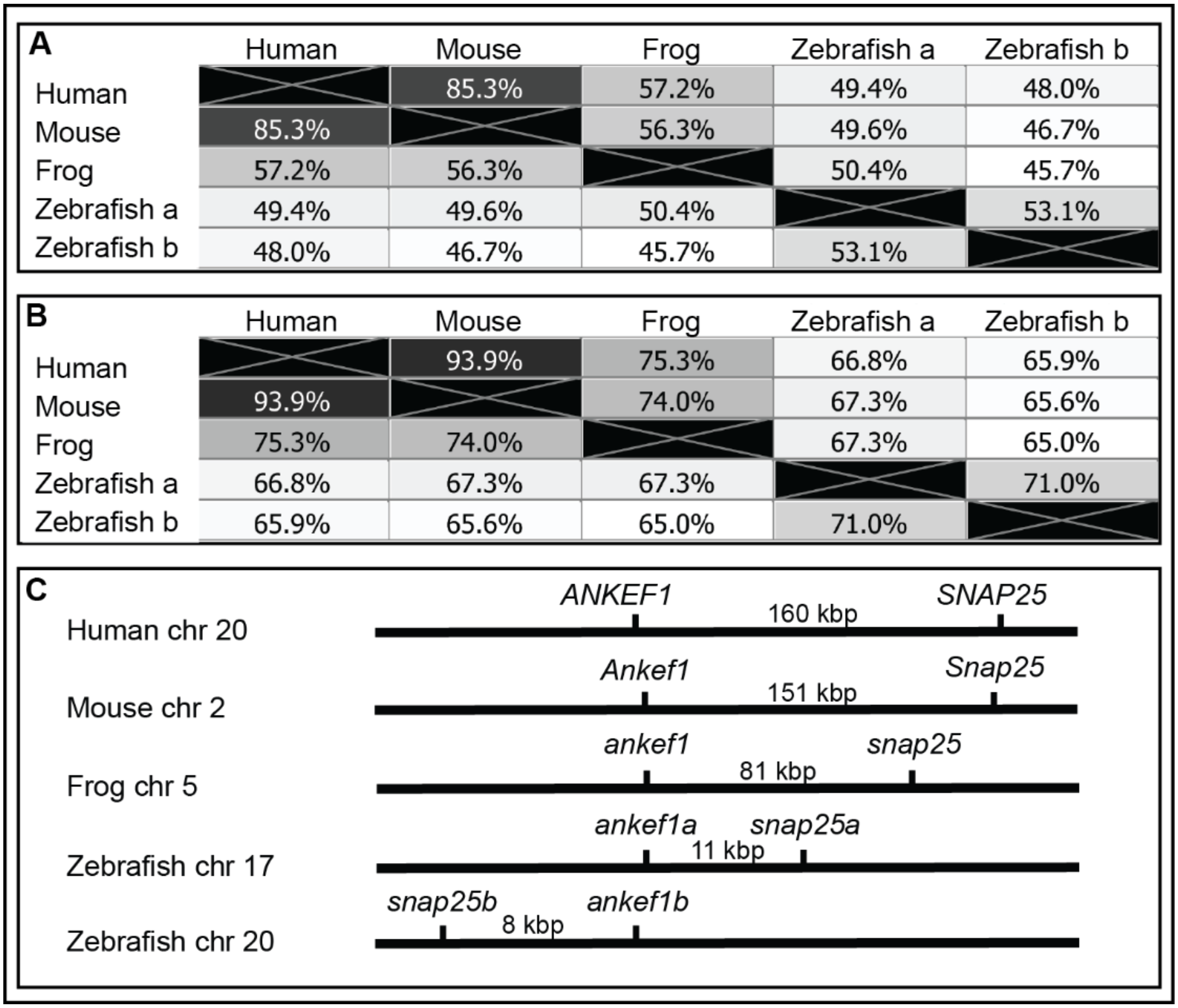

A

	Human	Mouse	Frog	Zebrafish a	Zebrafish b
Human		85.3%	57.2%	49.4%	48.0%
Mouse	85.3%		56.3%	49.6%	46.7%
Frog	57.2%	56.3%		50.4%	45.7%
Zebrafish a	49.4%	49.6%	50.4%		53.1%
Zebrafish b	48.0%	46.7%	45.7%	53.1%	

B

	Human	Mouse	Frog	Zebrafish a	Zebrafish b
Human		93.9%	75.3%	66.8%	65.9%
Mouse	93.9%		74.0%	67.3%	65.6%
Frog	75.3%	74.0%		67.3%	65.0%
Zebrafish a	66.8%	67.3%	67.3%		71.0%
Zebrafish b	65.9%	65.6%	65.0%	71.0%	

Figure 3.2: Percent identity (**A**) and percent similarity (**B**) matrices of Ankef1 proteins across several common vertebrate model organisms. *Homo sapiens*, **human** - NP_071379.3; *Mus musculus*, **mouse** - NP_783598.1; *Xenopus laevis*, **frog** - NP_001085241.1; *Danio rerio,* **zebrafish Ankef1a** – reported here; *Danio rerio*, **zebrafish Ankef1b** – reported here. The syntenic relationship of Ankef1 proteins across these model organisms is demonstrated in **C**, with chromosome number and approximate distance between ANKEF1 and SNAP25 homologs given for each.

terminal ankyrin repeat regions for these proteins revealed 50% identity (68% similarity) and 56% identity (74% similarity), respectively, while the EF-hand region of Ankef1b shows 35% identity (52% similarity) as compared to hANKEF1. Furthermore, Ankef1a and Ankef1b full-length amino acid sequences showed 53% identity (71% similarity) to one another, excluding the truncated C-terminal sequence. Similar degrees of identical and similar amino acid sequences are observed when either zebrafish protein is compared to frog and mouse homologs. Interestingly, analysis of the chromosomal location of *ANKEF1* genes in all four organisms revealed a syntenic relationship for the proximal chromosomal regions, whereby *SNAP25* is found as a neighboring gene (**Fig. 3.2C**).

***Ankef1* phylogenetic tree**

Full-length amino acid sequences were used to generate a phylogenetic tree (**Fig. 3.3**) using the neighbor-joining method in MEGA7. Two proteins with the ANKEF1 domain architecture are predicted in the *Ciona* genus and were included in the phylogenetic tree. Teleost Ankef1 branched off from the other vertebrate lineages and underwent a gene duplication event, thus creating two protein products. These products clustered in two distinct clades of paralogous Ankef1 proteins. A BLAST-P **(Altschul *et al.*, 1990; Altschul and Lipman, 1990)** search of zebrafish and human ANKEF1 against *Chlamydomonas reinhardtii*, *Caenorhabditis elegans*, and *Drosophila melanogaster* revealed no proteins displaying the ankyrin—EF-hand—ankyrin architecture.

2.3 Spatiotemporal expression of *ankef1a* and *ankef1b* during development

WISH for *ankef1a* and *ankeflb* revealed ubiquitous expression beginning at cleavage and continuing through 50% epiboly (**Fig 3.4. A-C**). The first mildly apparent tissue-restricted staining

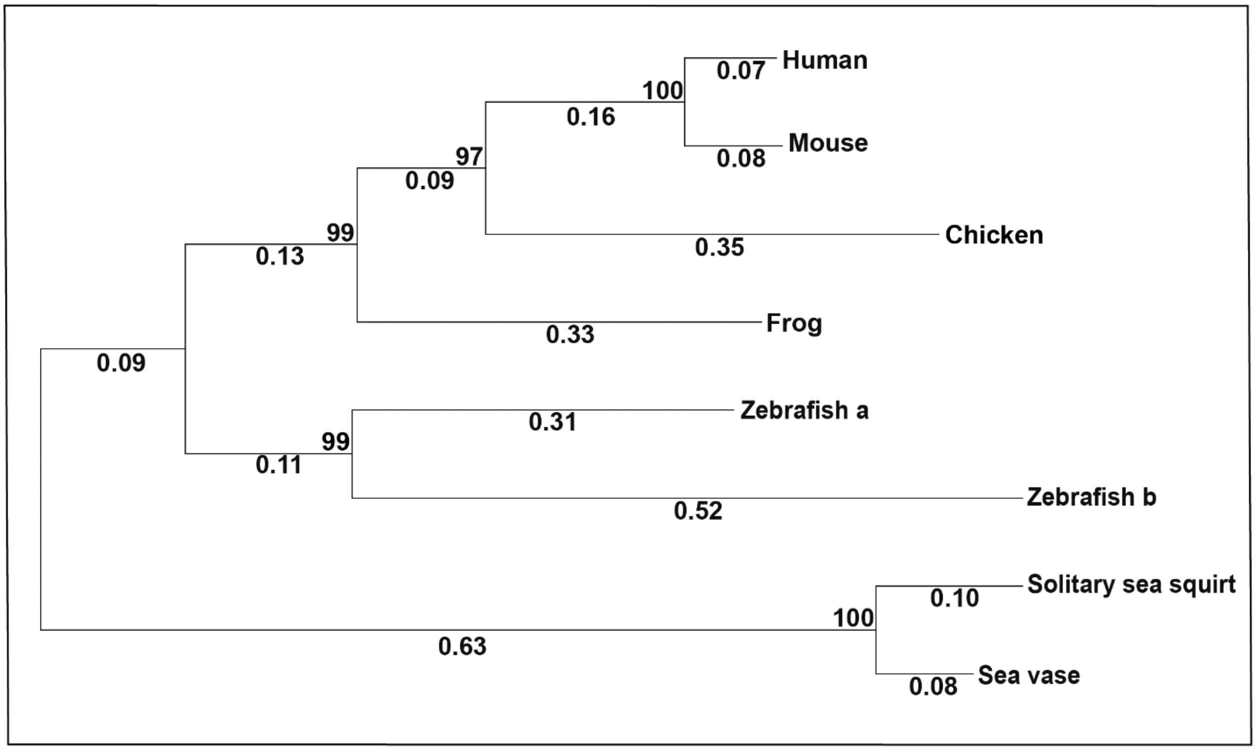

Figure 3.3: Phylogenetic relationship between select Ankef1 protein homologs. Bootstrap values are indicated at nodes and tree distances are listed under branches. *Homo sapiens*, **human** - NP_071379.3; *Mus musculus*, **mouse** - NP_783598.1; *Gallus gallus*, **chicken** - XP_004935298.2; *Xenopus laevis*, **frog** - NP_001085241.1; *Danio rerio,* **zebrafish Ankef1a** – reported here; *Danio rerio*, **zebrafish Ankef1b** – reported here; *Ciona savignyi*, **solitary sea squirt** - ENSCSAVT00000004681; *Ciona intestinalis*, **sea vase** - F6ZTU7.

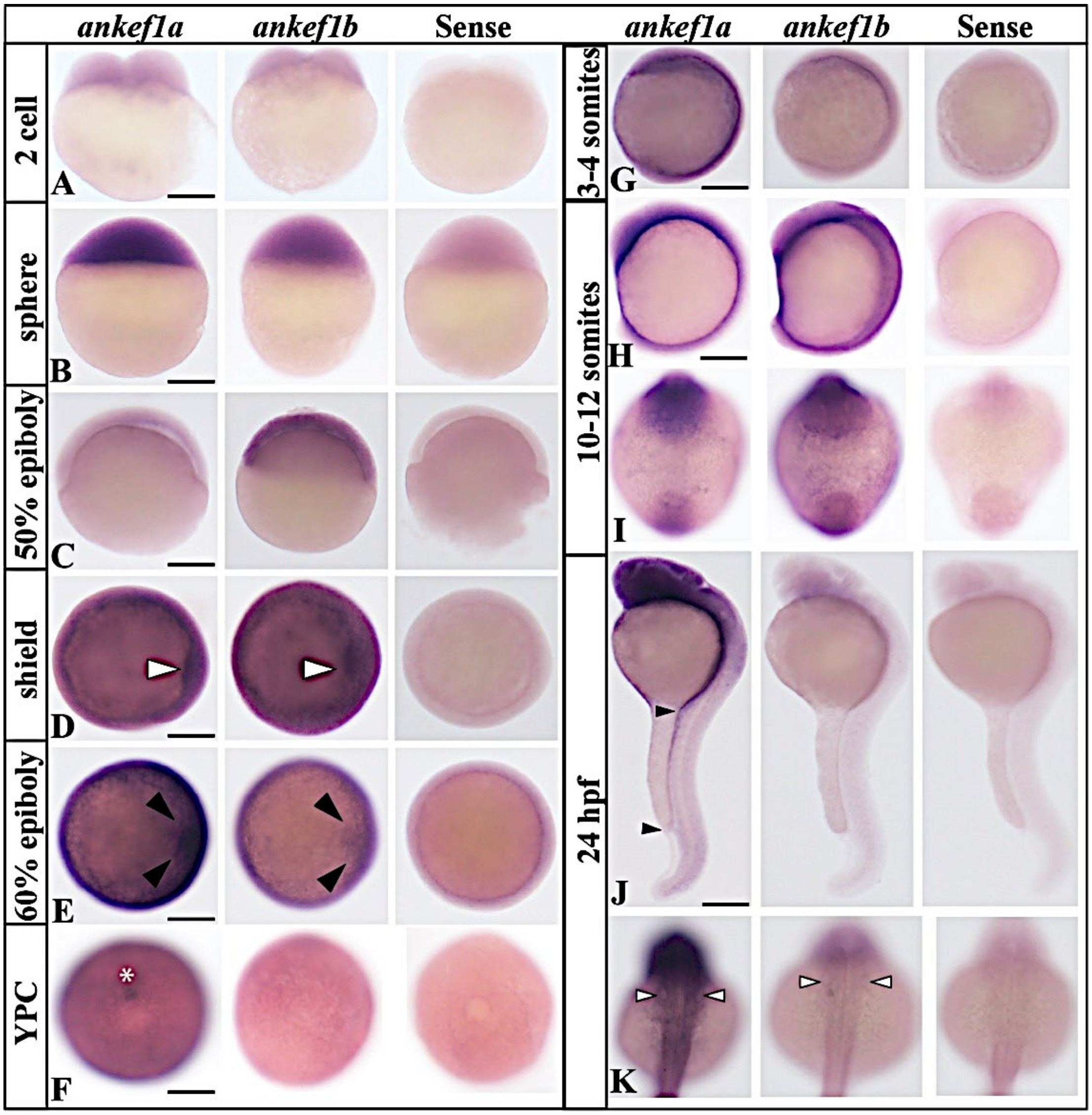

Figure 3.4: *Ankef1a and ankef1b* is expressed in early embryos. Rows: **A-C**, **G**, **H**, and **J** are lateral views; Row **D** and **E** are animal pole view; Row **F** are vegetal pole views; Row **I** are ventral view; Row **K** are dorsal view. The white arrowheads at shield (**D**) and black arrowheads at 60% epiboly (**E**) indicate *ankef1a* and *ankef1b* expression along the site of involution and convergent extension during gastrulation. Note the DFCs indicated at the YPC stage (asterisk in **F**), which was not seen in *ankef1b* YPC-stage embryos. Black arrowheads in 24 hpf lateral view (**J**) indicates *ankef1a* expression along the dorsal side of the yolk extension. Otic vesicle expression of *ankef1a* is indicated by white arrowheads in the 24 hpf dorsal view (**K**). Scale bars for each stage = 200 μm.

of both transcripts was observed in the shield stage, extending from the leading edge and following the region of convergent extension toward the animal pole (**Fig. 3.4D-E**). At yolk plug closure, *ankef1a* was observed in the dorsal forerunner cells (DFCs; **Fig. 3.4F**), which coalesce to form the motile-ciliated Kupffer's vesicle (Cooper and D'Amico, 1996; Melby *et al.*, 1996).

During early somitogenesis, expression of both genes was found to be relatively ubiquitous throughout the embryo body (**Fig. 3.4G-I**). Beginning at 24 hpf and at 48 hpf, both transcripts are strongly expressed in the head (**Fig. 3.4J-K** and **Fig. 3.5A-F**), with more specific expression occurring at 96 and 120 hpf (**Fig. 3.5G-L**). Expression patterns are remarkably similar, with the exception of *ankef1a* expression along the dorsal side of the yolk extension at 24 hpf (**Fig. 3.4J**). *Ankef1a* and *ankef1b* are weakly expressed in the otic vesicle at 24 hpf (**Fig. 3.4J-K**), then at higher levels in the same region at 96 and 120 hpf (**Fig. 3.5G-L** and **Fig. 3.6M-N)**. Both transcripts are apparent along the ventral side of the swim bladder, in the pharynx and brain at 96 hpf through 120 hpf (**Fig. 3.5G-L** and **Fig 3.6O-P**), as well as possibly in the pancreas at 120 hpf (**Fig. 3.6Q-R**).

2.4. qPCR of *ankef1a* and *ankef1b* in adult male and female tissues and embryonic stages

To more quantitatively analyze overall expression levels of *ankef1a* and *ankef1b*, we performed qPCR on the 14 developmental stages used for WISH. Our qPCR analysis of *ankef1* during embryonic stages confirmed presence of both forms in 2-16 cell and sphere stages (**Fig. 3.7**). *Ankef1a* shows little expression change from cleavage through 120 hpf. On the other hand, *ankef1b* relative transcript levels taper off much more slowly, until another increase at the 3-4 somite stage. The *ankef1b* transcript relative expression level remained low from the end of somitogenesis to 120 hpf.

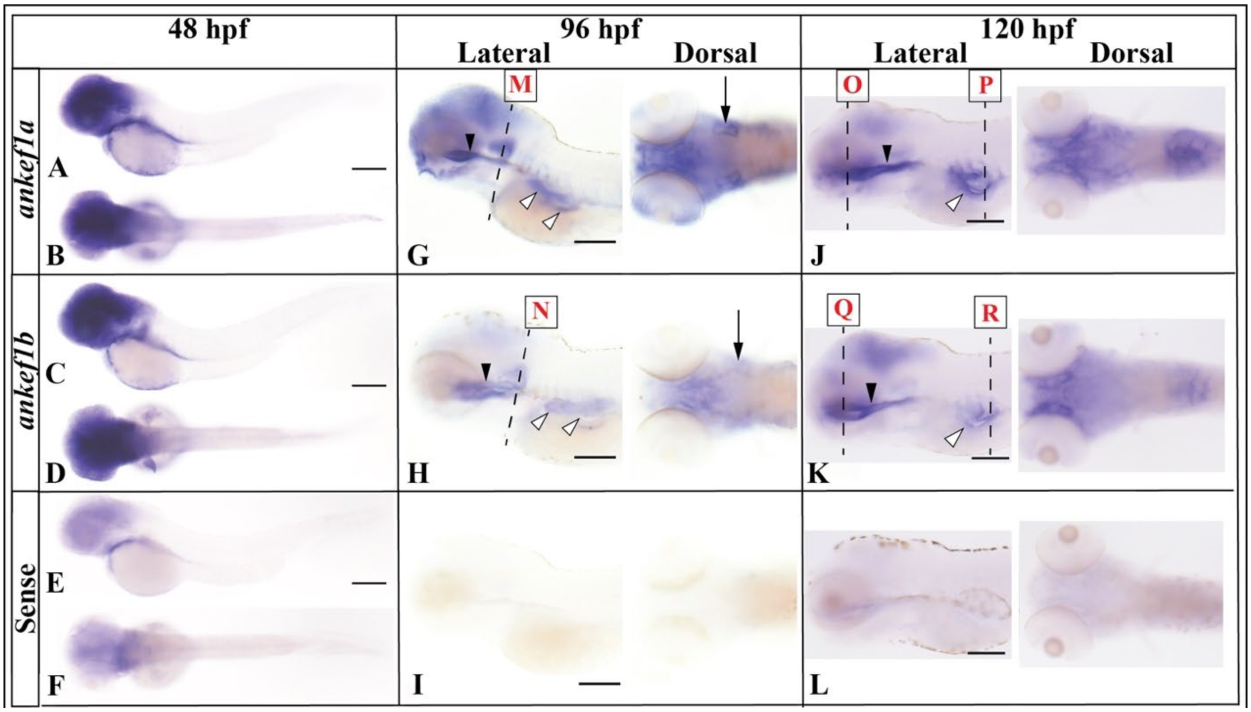

Figure 3.5: *Ankef1a* and *ankef1b* expression in 48, 96, and 120 hpf embryos. **A**,**C**,**E** are lateral views, while **B**,**D**, and **F** are dorsal views. Black arrowheads in **G-H** and **J-K** indicate pharyngeal staining. Staining in the swim bladder region in 96 and120 hpf is denoted by white arrowheads in **G-H** and **J-K**. Arrows in **G-H** point to otic vesicles. Scale bars for each whole mount images **A-L** = 200 μm.

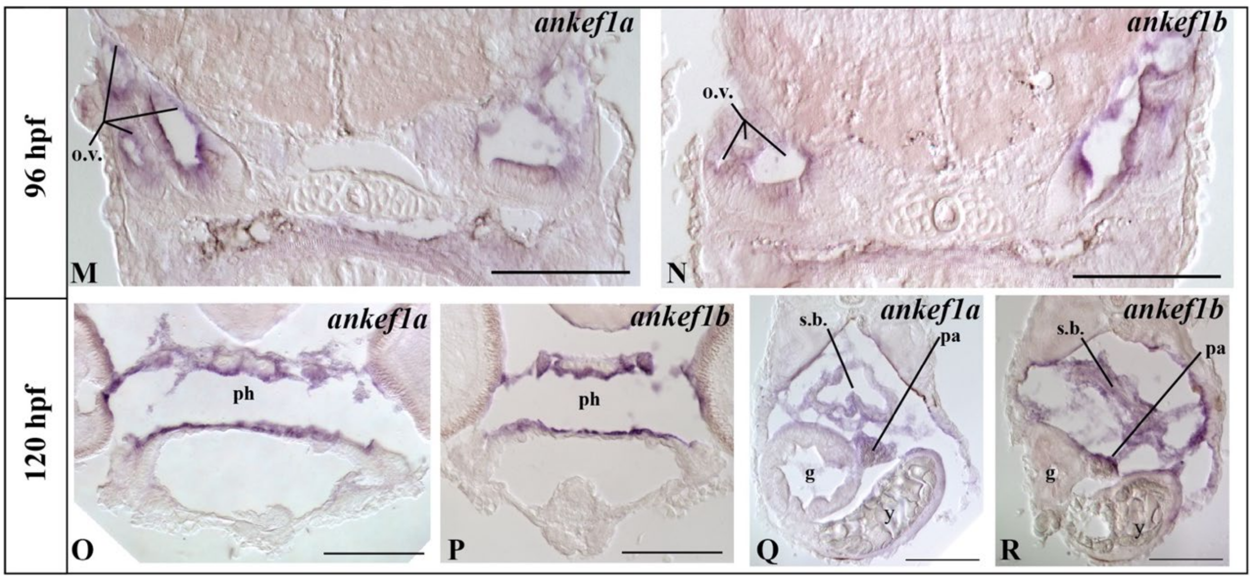

Figure 3.6: Cryosections of 4-5 dpf WISH embryos. **M-N** demonstrate *ankef1a* and *ankef1b* expression in the otic vesicles of a 96 hpf embryos. **O-P** show *ankef1a* and *ankef1b* expression in the pharynx of 120 hpf embryos. **Q-R** indicate *ankef1a* and *ankef1b* expression in the swim bladder of 120 hpf embryos. **g**: gut; **o.v**.: otic vesicle; **pa**: pancreas; **ph**: pharynx; **s.b**.: swim bladder; **y**: yolk. Scale bars for cryosections **M-R** = 100 μm.

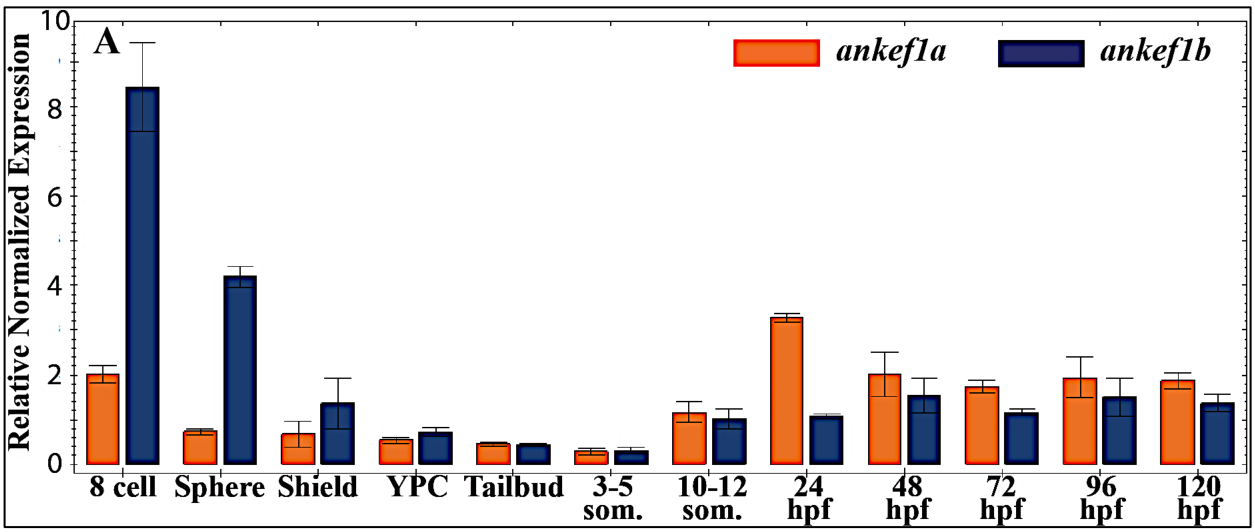

Figure 3.7: Early developmental expression of *ankef1a* and *ankef1b,* as measured by qPCR. For developmental stages (**A**), total RNA from a mix of all 12 stages was used to prepare control cDNA. *Ef1α* and *β-actin* were used as reference genes. C_q standard error bars shown (+/-1 SEM). **hpf**: hours post fertilization; **som.**: somites; **YPC**: yolk-plug closure.

Comparison of *ankef1a* and *ankef1b* relative expression in adult male and female tissues was performed next. As expression of both genes in intestines appeared very low, this tissue was used as control comparison. In female tissues, expression of both was highest in the brain, with elevated expression also present in the liver and low to moderate expression in all other tested tissues (**Fig. 3.8B**). Similar to that of female tissues, adult male tissue expression of *ankef1a* and *ankef1b* was enriched in the brain, with markedly higher levels of ankef1a in the brain than *ankef1b* (**Fig. 3.8C**). Additionally, high levels of *ankef1a* and *ankef1b* were observed in liver and swim bladder of males, with moderate expression levels also in other tissues analyzed. Notably, both *ankef1a* and *ankef1b* were highly expressed in whole testes preparations (**Fig. 3.8C′**) with *ankef1b* showing most enriched expression.

<u>3. Discussion</u>

Given the ANKEF1 amino acid sequence homology between zebrafish, frog, mouse, and human, we predict some degree of conserved function between species. Conserved chromosomal synteny of *ankef1* and *snap25* in all four species, as well as strong similarities between mammalian EST data and our organ-specific qPCR analyses, suggests that the *ankef1* genes analyzed here are orthologous. The genetic persistence of Ankef1 in species ranging from sea squirts to humans suggests it is of functional importance to the survival of these organisms.

Ubiquitous *ankef1a* and *ankef1b* expression in early development indicates a maternal contribution of both these genes, particularly *ankef1b*, suggesting they are required for early developmental processes. More restricted tissue expression after 24 hpf suggests additional later roles in development of the zebrafish, particularly in the otic vesicles, pharynx, and swim bladder. The overlapping developmental expression patterns shown by WISH suggest that both forms may

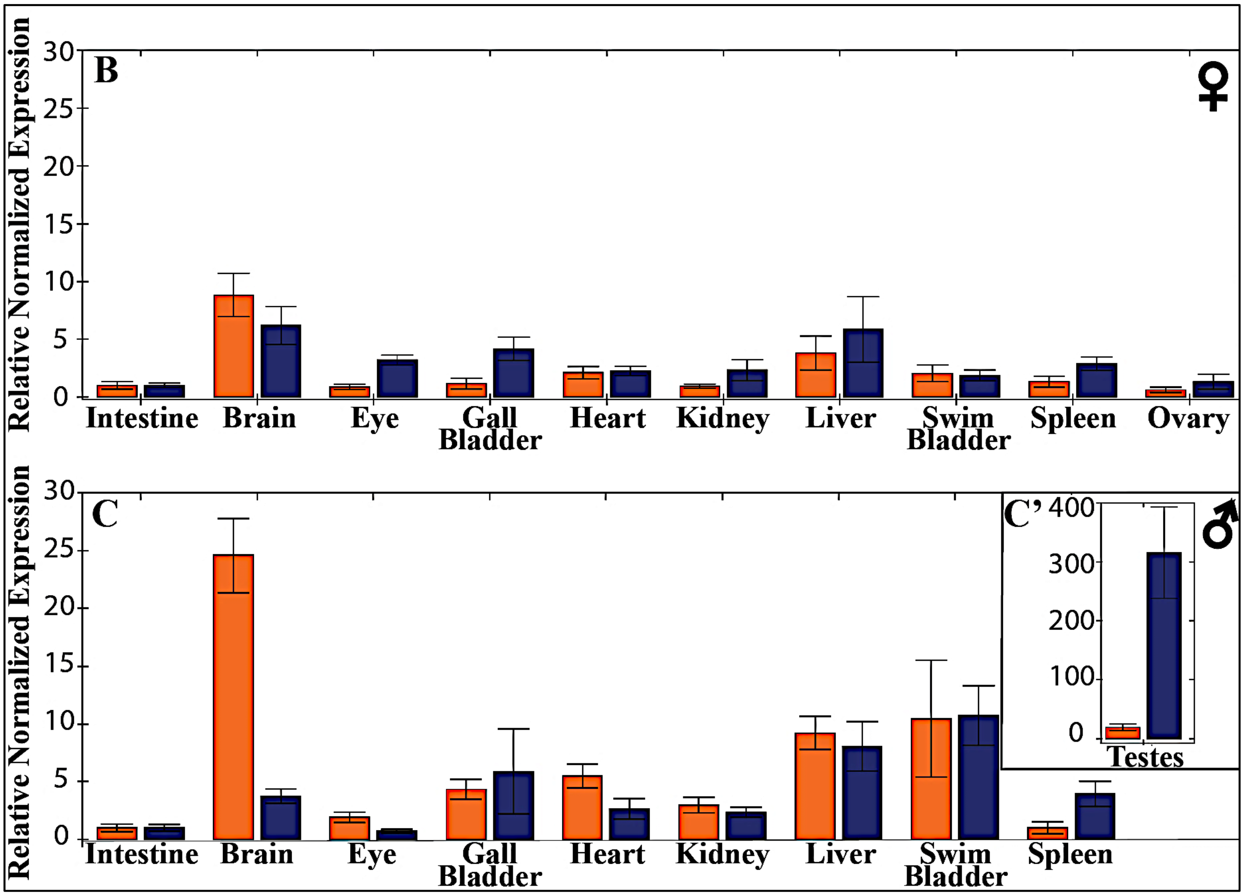

Figure 3.8: Adult organ expression in female and male fish. Graph **B** depicts *ankef1a* and *ankef1b* expression in female organs. In **C**, *ankef1a* and *ankef1b* expression in male organs is depicted. Inset box **C′** further shows relative normalized expression (y-axis) in testes preparations. For **B**, **C**, and **C′**, cDNA preparations from adult intestine of the corresponding sex were used as controls and set as “1”, while *ef1α* and *β-actin* were used as reference genes. Detailed description may be found in methods. C_q standard error bars shown (+/-1 SEM). **hpf**: hours post fertilization; **som.**: somites; **YPC**: yolk-plug closure.

possess some functional redundancy, however, the two share only 53% identity and the C-terminal end of Ankef1b is truncated by 116 amino acids. Interestingly, *ankef1a* and *ankef1b* did not always show overlapping expression patterns during development, supporting some level of functional divergence. Indeed, *ankef1a* appeared in the DFCs at the YPC stage, as well as *ankef1a* staining along the dorsal side of the yolk extension at 24 hpf, both of which were not present in *ankef1b*-stained embryos at the respective stages.

To our knowledge, functional work on ANKEF1 is limited to one study using *Xenopus* as the model organism (Chung *et al.*, 2007). That study showed that *ankef1* is down-regulated in response to an FGF-R inhibitor (SU5402) and provided evidence that Ankef1 is involved in cell protrusion and cell-cell adhesion. Furthermore, paraxial protocadherin, a calcium-dependent cell adhesion molecule also expressed in the dorsal midline of the zebrafish gastrula, was found to directly interact with Ankef1 (Chung *et al.*, 2007). We found that *ankef1a* expression was enhanced during the shield stage along the site of involution, which is also a region of *papc* expression (Yamamoto *et al.*, 1998). Further experiments are required to determine if these genes co-localize in the zebrafish.

Other studies have revealed Ankef1 presence in the mouse auditory forebrain (Hackett *et al.*, 2015), gastrula of frogs (Chung *et al.*, 2007), airway cilia in humans (Blackburn *et al.*, 2017), and kidney cells in the adult zebrafish (Tang *et al.*, 2017). Similar to our findings in adult zebrafish, *ANKEF1* transcripts are also enriched in the adult human testes (Fagerberg *et al.*, 2014), indicating possible functional conservation in the zebrafish, potentially in spermatogenesis. This, as well as specific expression of *ankef1a* in the DFCs, *ankef1a* and *ankef1b* in the otic vesicles and brain indicate a possible connection to cilium formation and/or function. *Ankef1* was also previously found to be enriched in mouse inner ear hair cells versus epithelial non-hair cells, perhaps implying a role for ANKEF1 in MCC differentiation.

Many tissues examined by qPCR exhibited similar expression levels for both genes, with the exception of the male brain and male testes. In the male brain, it appears that *ankef1a* is the predominant paralog expressed, whereas in the testes, *ankef1b* appears to be more highly expressed. Given our qPCR data collection and normalization protocol, and that high relative expression of *ankef1b* in testes and *ankef1a* in male brain versus other male organs was consistently seen in both RT-PCR (data not shown) and qPCR assays, we feel these data are accurate under the conditions used. Several possibilities may account for the differences in relative expression ratios of *ankef1a* and *ankef1b*. The most obvious explanation is that they have divergent functions in these specific tissues. As both are tissues containing ciliated/flagellated cells, it is tempting to hypothesize a role in the formation of or signaling in those organelles. However, further exploration, such as immunohistochemical analysis of adult brain and testes tissues with protein-specific antibodies, is warranted to shed more light on this possibility.

This study is the first to provide localization and quantification of *ankef1a* and *ankef1b* expression in zebrafish embryos and adults. Data presented here will serve to inform further experiments as to the function of these important genes in developmental and organ-specific processes.

Materials and methods

Zebrafish care and maintenance

Adult wild-type (WT) fish (AB, TU, and TUAB lines) were maintained in a circulating system (Aquarius Fish Systems) at 28.5º C on a 14h/10h light/dark cycle, with other parameters maintained as previously described (Lawrence, 2007). Embryos were collected from natural crosses and grown in 0.5x E2 media (7.5mM NaCl, 0.25mM KCl, 0.5mM $MgSO_4$, 75µM KH_2PO_4, 25µM Na_2HPO_4, 0.5mM $CaCl_2$, 0.35mM $NaHCO_3$, pH 7.2-7.6) at 28.5º C. Embryonic staging criteria was used according to previous studies (Kimmel *et al.*, 1995). All protocols and experiments used in this paper were monitored and approved by the Auburn University Institutional Animal Care and Use Committee (IACUC).

Cloning and characterization of *ankef1a* and *ankef1b*

Total RNA was isolated from 12 embryonic stages (WT, AB strain) using the TRIzol reagent (Invitrogen 15596026). Total RNA concentration and purity was checked on a spectrophotometer (DeNovix DS-11), and integrity was verified on both a 1.2% agarose gel stained with GelRed (Biotium 41003). cDNA was then produced with the Superscript IV First-Strand synthesis system (Thermo Fisher Scientific 18091200) via oligo-dT primers. Primers spanning the predicted stop and start codons of *ankef1a* were designed using Primer3 Plus (Untergasser *et al.*, 2012a), checked for specificity via the NCBI-BLASTn tool (Altschul, Gish, Miller, Myers, & Lipman, 1990) and ordered from Eurofins Genomics. The forward primer was kept in-frame to allow for subcloning into destination vectors with N-terminal fusion proteins. cDNAs from each embryonic stage were pooled, and gene-specific primers with attB1/attB2 adapter sites (**Table 3.1**) were used to amplify *ankef1a*, using the AccuPrime Pfx Supermix (Thermo Fisher Scientific 12344040). In addition to standard PCR conditions recommended for AccuPrime Pfx, the following *ankef1a*-specific protocol (T100, Bio-Rad) was used: 52° C annealing, 5-minute extension, 35 cycles. Amplicons were gel-purified with the QIAquick gel extraction kit (Qiagen) and used in a BP recombination reaction for insertion into the pCS2-Dest vector (Villefranc *et al.*, 2007) then transformed into NEB-10β chemically competent cells (New England BioLabs

C3019I), using manufacturer's protocols. pCS2-Dest was a kind gift from Dr. Nathan Lawson (Addgene plasmid #22423). Isolated colonies were used to inoculate preps, and plasmids were extracted using plasmid miniprep kit (Qiagen 27104). Plasmid sequences were verified by Sanger sequencing (Eurofins Genomics) using the Sequencher sequence analysis software (version 5.4.6).

For *ankef1b*, primers (see Table 3.1) were designed to span the 5′-and 3′-UTR, including putative start and stop codons (ZDB-GENE-060810-68). *Ankef1b* was amplified from pooled embryonic cDNA as described above, using DreamTaq PCR Master Mix (Thermo Fisher Scientific K9011). In addition to standard PCR conditions recommended for DreamTaq, the following thermocycler protocol was used: 60° C annealing, 1.5-minute extension, 35 cycles. The *ankef1b* amplicons were gel-purified and used for TA cloning with the pCRII-TOPO plasmid (Thermo Fisher Scientific K460001), then verified via Sanger sequencing and analyzed with Sequencher.

Whole-mount *in situ* hybridization and cryosectioning

Regions spanning the stop codon and 3′ UTR of *ankef1a* and *ankef1b* (Table 3.1) were amplified from cDNA using DreamTaq PCR Master Mix. In addition to standard PCR conditions recommended for DreamTaq, the following thermocycler protocol was used: 56° C annealing, 1-minute extension, 35 cycles. The amplicons were gel-purified using the QIAquick gel extraction kit (Qiagen 28704), inserted into the pCRII-TOPO (Thermo Fisher Scientific) plasmid via TA cloning, and transformed into NEB-5α chemically competent cells (New England BioLabs C2987I) according to the manufacturer's protocol. Sequences of plasmids containing the ISH probes were verified by Sanger sequencing (Eurofins Operon). Sense (SpeI restriction enzyme digest/T7 polymerase) and antisense (NotI restriction enzyme digest/T3 polymerase) probes for *ankef1a* and *ankef1b* were synthesized from linearized plasmids with digoxigenin-labeled NTPs

(Sigma-Aldrich 11277065910). The DiG-labelled RNA probes were the following lengths: *ankef1a* antisense – 50 bp of 3' UTR and 594 bp of coding sequence—644 bp; *ankef1b* antisense – 147 bp of 3'UTR and 547 of coding sequence bp; *ankef1b* sense – 694 bp.

Embryos from the AB strain were fixed in 4% PFA + PBS, and the WISH protocol was performed as previously established (Thisse and Thisse, 2008). After staining, later stages (24, 96, and 120 hpf) were cleared by incubation in 100% methanol following progressive dehydration. Once the desired stain intensity was reached, embryos were progressively rehydrated back into PBS and whole-mount images were taken. For cryosections, stained WISH samples were first soaked in 4% paraformaldehyde and embedded in a 1.2% agarose/5% sucrose solution. The agarose blocks were stored in a 30% sucrose solution at 4°C until use. The blocks were positioned on chucks using Surgipath FSC22 medium (Leica Microsystems) and 16 µm sections were produced with a Microm HM 525 cryostat.

Imaging

WISH images were obtained using an Olympus MVX10 stereo microscope equipped with a DP74 digital camera. Images were captured using the CellSens software package and processed identically at each stage using Adobe Illustrator. Sections were imaged using a Nikon Eclipse E800 using a 20x objective (Nikon, Plan Fluor) using the Nikon Elements AR software and prepared with Adobe Illustrator.

Quantitative RT-PCR

All parameters described in 4.5 were checked to be in accordance with the MIQE guidelines for RT-qPCR data submission (Bustin *et al.*, 2009). Developmental stages were collected from three biological replicates of 4-6 adult crosses per replicate, with at least 100 fertilized embryos per adult pair included in each replicate. Ten embryos from each stage were dechorionated and total RNA was extracted using the TRIzol reagent (Invitrogen 15596026). Total RNA purity, concentration, and integrity were checked as described in 4.2, and reverse transcription was performed using the SuperScript IV First-Strand Synthesis system according to manufacturer protocol. The same total RNA input for all samples (550 ng) was used in each 20 mL reaction.

Adult organs were collected individually in triplicate from sibling males or females (1-year old, AB strain), with smaller organs (spleen, gall bladder, heart, swim bladder) pooled from 3 adults and in triplicate. All were rinsed in Hanks Balanced Salt Solution immediately after removal. Total RNA was extracted by adding 650 mL TRIzol reagent (Invitrogen 15596026) according to manufacturer protocol following tissue disruption from two rounds of rapid freeze-thaw and 15 minutes of high speed vortexing. Resultant organ RNA was brought to volume of 300 ml with nuclease free water (Ambion AM9937) and further purified using ReliaPrep RNA Clean-Up and Concentration System (Promega Z1073) according to manufacturer instructions. After assaying all total RNA preparations for purity, quality, and concentration, as above for developmental stages, reverse transcription was performed with qScript cDNA synthesis kit (Quanta Biosciences 95047) according to manufacturer protocol, using the same RNA input (200 ng) for all samples. Reactions were set up in triplicate with total reaction volumes of 20 µL using 2X PerfeCTa SYBR green (Quanta Biosciences 95072), primer concentrations of 200 nM, and 1.0 µL of cDNA template from adult tissues or developmental stages.

Primers for *ankef1a* and *ankef1b* (Table 3.1) were designed as described above. Amplicon size (*ankef1a* – 129 bp; *ankef1b* – 252 bp) was confirmed on a 1.2% agarose gel and by sequencing after PCR amplification using a cDNA mixture of all stages used in the qPCR study. Primer efficiency was checked using serial dilutions of ApaI-linearized pCRII-TOPO plasmid containing the *ankef1a* and *ankef1b* qPCR amplicons and melt curves were checked for single peaks. The geometric mean of both *ef1α* and *β-actin* C_q values were used as housekeeping genes for developmental stages and adult tissues. These genes were selected on the basis that they were previously shown to have high stability throughout development and among adult tissues (Casadei *et al.*, 2011; McCurley and Callard, 2008; Tang *et al.*, 2007). Reactions were set up in triplicate with total reaction volumes of 20 µL using 2X PerfeCTa SYBR green (Quanta Biosciences 95072), primer concentrations of 300 nM, and 1.0 µL of cDNA template from adult tissues or developmental stages. The following PCR protocol was used (CFX96, Bio-Rad) for all reactions: 1) 95° C for 3 minutes; 2) 95° C for 10 seconds; 3) 58° C for 20 seconds; 4) plate read; 5) repeat steps 2-4 39x; 6) melt curve 65° C, increase by 0.5° C every 5 seconds up to 95° C, with plate read after each increase. CFX manager software (version 3.1, Bio-Rad) was used in the analysis and display of real-time data, using the single-threshold method for C_q determination. Relative expression for developmental stages and adult organs was calculated using the $2^{-\Delta\Delta Ct}$ method (Livak and Schmittgen, 2001). Developmental stages were normalized to expression data from an equal-proportioned mixture of all 12 embryonic-stage cDNAs produced from the synthesis reaction. Relative expression for adult tissues was normalized to intestinal expression.

4.6. Phylogenetics and protein alignment

Zebrafish amino acids sequences were translated from *ankef1a* and *ankef1b* cloned sequences mentioned above in method 4.2. Our Ankef1a and Ankef1b sequence data were used in both the phylogenetic analysis and protein alignments. Ankef1 amino acid sequences for all non-zebrafish species were: *Xenopus laevis*, frog - NP_001085241.1; *Homo sapiens*, human - NP_071379.3; *Mus musculus*, mouse - NP_783598.1; *Gallus gallus*, chicken - XP_004935298.2; *Ciona savignyi*, solitary sea squirt - ENSCSAVT00000004681; *Ciona intestinalis*, sea vase -

F6ZTU7. Multiple sequence alignment by MUSCLE and pairwise distances were produced by Genious 2019.1. Sequences used in the cladogram construction were aligned using MUSCLE in MEGA7 (Kumar *et al.*, 2018). The evolutionary history was determined using the Neighbor-Joining method (Saitou and Nei, 1987) with 1000 bootstrap replications (Felsenstein, 1985). The JTT matrix-based method was used to calculate evolutionary distances (Jones *et al.*, 1992). Specific domains were checked for homology using the protein sequence alignment function of NCBI-BLAST (Altschul *et al.*, 1990; Altschul and Lipman, 1990).

REAGENT or RESOURCE	SOURCE	IDENTIFIER
Oligonucleotides		
Primer: *ankef1a* forward, without Gateway adapter site (cDNA cloning) - TACAGCTGCTCCTAGAGGCA	Eurofins Genomics	N/A
Primer: *ankef1a* reverse, without Gateway adapter site (cDNA cloning) - TGCAAGCATCTCCTGAAACCT	Eurofins Genomics	N/A
Primer: *ankef1b* forward, without Gateway adapter site (cDNA cloning) - AGGTTTCAGGAGATGCTTGCA	Eurofins Genomics	N/A
Primer: *ankef1b* reverse, without Gateway adapter site (cDNA cloning) - GAAGCTGGCATTGAAGCAGG	Eurofins Genomics	N/A
Primer: *ankef1a* forward (qRT-PCR) - GCAAGCATCTCCTGAAACCTT	Eurofins Genomics	N/A
Primer: *ankef1a* reverse (qRT-PCR) - GTCGTAATGCACGTGGGGTT	Eurofins Genomics	N/A
Primer: *ankef1b* forward (qRT-PCR) - CTCTCCACCATGCTTGCCAT	Eurofins Genomics	N/A
Primer: *ankef1b* reverse (qRT-PCR) - TCGCTCCATTCATTGCCACT	Eurofins Genomics	N/A
Primer: *ef1α* forward (qRT-PCR) – CCTCTTTCTGTTACCTGGCAA	Eurofins Genomics	N/A
Primer: *ef1α* reverse (qRT-PCR) – CTTTTCCTTTCCCATGATTGA	Eurofins Genomics	N/A
Primer: β-*actin* forward (qRT-PCR) – GCTGTTTTCCCCTCCATTGTT	Eurofins Genomics	N/A
Primer: β-*actin* reverse (qRT-PCR) – TCCCATGCCAACCATCACT	Eurofins Genomics	N/A
Primer: *ankef1a* forward (WISH) - TACAGCTGCTCCTAGAGGCA	Eurofins Genomics	N/A
Primer: *ankef1a* reverse (WISH) - AGGTTTCAGGAGATGCTTGCA	Eurofins Genomics	N/A
Primer: *ankef1b* forward (WISH) - TGAGAACGATTCGGCTTGGT	Eurofins Genomics	N/A
Primer: *ankef1b* reverse (WISH) - TTCATTTATTCCTCCCCAGT	Eurofins Genomics	N/A
Recombinant DNA		
ankef1a (full-length) + pCS2-Dest	This paper	N/A
ankef1b (full-length) + pCRII-TOPO	This paper	N/A
ankef1a 3’ UTR ISH probe + pCRII-TOPO	This paper	N/A
ankef1b 3’ UTR ISH probe + pCRII-TOPO	This paper	N/A

Table 3.1: Key resources used in experiments.

Chapter 4

Functional characterization of ankyrin and EF-hand containing protein 1 (Ankef1) in *Danio rerio*

Abstract:

Previous studies on ankef1 function and expression patterns suggest a role in cell protrusion and extension. Widespread expression during gastrulation indicates that ankef1 may play a role in the morphogenetic movements that precede the establishment of the zebrafish body plan. This study uses MO knockdown to probe for a functional role of *ankef1* during early zebrafish development. MO-mediated knockdown of *ankef1a* revealed defects in heart laterality establishment; however, rescue experiments to control for off-target effects were inconclusive. Furthermore, two *ankef1a* KO mutant lines were generated by CRISPR/Cas9 technology in order to provide a robust method for determining functional overlap and compensation that may be occurring between *ankef1* paralogs. We also used in silico structure prediction methods due to a lack of crystallography data on Ankef1. Data from Iterative Threading Assembly Refinement (I-TASSER) provided additional virtual evidence toward the predicted ankyrin—EF-hand—ankyrin domain structure of Ankef1.

1. Introduction:

Eukaryotic cell migration is a critical process that mediates cell movement to a new area (e.g., within an organ or between organs). Wound healing, embryonic development, neutrophil migration, and tumor metastasis are examples of processes that require cells to generate force against the viscous extracellular environment (Katz and Lasek, 1980; Leick *et al.*, 1994). Cells move chemotactically or mechanotactically in response to guidance cues (Yam *et al.*, 2009). Neutrophils migrating through capillaries use these guidance cues, such as interleukin 8 (IL-8), Leukotriene B4 (LTB-4), and interferon γ (IFN-γ), to switch from rolling to amoeboid movement

(Nieminen *et al.*, 2005; Valerius *et al.*, 1983). Upon receiving chemoattractant cues, neutrophils must first polarize in order to move in the correct direction. Cell polarity established the leading and trailing edges of the cell and polarity is mediated by the three most common forms of the Rho family of GTPases: Ras-related C3 botulinum toxin substrate 1 (Rac1), cell division control protein 42 (cdc42), and Ras homolog family member A (RhoA) (Burridge and Wennerberg, 2004; Raftopoulou and Hall, 2004; Wunnenberg-Stapleton *et al.*, 1999). These three Rho GTPases act as protein switches, and each mediates different aspects of cell motility—sheet-like actin-dependent projections on the leading edge (lamellipodia), long cell projections containing actin filaments (filopodia), and contractile actin-myosin II arrangements (stress fibers), respectively. Migrating cells during gastrulation form tight junctions, focal adhesions, and adherens junctions as motile cells participating in involution, convergence and extension (C&E), and epiboly contact other cell types (Kim *et al.*, 1998; Medina *et al.*, 2004; Shimizu *et al.*, 2005; Yamamoto *et al.*, 1998).

Gastrulation establishes the three embryonic germ layers into their appropriate positions through a coordinated serious of morphogenetic processes (Gong and Brandhorst, 1988; Holland, 1976; Smith *et al.*, 1976). Mesoderm is established between the ectoderm (outer surface) and endoderm (inner surface). Furthermore, gastrulation establishes a basic body plan with dorsoventral and anteroposterior symmetries. Zebrafish gastrulation begins at 50%-epiboly, during which the marginal germ ring appears (Hammerschmidt *et al.*, 1996b; Kimmel *et al.*, 1995; Melby *et al.*, 1996). To form the germ ring, the leading edge of the spreading blastoderm involutes upon itself and forms the epiblast and hypoblast. Involution continues during epiboly as the hypoblast spreads toward the animal pole, and the epiblast continues spreading over the remainder of the yolk. As the germ ring begins its involution, a cell aggregation (embryonic shield; ES) is formed by convergence movements and is located at a single position on the germ ring (Cooper and D'Amico, 1996; Warga and Nusslein-Volhard, 1999). The ES defines the dorsal side, and the involuting shield cells become the axial hypoblast. The axial hypoblast extends toward the animal pole through convergence and extension movements (CE) (Rebagliati *et al.*, 1998). Many morphological defects can arise from errors in gastrulation, including fused eyes (one-eyed pinhead; oep), absent notochord (floating head; flh), shortened body axis (trilobite and pipetail; tri and ppt), and an enlarged tailbud (spadetail; spt)(Hammerschmidt *et al.*, 1996b; Solnica-Krezel *et al.*, 1996).

Ankyrin and EF-hand containing protein 1 (ankef1, anr5 in *Xenopus*) is a putative calcium-binding protein that plays a role in mediating cell adhesion and protrusion processes in *Xenopus* (Chung *et al.*, 2007). Anr5 was downregulated in response to SU5402, an FGF-R inhibitor. Morpholino oligonucleotide (MO) knockdown of anr5 caused an irregular Branchet's cleft and shortened tail in injected embryos. Anr5 acts upstream of Rho and is an important paraxial protocadherin (papc) interactor. Papc is a calcium-dependent cell adhesion molecule that is first expressed in the prechordal plate at 30% epiboly and in the paraxial mesoderm at the shield stage. Here, we sought to evaluate the effects of KD via a splice-blocking MO. To reinforce our KD results, we generated KO lines of *ankef1a* via CRISPR/Cas9 in order to use various mutant allele combinations in future studies.

2. **Results and Discussion**

2.1 MO injections

Eleven different clutches were injected with 2.3 nL of a solution consisting of p53/Ankef1aIn2-3_Ex3/Ankef1aEx3In3-4 morpholinos and control groups were set aside for comparison. WISH images of each phenotype are shown in **Fig. 4.3**. The mean percentage of heart laterality phenotypes from the control and MO-injected clutches are displayed in **Fig. 4.2**. All three phenotype groups showed statistically significant differences between control and MO-injected groups (Fig. 4.2). Two clutches from separate parents were injected with *p53* alone, and there was no difference in heart laterality percentages between the control and *p53*-injected groups (data not shown). Mean laterality percentages in the *p53* injected group followed the same trend as the control group from the *ankef1a*/p53 control group. Rescue experiments with *ankef1a* were inconclusive, with only a partial rescue (50% situs solitus, 50% situs medialis); therefore, off-target effects cannot be definitively ruled out (Stainier *et al.*, 2017). The *ankef1a* morpholino sequences were queried against the Ensembl genomic database, which returned *ankef1a* as the top matching gene sequence. WISH staining revealed that *ankef1a* was enriched in the dorsal forerunner cells (Daniel and Panizzi, 2019), which coalesce to form the Kupffer's vesicle, raising the possibility that *ankef1a* does play a role in determining heart laterality.

2.2 Generation of mutant line

Given that our morpholino rescue results could not rule out off-target effects from the *ankef1a* MOs, we sought to create an *ankef1a* mutant line carrying a loss-of-function allele. An *ankef1b* loss-of-function mutant was bought from ZIRC. Amplicon sequences of the six putative CRISPR-edited regions were analyzed for sequence changes near the Cas9 cut site (**Fig. 4.4**). Amplicons with a successful edit contained a string of single chromatogram peaks, followed by double peaks for the rest of the sequence. Double peak sequences were compared to the WT sequence to compile the new sequence at the edited site. Sequences from fin-clipped F_1 adults revealed several edited alleles, including two with early stop codons (Leu54fs*5, Gly93fs*5), as

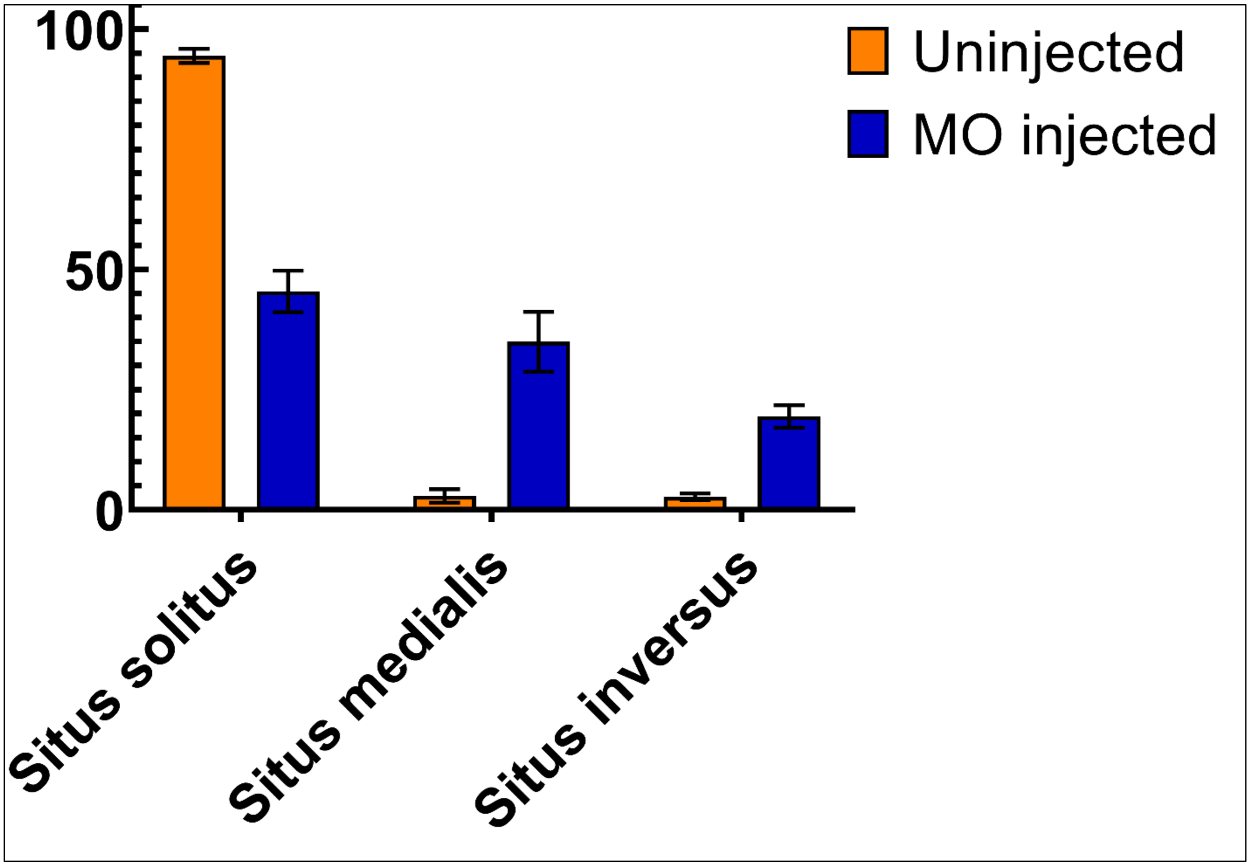

Figure 4.2: Mean heart laterality percentages from control and MO-injected clutches (n = 10 clutches of >100 fertilized embryos) observed at 32 hpf.

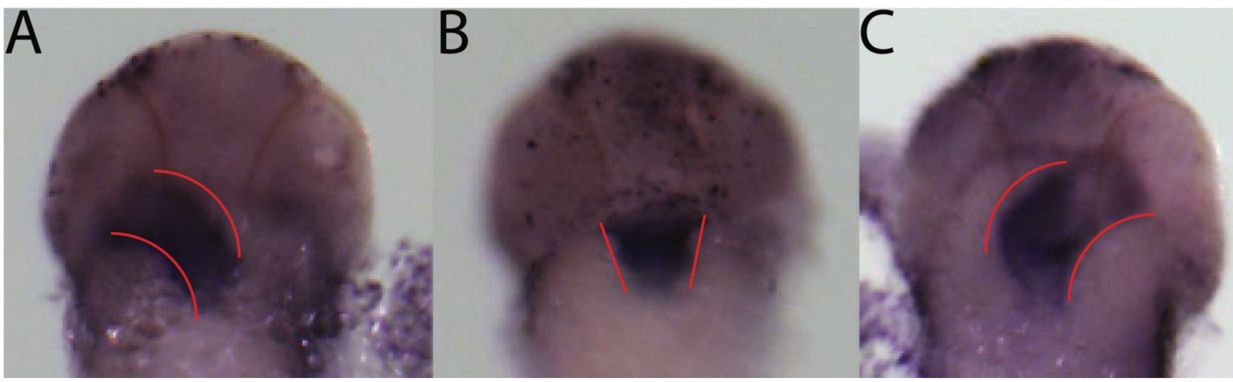

Figure 4.3: Ventral view of 32 hpf embryos labeled with the *cmlc2* ISH probe. Yolks were removed prior to imaging. A. situs inversus, B. situs medialis, C. situs solitus.

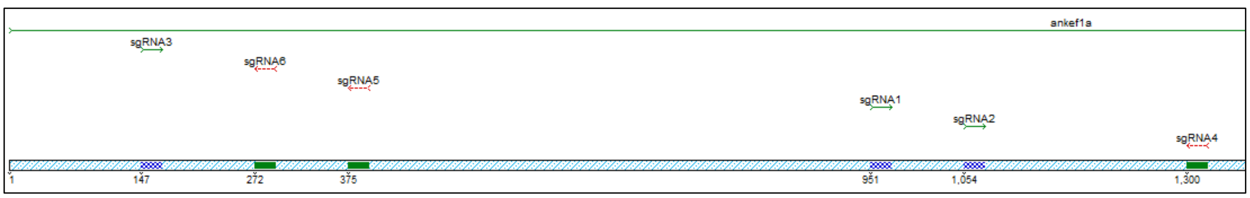

Figure 4.4: Germline KO of ankef1a using nCas9n-nanos3'UTR mRNA. Six sgRNAs were designed to the coding region of *ankef1a* (Daniel and Panizzi, 2019). sgRNA3 and sgRNA6 generated early stop codons.

shown in **Fig. 4.5**. Other edited alleles were in-frame edits, which we did not expect to have deleterious effects as compared to the alleles with early stop codons. F_1 fish carrying the two early stop alleles were outcrossed by the AB (WT) strain to enrich for ankef1a$^{+/-}$ carriers. Furthermore, we crossed the ankef1a$^{+/-}$ F_2 generation by the *ankef1b*$^{+/-}$ (**Fig. 4.6**) mutants to obtain *ankef1a*$^{+/-}$/*ankef1b*$^{+/-}$ offspring. We then searched for restriction sites in the WT and mutated sequences of the amplicons. The Leu54fs*5 mutation induced by sgRNA3 did not have a restriction site near the Cas9 binding site, nor did the WT sequence. However, the sgRNA1 editing site did disrupt an HaeIII recognition site, which provides a genotyping site linked to the upstream sgRNA3 edit. The Gly93fs*5 mutation disrupted an AvaII recognition sequence at the sgRNA6 editing site.

2.3 Structural modeling

Protein sequences translated from cloned coding sequences were submitted to the I-TASSER web server for *in silico* modeling (Roy *et al.*, 2010; Yang *et al.*, 2015; Yang and Zhang, 2015). Neither paralog was predicted to have enzymatic activity. Both Ankef1a and Ankef1b shared significant structural homology (TM-score > 0.5) with human Ankyrin-2 (Ank2), which plays a wide variety of roles across cell types. Ank2 binds dynactin to promote cell motility, and Ank2 has been shown to form a complex with RABGAP1L. The Ank2/RABGAP1L complex recruits PI(3)P-positive early endosomes and thus promotes trafficking to the leading edge of a migrating cell. The high protein promiscuity of Ank2 suggests that Ankef1 may also participate in multiple cellular processes; however, I-TASSER ligand-binding site prediction C-scores for both proteins were very low, indicating random associations. Ankef1 was shown to bind ccdc103 in a mouse Y2H study, and also physically interacted with frog paraxial protocadherin (papc) in a separate study. The I-TASSER models further support that Ankef1a and Ankef1b display the ankyrin-EF-ankyrin domain structure (**Figs. 4.7, 4.8**.). Furthermore, sequence submission to

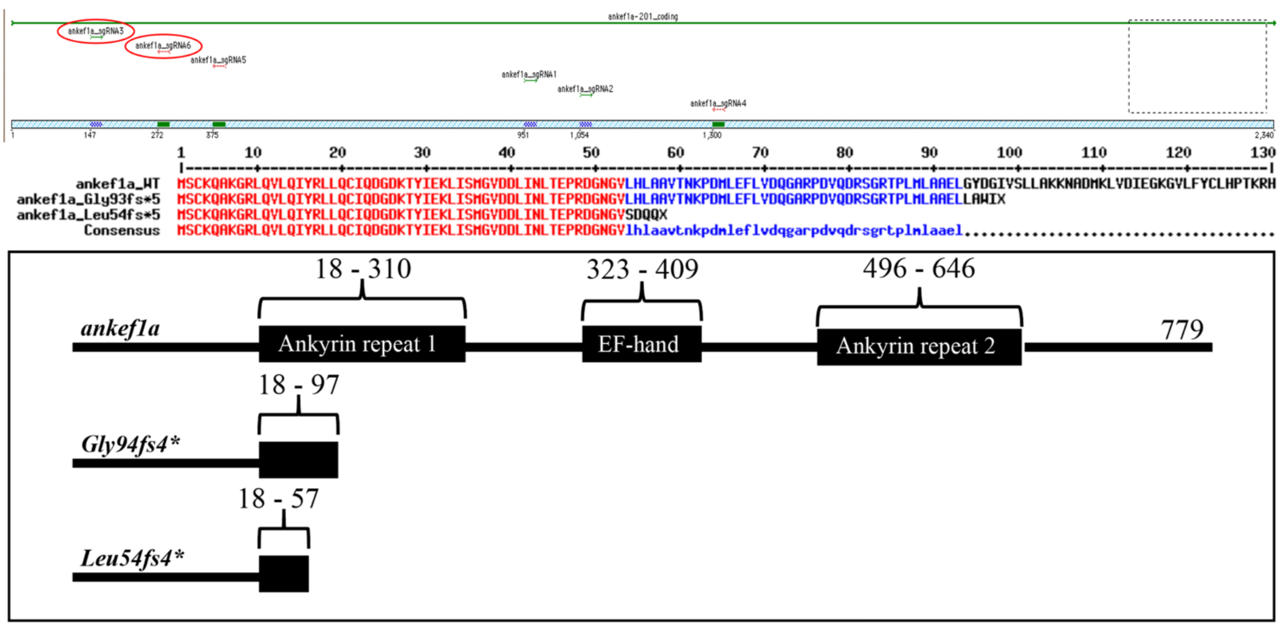

Figure 4.5: Sequence and domain diagrams of WT and CRISPR-edited alleles. Two alleles with premature stop codons introduced at the sgRNA1/3 sites produced truncated proteins as shown above.

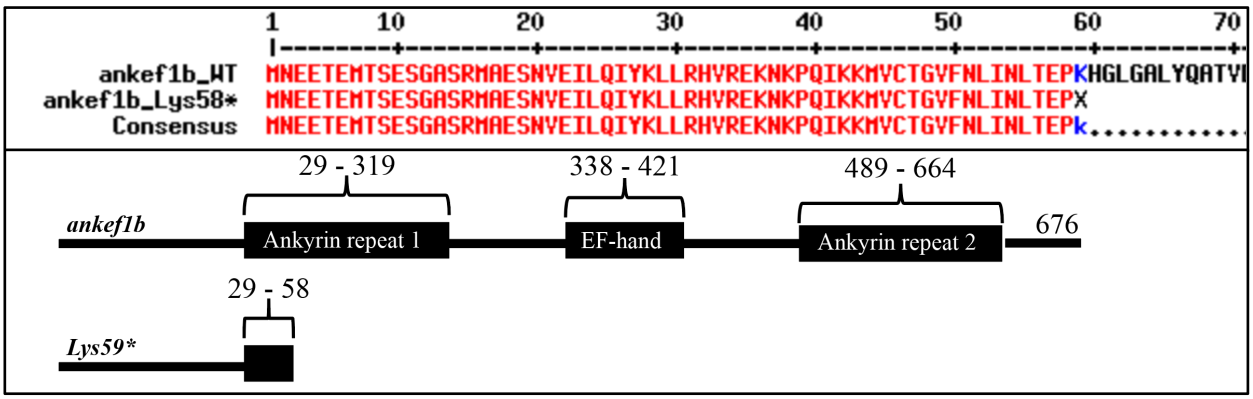

Figure 4.6: Domain schematics of *ankef1b* and *ankef1b*$^{+/-}$ obtained from ZIRC.

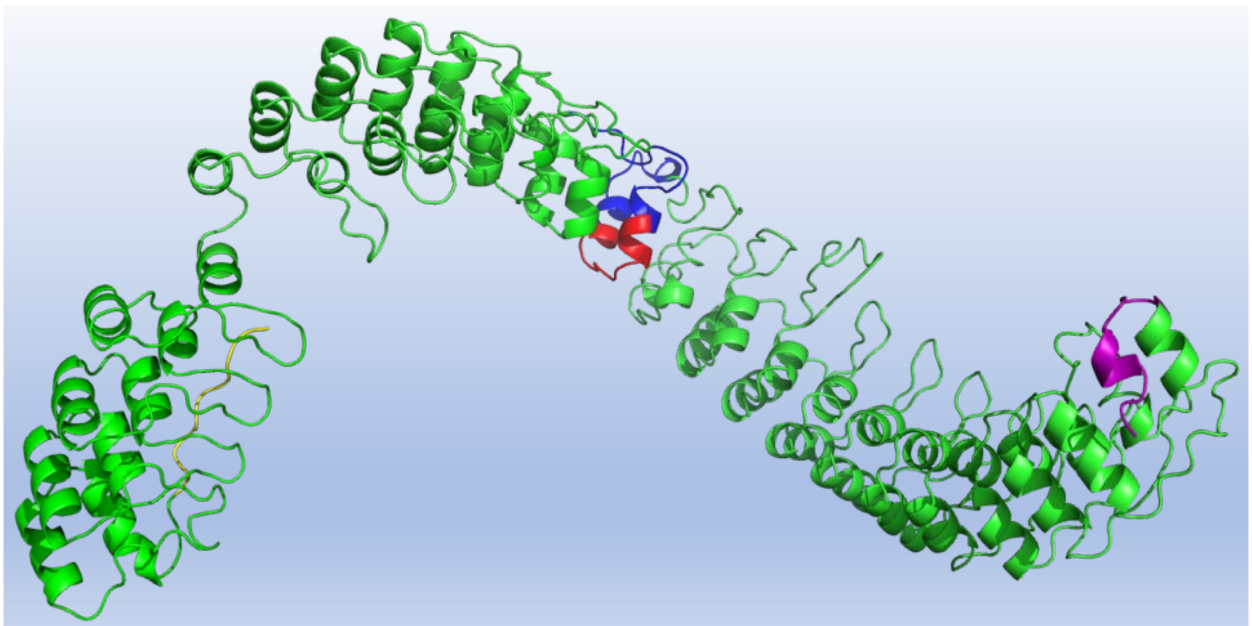

Figure 4.7: Ankef1a structure prediction using I-TASSER. Yellow: N-terminus; purple: C-terminus; green: ankyrin repeats; blue: EF-hand motif; red: calcium-binding region.

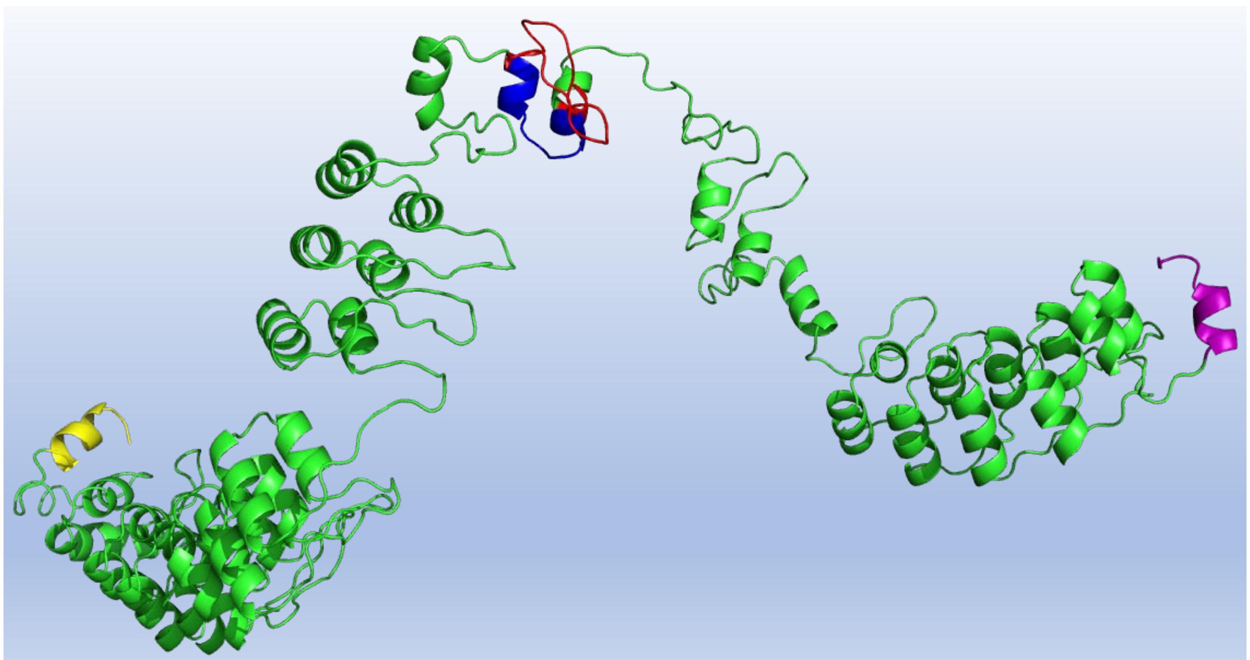

Figure 4.8: Ankef1b structure prediction using I-TASSER. Yellow: N-terminus; purple: C-terminus; green: ankyrin repeats; blue: EF-hand motif; red: calcium-binding region.

PROSITE predicted at least one calcium-binding region within the EF-hand motifs of both proteins.

3. <u>Conclusions</u>

A BLASTn search of the *ankef1a* MO sequences suggest a low probability of off-target effects; however, a successful rescue experiment is the gold standard for providing robust evidence that the MO-induced phenotypes are due to successful *ankef1a* knockdown. Furthermore, genetic compensation from *ankef1b* could mask *ankef1a* knockdown or knockout phenotypes. Expression data for *ankef1a* and *ankef1b* shown in this paper suggests a widespread role throughout zebrafish development. We did however see only *ankef1a* expression in structures related to motile cilia, which supports the hypothesis that *ankef1* plays a role in motile cilia development or function. Transcripts from both genes show almost identical expression patterns in zebrafish embryos (Daniel and Panizzi, 2019), with several exceptions noted above. DFC are the precursors to the laterality-establishing KV in development, thus providing some evidence that we were specifically knocking down *ankef1a* without off-target effects. WISH of MO-injected embryos using other established laterality probes (e.g. *insulin*, *lefty*) could provide further evidence of situs defects. Splice-site targeted MOs revealed abnormal heart looping phenotypes in injected embryos.

Due to inconclusive rescue experiments, we sought to produce and propagate fish containing putative loss-of-function genetic lesions in both genes. An *ankef1b* mutant containing an early stop codon was obtained from ZIRC. Two *ankef1a* mutants with early stop codons were produced using CRISPR/Cas9 technology. Future mating experiments with $ankef1a^{+/-}/ankef1b^{+/-}$, $ankef1a^{-/-}/ankef1b^{+/-}$, and $ankef1a^{+/-}/ankef1b^{-/-}$ combinations will provide more robust evidence toward the role of *ankef1* gene*s* during zebrafish embryonic development. Structural modeling predicted overlapping features and functions between Ankef1a and Ankef1b. Gene ontology for both proteins suggested that they function in protein binding (GO-score > 0.5); however, ontology prediction for biological processes and cellular component were inconclusive. The lack of ligand binding prediction and the inconclusive biological process ontology perhaps suggest that Ankef1 requires increased calcium concentrations to change conformation and thus perform its cellular functions, as shown in *Xenopus* cell reaggregation assays (Chung *et al.*, 2007).

Although a zebrafish Ccdc103 antibody is already available, future functional experiments with zebrafish Ankef1a/b would greatly benefit from the production of polyclonal antibodies for both forms. A recently produced mouse Ankef1 antibody will allow Co-IP studies with untagged proteins, thus eliminating the need for fusion proteins which may not retain their native conformation. Another protein containing ankyrin repeats and an EF-hand domain, transient receptor potential channel A1 (TRPA1), extends an ankyrin repeat string from the cation channel into the intracellular domain (Zayats *et al.*, 2013). An N-terminal EF-hand motif increases its stiffness upon calcium binding, causing an increase in channel permeability. Co-IP experiments with Ankef1 present a similar problem, so calcium concentrations may need to be adjusted to determine the range of concentrations through which Ankef1 possibly interacts with Ccdc103.

4. <u>Materials and Methods</u>

4.1. Zebrafish care and maintenance

Adult wild-type (WT) fish (AB line) were maintained in a circulating system (Aquarius Fish Systems) at ~28.5º C on a 14h/10h light/dark cycle, with other water parameters (pH and conductivity) maintained as previously described (Lawrence, 2007). Embryos were collected from matings and grown in 0.5x E2 media (7.5mM NaCl, 0.25mM KCl, 0.5mM $MgSO_4$, 75µM

KH_2PO_4, 25µM Na_2HPO_4, 0.5mM $CaCl_2$, 0.35mM $NaHCO_3$, pH 7.2-7.6) in a 28.5º C incubator. Embryos were staged according to previous studies (Kimmel *et al.*, 1995). All protocols and experiments used in this paper were monitored and approved by the Auburn University Institutional Animal Care and Use Committee (IACUC).

4.2. Production of nCas9n-nanos 3'UTR mRNA and sgRNA

Guide RNA sequences were designed using the CRISPRscan tool (https://www.crisprscan.org/) with sequence selection guidelines previously established (Moreno-Mateos *et al.*, 2015). The gene-specific DNA oligonucleotides were ordered from Eurofins Genomics and inserted into the pCRII vector via TA cloning for long-term storage after the full-length DNA oligonucleotide was made (K457501, Thermo-Fisher). The full-length sgRNA template was produced via PCR (DreamTaq 2x SuperMix #K1081, Thermo-Fisher), column-purified with the QIAquick PCR purification kit (Qiagen), and used as the DNA template to make the sgRNA via IVT (Ampliscribe-T7 Flash Transcription kit, Epicentre), with all procedures following established protocols (Vejnar *et al.*, 2016b).

pCS2-nCas9n-nanos 3'UTR was a gift from Antonio Giraldez (Addgene plasmid #62542; http://n2t.net/addgene:62542; RRID:Addgene_62542). The supplied bacterial stab was streaked onto LB/ampicillin agarose plates and grown overnight at 37° C. A well-isolated colony was used to inoculate 50 mL LB broth containing carbenicillin 50 µg/mL. The liquid culture was grown overnight at 37° C under a rotation of 225 rpm. A Qiagen (Cat.# 12145) midi kit was used to extract and purify the plasmid, which was then submitted to Eurofins Operons for sequence confirmation. pCS2-nCas9n-nanos 3'UTR was linearized with NotI (New England BioLabs, #R3189) using the manufacturer's protocol. Plasmid concentration and purity was checked on both a 2% agarose gel and a spectrophotometer (DeNovix DS-11). The manufacturer's protocol for IVT was performed with the mMessage mMachine SP6 transcription kit (#AM1340, Thermo-Fisher) using the linearized pCS2-nCas9n-nanos 3'UTR plasmid (300 ng) as the template for SP6 polymerase. The mRNA product was column purified (mini Quick Spin RNA columns, 11814427001, Millipore Sigma), then checked on both a 2% agarose gel and a spectrophotometer to assess purity and concentration.

4.3. Morpholino and CRISPR injection

Microinjections were performed with a Nanoliter 2010 (World Precision Instruments) and dosage accuracy and precision were confirmed with a stage micrometer. All morpholinos (MO) in this paper (**Fig. 4.1**, **Table 4.1**) were designed by and ordered from Gene Tools LLC (Philomath, OR). MOs were stored at 4° C and heated to 65° C just before use to ensure homogeneity. The MO mixture consisted of 1:4 dilutions of three MOs (*p53*, Ankef1aIn2-3_Ex3, Ankef1aEx3In3-4) with stock concentrations of 8.47 ng/nL, and ultrapure water. *P53* was included to eliminate potential *ankef1a* MO-mediated toxicity. Embryos were injected with ~2.3 nL of the MO solution into the blastodisc-yolk interface at the 1-cell stage. For germline editing with CRISPR/Cas9, 1-cell embryos were injected with ~2.3 nL of a solution containing 200 pg of the nCas9n-*nanos* 3'UTR mRNA and 15 pg of each of the six sgRNAs produced in 3.2 (see Figure 4.4 for sgRNA sites).

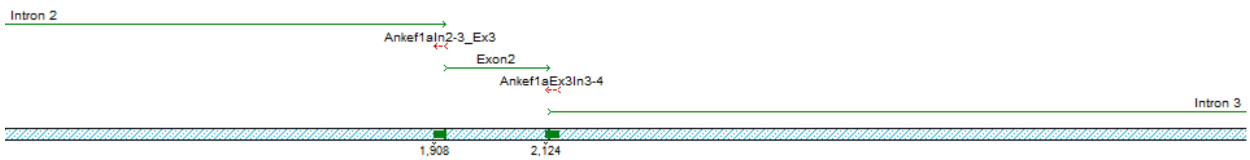

Figure 4.1: Location of *ankef1a* splice-blocking morpholinos.

Oligo name	Sequence
Ankef1a sgRNA1	taatacgactcactataGGGAGGCACGAATGGGCCATgttttagagctagaa
Ankef1a sgRNA2	taatacgactcactataGGAGTAGAGTTTGTGCCCAAgttttagagctagaa
Ankef1a sgRNA3	taatacgactcactataGGGCAATGGGGTCCTGCACTgttttagagctagaa
Ankef1a sgRNA4	taatacgactcactataGGGACTGTACAGATGGGCAAgttttagagctagaa
Ankef1a sgRNA5	taatacgactcactataGGCGCATGTGTCTTTTGGTGgttttagagctagaa
Ankef1a sgRNA6	taatacgactcactataGGTACCATCATATCCAAGTTgttttagagctagaa
p53 MO	GCGCCATTGCTTTGCAAGAATTG
Ankef1aIn2-3_Ex3	ACGCCTGGCAGAGAAGCCACAGTAC
Ankef1aEx3In3-4	ATTACACCATTTGCATACCTGAT

Table 4.1: sgRNA and morpholino sequences.

4.4. Crispant PCR and sequencing

Primers flanking the sgRNA target sites within *ankef1a* (**Table 4.1**) were designed using Primer3 Plus (Untergasser *et al.*, 2012a), checked for specificity via the NCBI-BLASTn tool (Altschul, Gish, Miller, Myers, & Lipman, 1990) (Altschul *et al.*, 1990), and ordered from Eurofins Genomics. Crispants were grown to adult stage (F_0 generation) and outcrossed with an AB strain to obtain *ankef1a*$^{+/-}$ offspring. To spot-check for successful germline edits, genomic DNA was extracted from individual 5 dpf F_1 embryos using lysis buffer (10 mM TrisCl pH 8.3; 50 mM KCl; 0.3% Tween20; 0.3% Nonidet40; 0.5 mg/mL Proteinase K), incubated overnight at 55° C. DreamTaq 2x SuperMix (Thermo Fisher Scientific K9011) was used to amplify a 100-200 bp region centered on the putative Cas9 cut sites within *ankef1a*, using 1 µL genomic DNA as the template in a 25 µL reaction (Table 4.2). In addition to standard PCR conditions recommended for DreamTaq, the following *ankef1a*-specific protocol (T100, Bio-Rad) was used: 58° C annealing, 1-minute extension, 35 cycles. Amplicons were column purified with the QIAquick PCR cleanup kit (Qiagen, 28104). Amplicon sequences were verified by Sanger sequencing (Eurofins Genomics) using T7/SP6 promoters contained in the primer sequences). Amplicon sequences were visualized with the Sequencher sequence analysis software (version 5.4.6). Fin clips were obtained from adults of the F_1 generation in order to screen for the presence of edited *ankef1a* alleles. Each of the six putative edit sites was amplified with DreamTaq 2x SuperMix and Cas9 site amplicons submitted for Sanger sequencing. Results were visualized with Sequencher. F_1 fish carrying deleterious mutant alleles were outcrossed with the AB strain to obtain 50% *ankef1a*$^{+/-}$ offspring. Fin clips on adult F_2 offspring were again used to screen for carriers of the mutant allele, as described above.

Primer	Sequence
Ankef1a sgRNA1 check F	GACTTTCCATGCAGCCGTT
Ankef1a sgRNA1 check R	AGTTTGTGCCCAAGGGAACA
Ankef1a sgRNA2 check F	GCTTCATGACTGGTCTCATG
Ankef1a sgRNA2 check R	TAAATATAAACGACTTCTTAAGAGGT
Ankef1a sgRNA3 check F	GCAAACAGGCCAAAGGAAGG
Ankef1a sgRNA3 check R	CCAACAAACCCGACATGCTG
Ankef1a sgRNA4 check F	GCTTCCTATGGGCCGAAGAA
Ankef1a sgRNA4 check R	CAGCATGCTACAGACACCCA
Ankef1a sgRNA5 check F	CGTGCTCTTCTACTGCCTCC
Ankef1a sgRNA5 check R	AGAGAGGAGCAGACCCCAAT
Ankef1a sgRNA6 check F	CATGGGTGTTGACGACCTCA
Ankef1a sgRNA6 check R	CATGGGTGTTGACGACCTCA

Table 4.2: Sequences of primer pairs used to amplify and sequence amplicons containing *ankef1a* sgRNA edit sites.

For genotyping *ankef1a*$^{+/-}$ offspring or adults, restriction digests were used on amplicons from the sgRNA1 and sgRNA6 edited sites, which correspond to the Leu54fs*5 and Gly93fs*5 mutants, respectively. HaeIII was used to digest the sgRNA1 site amplicons, and AvaII was used with sgRNA6 site amplicons. Digests were performed overnight according to the manufacturer's protocol. The digest products were analyzed on a 2.0% agarose gel. Ankef1b genotyping was performed by amplifying a short section centered on the mutation. Amplicons were run on a 2.0% agarose gel, gel-purified (Qiaquick gel extraction kit, Qiagen), and submitted for Sanger sequencing.

4.5. Statistics on MO injections

Distributions of each heart looping phenotype (situs solitus, situs medialis, and situs inversus) in control and injected groups (n = 10 replicates) were tested for normality and lognormality using the Shapiro-Wilk and Kolmogorov-Smirnov tests. Each phenotype was tested pairwise (control vs. injected) using the Mann-Whitney signed ranks nonparametric test using $\alpha = 0.01$. Prism 8.4 was used for graphing and all statistical calculations.

4.6. Whole-mount in situ hybridization

Sequences of plasmids containing the *cmlc2* ISH probe (a kind gift from Dr. Lilianna Solnica-Krezel at Washington University in St. Louis) were verified by Sanger sequencing (Eurofins Operon). The antisense (NotI restriction enzyme digest/T7 polymerase) probe for *cmlc2 was* synthesized from a linearized plasmid with digoxigenin-labeled NTPs, according to the manufacturer's protocol (Sigma-Aldrich 11277065910). MO-injected embryos from the AB strain were fixed in 4% PFA + PBS, and the WISH protocol was performed as previously established (Thisse and Thisse, 2008). Whole-mount embryos were examined with an Olympus MVX10 stereomicroscope equipped with a DP74 digital camera. Images were then obtained using the CellSens software package.

4.7. Structural modeling

We submitted the Ankef1a and Ankef1b amino acid sequences to the I-TASSER server to model possible protein structures, using default settings. Protein structures were viewed using PyMOL (The PyMOL Molecular Graphics System, Version 2.0 Schrödinger, LLC). The Ankef1a and Ankef1b amino acid sequences were submitted to the PROSITE motif prediction tool. PyMOL was also used to color various features of both proteins.

Chapter 5: Conclusions and Future Directions

<u>Research problem summary</u>:

Motile ciliogenesis requires the attachment of dynein arms to axonemal microtubules using ccdc103 as an adapter. Functional and structural data from previous studies (King and Patel-King, 2019; Panizzi *et al.*, 2012) show that Ccdc103 is a dynein adapter which binds microtubules at regular intervals; however, little is known about its regulation or broader cellular context. This study was designed to identify and characterize putative ccdc103 interactors. Data from our Y2H study yielded 14 possible ccdc103 interactors. We selected *ankef1* for further study on the basis of its dearth of molecular data, as well as its relevance to human health. Interestingly, the only ankef1 direct functional data comes from its link to cell adhesion and protrusion processes in *Xenopus laevis* (Chung *et al.*, 2007). In the same study, an FGFR inhibitor induced downregulation of *ankef1* transcripts, which could be rescued by injection with RhoA mRNA. Finally, the Chung *et al*. study demonstrated a physical interaction and cellular colocalization between Papc (paraxial protocadherin; protocadherin-8) and Ankef1. No evidence has yet been found for a direct functional link between ankef1 and ccdc103. Furthermore, a knowledge gap exists in molecular evidence for zebrafish ankef1 expression and function. Here, we hypothesized that expression data would show that *ankef1* is expressed throughout zebrafish development. In terms of function, we expected to see that *ankef1* transcripts are enriched in tissues with motile cilia. Finally, we hypothesized that loss-of-function studies would show phenotypes related to motile cilia dysfunction (i.e. curved tail, kidney cysts, situs defects, hydrocephalus).

<u>Approach summary</u>:

In this study, we sought to uncover candidates for the interactome of ccdc103. A yeast-two-hybrid assay with a mouse cDNA library identified Ankef1 as a putative Ccdc103 interactor. Given that our downstream functional modeling of *ankef1* would be performed in zebrafish, we first characterized *ankef1* expression in the developing embryo and in adult organs using WISH and RT-qPCR. Splice- and ATG-blocking MOs were used to study *ankef1* LoF phenotypes in developing embryos. We also generated *ankef1a* KO mutants through the CRISPR/Cas9 system, which will provide maternal-zygotic mutant data when paired with our purchased *ankef1b* KO mutant line.

Discussion:

Identification of ccdc103 interactors

Our Y2H study uncovered 14 potential ccdc103 interactors, 12 of which were successfully subcloned into plasmid vectors using zebrafish embryo cDNA. Ankef1 was selected for further expression and functional analysis in zebrafish based on several lines of molecular evidence linking it to motile cilia. Mouse Ankef1 localized to motile cilia in cultured tracheal MCC (Hoh *et al.*, 2012). RNA-Seq data also showed that ankef1 transcripts are enriched in the human testis (Fagerberg *et al.*, 2014), an organ with high levels of ciliogenesis. Conserved synteny and protein structure suggested that zebrafish Ankef1 function is similar to its mammalian counterparts. Further co-IP studies with mouse Ccdc103 and Ankef1 proteins should be done to validate the mouse Ccdc103 Y2H data. While antibodies for Ankef1a and Ankef1b are not yet available for zebrafish, co-IP experiments with various tagged proteins (His, FLAG, etc.) would be the best available option for testing interactions in zebrafish.

Expression patterns of ankef1

The results presented here provide groundwork knowledge of *ankef1* spatiotemporal expression patterns in both embryos and adult zebrafish, as well as mutant lines for further studies of the role of *ankef1* paralogs during zebrafish embryonic development. Our Y2H study and subsequent WISH and qPCR results, as well as studies by other groups, suggest a link to motile cilia. Expression studies of *ankef1* in zebrafish embryos revealed widespread expression during the first 24 hours of development, with expression restricted to the otic vesicles after organogenesis (Daniel and Panizzi, 2019). Our expression studies demonstrated widespread *ankef1a/b* expression during gastrulation and somitogenesis. During those stages, constant morphogenetic movements, which involve cell adhesion and protrusion processes, occur until the basic body plan is established.

In the frog, paraxial protocadherin (papc/pcdh8) was shown to colocalize and physically interact with ankef1 (Chung *et al.*, 2007), so we expected to see some overlap between their expression patterns. In zebrafish, *papc* is highly expressed in the paraxial mesoderm during gastrulation (Yamamoto *et al.*, 1998), in the tail during segmentation (Weidinger *et al.*, 1999; Yamamoto *et al.*, 1998), and in the retina after 24 hpf (Thisse and Thisse, 2005). The *ankef1* developmental expression pattern did not overlap with *papc* in stages past 3 dpf. Likewise, *ankef1* was ubiquitously expressed until 24 hpf, which did not fit the pattern of *papc* expression during this period; however, ankef1 is expressed in the zebrafish retina at 48 hpf, so some *papc* and *ankef1* colocalization may be present during development. Conversely, *ankef1* and *ccdc103* shared some important expression features. *Ankef1a* and *ccdc103* are enriched in the DFC and otic placode (Daniel and Panizzi, 2019; Panizzi *et al.*, 2012), two structures featuring motile cilia. *Ankef1b* was not seen in either structure, suggesting functional divergence between *ankef1a* and *ankef1b*.

Conclusion: Possible ankef1 functions in zebrafish

High expression of *ankef1* in the testes of zebrafish, mouse, and humans suggests a conserved role in vertebrates. Likewise, conserved synteny and amino acid sequences strengthen the idea that zebrafish and human *ankef1* likely share functional roles. Genome duplication in zebrafish led to two ankef1 paralogs. Their overlapping expression patterns suggest strong functional redundancy; however, ankef1a splice-blocking MO knockdown did result in heart looping dysfunction. Heart laterality dysfunction may be related to the ankef1a-specific expression in DFC, which precede KV. Heart loop laterality is mediated by motile cilia that line Kupffer's vesicle (KV), which generates asymmetric Nodal signaling. Conversely, overexpression of ankef1a did not cause any observable morphological defects; however, Anr5 overexpression in *Xenopus* embryos did produce similar phenotypes seen with MO KD, indicating that proper Anr5/Ankef1 function may be dose-dependent and our mRNA dose was too low to cause morphological defects. We were unable to knock down *ankef1b*, as the full coding sequence was not available until it was clarified in this study.

Paraxial protocadherin (papc/pcdh8), along with ankef1, has been shown to mediate tissue separation processes in the frog (Chung *et al.*, 2007; Kim *et al.*, 1998; Nutt *et al.*, 2001). Multiple protocadherins are also expressed in the adult rat testis along with ankef1 (Yu *et al.*, 2014), which suggests that both proteins may play a role in testis function. Spermatozoa use a motile cilium (also called a flagella) to generate forward motion, thus ankef1 could play a role during the formation of these cilia. Given the close interaction between the developing sperm and Sertoli cells, Ankef1 may also be involved in the separation of Sertoli cells as sperm move to the lumen. Further studies on *ankef1* expression and localization patterns in mouse and zebrafish testes would provide important evidence toward its role in testis function. Additionally, the interaction data between Ccdc103 and Ankef1 presented here also raise the possibility that Ankef1 could play a role in motile cilia (i.e. sperm tail) formation during spermatogenesis. Ankef1 may interact with other protocadherins during development, so it would be interesting to perform interaction studies between zebrafish ankef1 and protocadherin proteins. **Fig. 5.1** depicts a potential pathway through which Ankef1 may act in vertebrates. Furthermore, protocadherins are associated with several cancers, including those of the colon (Hinkel *et al.*, 2012; Ose *et al.*, 2012), liver (Okazaki *et al.*, 2002), and prostate (Giannakopoulos *et al.*, 2007; Shishodia *et al.*, 2019).

Ankef1 and *ccdc103* transcripts are both enriched in testis tissue. Future studies should include immunostaining of zebrafish, assuming a zebrafish antibody is available, and mouse testes. Without zebrafish Ankef1 antibodies, mouse testes are the best option for analyzing colocalization with Ccdc103; however, various crosses our stable *ankef1a/b* zebrafish KO lines will allow us to assay for sperm morphology and motility. Functional studies on the role of Ankef1 in mammalian and piscine testes will provide insights into additional mechanisms that may lead to infertility. Furthermore, given the link between *ankef1* and prostate cancer in humans, future studies in zebrafish will provide critical evidence toward clarifying its potential role in human homeostasis and pathology.

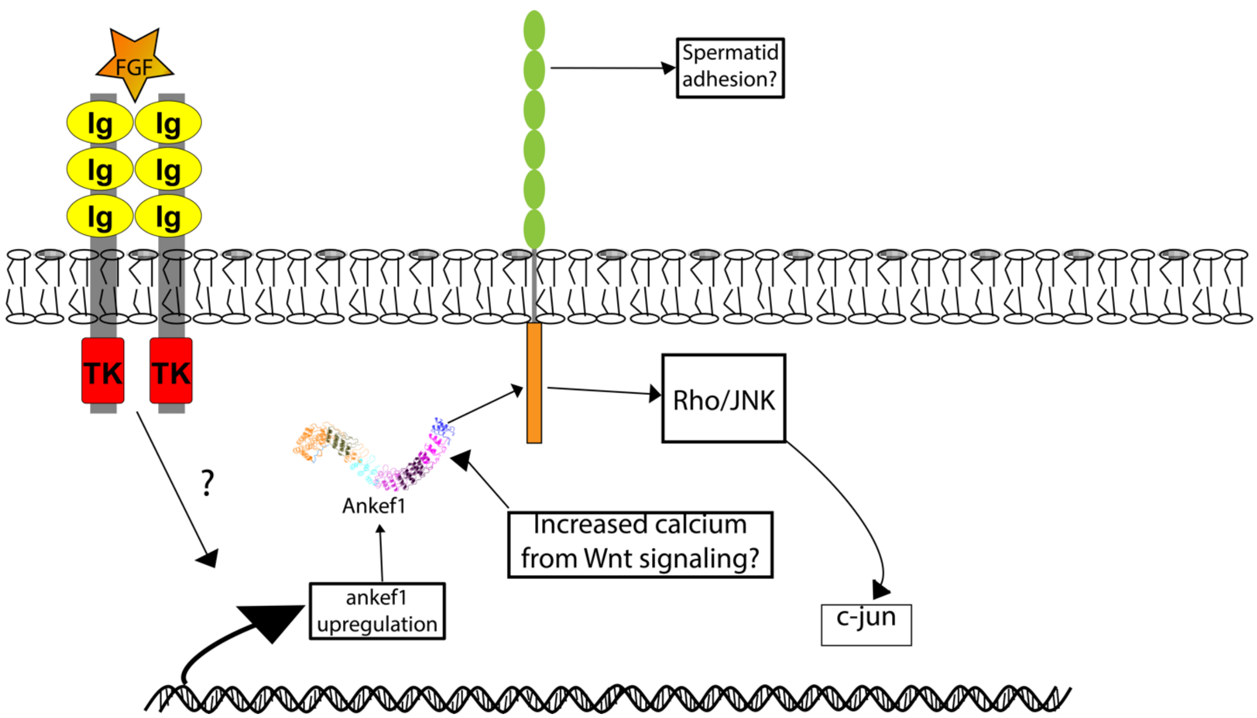

Figure 5.1: Suggested model through which Ankef1 regulates cell adhesion in the frog testis. FGF binds to FGF-R (an Ig-like receptor with tyrosine kinase activity). The FGF receptor then activates the Ras-ERK pathway, which may upregulate ankef1 transcription. Increased calcium may also bind to the EF-hand domain and induce a conformational change in Ankef1. Ankef1 has been shown to interact with protocadherin in the frog. Protocadherin could then mediate spermatid adhesion in the testis through Rho and JNK activation.

REFERENCES

Abecasis, G.R., Altshuler, D., Auton, A., Brooks, L.D., Durbin, R.M., Gibbs, R.A., Hurles, M.E., and McVean, G.A. (2010). A map of human genome variation from population-scale sequencing. Nature *467*, 1061-1073.

Ablain, J., Durand, E.M., Yang, S., Zhou, Y., and Zon, L.I. (2015). A CRISPR/Cas9 vector system for tissue-specific gene disruption in zebrafish. Dev Cell *32*, 756-764.

Ablain, J., and Zon, L.I. (2016). Tissue-specific gene targeting using CRISPR/Cas9. Methods Cell Biol *135*, 189-202.

Abudayyeh, O.O., Gootenberg, J.S., Essletzbichler, P., Han, S., Joung, J., Belanto, J.J., Verdine, V., Cox, D.B.T., Kellner, M.J., Regev, A*., et al.* (2017). RNA targeting with CRISPR-Cas13. Nature *550*, 280-284.

Afzelius, B.A. (1961). The fine structure of the cilia from ctenophore swimming-plates. J Biophys Biochem Cytol *9*, 383-394.

Afzelius, B.A. (1976). A human syndrome caused by immotile cilia. Science *193*, 317-319.

Afzelius, B.A., Eliasson, R., Johnsen, O., and Lindholmer, C. (1975). Lack of dynein arms in immotile human spermatozoa. J Cell Biol *66*, 225-232.

Altschul, S.F., Gish, W., Miller, W., Myers, E.W., and Lipman, D.J. (1990). Basic local alignment search tool. J Mol Biol *215*, 403-410.

Altschul, S.F., and Lipman, D.J. (1990). Protein database searches for multiple alignments. Proc Natl Acad Sci U S A *87*, 5509-5513.

Amsterdam, A., Burgess, S., Golling, G., Chen, W., Sun, Z., Townsend, K., Farrington, S., Haldi, M., and Hopkins, N. (1999). A large-scale insertional mutagenesis screen in zebrafish. Genes Dev *13*, 2713-2724.

Aragon, L. (2018). The Smc5/6 Complex: New and Old Functions of the Enigmatic Long-Distance Relative. Annu Rev Genet *52*, 89-107.

Araki, M., Watanabe, K., and Yasuda, K. (1984). Immunocytochemical localization of rhodopsin-like immunoreactivity in the outer segments of the rods and single cones of chick retina. Cell Struct Funct *9*, 1-12.

Armstrong, M.E., and Thomas, C.P. (2019). Diagnosis of monogenic chronic kidney diseases. Curr Opin Nephrol Hypertens *28*, 183-194.

Arsov, T., Silva, D.G., O'Bryan, M.K., Sainsbury, A., Lee, N.J., Kennedy, C., Manji, S.S., Nelms, K., Liu, C., Vinuesa, C.G.*, et al.* (2006). Fat aussie--a new Alstrom syndrome mouse showing a critical role for ALMS1 in obesity, diabetes, and spermatogenesis. Mol Endocrinol *20*, 1610-1622.

Auer, T.O., and Del Bene, F. (2014). CRISPR/Cas9 and TALEN-mediated knock-in approaches in zebrafish. Methods *69*, 142-150.

Avasthi, P., and Marshall, W.F. (2012). Stages of ciliogenesis and regulation of ciliary length. Differentiation *83*, S30-42.

Barnes, B.G. (1961). Ciliated secretory cells in the pars distalis of the mouse hypophysis. J Ultrastruct Res *5*, 453-467.

Barrangou, R., Fremaux, C., Deveau, H., Richards, M., Boyaval, P., Moineau, S., Romero, D.A., and Horvath, P. (2007). CRISPR provides acquired resistance against viruses in prokaryotes. Science *315*, 1709-1712.

Baxendale, S., van Eeden, F., and Wilkinson, R. (2017). The Power of Zebrafish in Personalised Medicine. Adv Exp Med Biol *1007*, 179-197.

Baxter, G.T., and Morse, D.E. (1992). Cilia from Abalone Larvae Contain a Receptor-Dependent G Protein Transduction System Similar to that in Mammals. Biol Bull *183*, 147-154.

Biswas, P., Chavali, V.R., Agnello, G., Stone, E., Chakarova, C., Duncan, J.L., Kannabiran, C., Homsher, M., Bhattacharya, S.S., Naeem, M.A., *et al.* (2016). A missense mutation in ASRGL1 is involved in causing autosomal recessive retinal degeneration. Hum Mol Genet *25*, 2483-2497.

Bitgood, M.J., and McMahon, A.P. (1995). Hedgehog and Bmp genes are coexpressed at many diverse sites of cell-cell interaction in the mouse embryo. Dev Biol *172*, 126-138.

Bitgood, M.J., Shen, L., and McMahon, A.P. (1996). Sertoli cell signaling by Desert hedgehog regulates the male germline. Curr Biol *6*, 298-304.

Blackburn, K., Bustamante-Marin, X., Yin, W., Goshe, M.B., and Ostrowski, L.E. (2017). Quantitative Proteomic Analysis of Human Airway Cilia Identifies Previously Uncharacterized Proteins of High Abundance. J Proteome Res *16*, 1579-1592.

Blechman, J., Anbalagan, S., Matthews, G.G., and Levkowitz, G. (2018). Genome Editing Reveals Idiosyncrasy of CNGA2 Ion Channel-Directed Antibody Immunoreactivity Toward Oxytocin. Front Cell Dev Biol *6*, 117.

Blum, J.J. (1971). Existence of a breaking point in cilia and flagella. J Theor Biol *33*, 257-263.

Blyth, M., and Wellesley, D. (2008). Ectopic pregnancy in primary ciliary dyskinesia. J Obstet Gynaecol *28*, 358.

Boisvieux-Ulrich, E., Laine, M.C., and Sandoz, D. (1985). The orientation of ciliary basal bodies in quail oviduct is related to the ciliary beating cycle commencement. Biol Cell *55*, 147-150.

Bolotin, A., Quinquis, B., Sorokin, A., and Ehrlich, S.D. (2005). Clustered regularly interspaced short palindrome repeats (CRISPRs) have spacers of extrachromosomal origin. Microbiology *151*, 2551-2561.

Brand, M., Heisenberg, C.P., Warga, R.M., Pelegri, F., Karlstrom, R.O., Beuchle, D., Picker, A., Jiang, Y.J., Furutani-Seiki, M., van Eeden, F.J.*, et al.* (1996). Mutations affecting development of the midline and general body shape during zebrafish embryogenesis. Development *123*, 129-142.

Breslow, D.K., Hoogendoorn, S., Kopp, A.R., Morgens, D.W., Vu, B.K., Kennedy, M.C., Han, K., Li, A., Hess, G.T., Bassik, M.C.*, et al.* (2018). A CRISPR-based screen for Hedgehog signaling provides insights into ciliary function and ciliopathies. Nat Genet *50*, 460-471.

Breuer, D.K., Yashar, B.M., Filippova, E., Hiriyanna, S., Lyons, R.H., Mears, A.J., Asaye, B., Acar, C., Vervoort, R., Wright, A.F.*, et al.* (2002). A comprehensive mutation analysis of RP2 and RPGR in a North American cohort of families with X-linked retinitis pigmentosa. Am J Hum Genet *70*, 1545-1554.

Burger, A., Lindsay, H., Felker, A., Hess, C., Anders, C., Chiavacci, E., Zaugg, J., Weber, L.M., Catena, R., Jinek, M.*, et al.* (2016). Maximizing mutagenesis with solubilized CRISPR-Cas9 ribonucleoprotein complexes. Development *143*, 2025-2037.

Burns, M.A., Liao, Z.W., Yamagata, N., Pouliot, G.P., Stevenson, K.E., Neuberg, D.S., Thorner, A.R., Ducar, M., Silverman, E.A., Hunger, S.P.*, et al.* (2018). Hedgehog pathway mutations drive oncogenic transformation in high-risk T-cell acute lymphoblastic leukemia. Leukemia *32*, 2126-2137.

Burridge, K., and Wennerberg, K. (2004). Rho and Rac take center stage. Cell *116*, 167-179.

Bush, A., Cole, P., Hariri, M., Mackay, I., Phillips, G., O'Callaghan, C., Wilson, R., and Warner, J.O. (1998). Primary ciliary dyskinesia: diagnosis and standards of care. Eur Respir J *12*, 982-988.

Bush, L.A., Herr, J.C., Wolkowicz, M., Sherman, N.E., Shore, A., and Flickinger, C.J. (2002). A novel asparaginase-like protein is a sperm autoantigen in rats. Mol Reprod Dev *62*, 233-247.

Bustin, S.A., Benes, V., Garson, J.A., Hellemans, J., Huggett, J., Kubista, M., Mueller, R., Nolan, T., Pfaffl, M.W., Shipley, G.L*., et al.* (2009). The MIQE guidelines: minimum information for publication of quantitative real-time PCR experiments. Clin Chem *55*, 611-622.

Buttitta, L., Mo, R., Hui, C.C., and Fan, C.M. (2003). Interplays of Gli2 and Gli3 and their requirement in mediating Shh-dependent sclerotome induction. Development *130*, 6233-6243.

Cao, L., Li, L., Li, Y., Zhuang, J., Chen, Y., Wang, Y., Shi, Y., Chen, J., Zhu, X., Wan, Y*., et al.* (2018). Loss of the Nodal modulator Nomo results in chondrodysplasia in zebrafish. Curr Mol Med *18*, 448-458.

Carrillo-Rosas, S., Weber, C., Fievet, L., Messaddeq, N., Karam, A., and Trottier, Y. (2019). Loss of zebrafish Ataxin-7, a SAGA subunit responsible for SCA7 retinopathy, causes ocular coloboma and malformation of photoreceptors. Hum Mol Genet *28*, 912-927.

Casadei, R., Pelleri, M.C., Vitale, L., Facchin, F., Lenzi, L., Canaider, S., Strippoli, P., and Frabetti, F. (2011). Identification of housekeeping genes suitable for gene expression analysis in the zebrafish. Gene Expr Patterns *11*, 271-276.

Chassaing, N., Davis, E.E., McKnight, K.L., Niederriter, A.R., Causse, A., David, V., Desmaison, A., Lamarre, S., Vincent-Delorme, C., Pasquier, L., *et al.* (2016). Targeted resequencing identifies PTCH1 as a major contributor to ocular developmental anomalies and extends the SOX2 regulatory network. Genome Res *26*, 474-485.

Chekuri, A., Guru, A.A., Biswas, P., Branham, K., Borooah, S., Soto-Hermida, A., Hicks, M., Khan, N.W., Matsui, H., Alapati, A., *et al.* (2018). IFT88 mutations identified in individuals with non-syndromic recessive retinal degeneration result in abnormal ciliogenesis. Human genetics *137*, 447-458.

Chen, Y., Wu, B., Xu, L., Li, H., Xia, J., Yin, W., Li, Z., Shi, D., Li, S., Lin, S., *et al.* (2012). A SNX10/V-ATPase pathway regulates ciliogenesis in vitro and in vivo. Cell Res *22*, 333-345.

Cheong, A., Degani, R., Tremblay, K.D., and Mager, J. (2019). A null allele of Dnaaf2 displays embryonic lethality and mimics human ciliary dyskinesia. Hum Mol Genet *28*, 2775-2784.

Chiang, C., Litingtung, Y., Lee, E., Young, K.E., Corden, J.L., Westphal, H., and Beachy, P.A. (1996). Cyclopia and defective axial patterning in mice lacking Sonic hedgehog gene function. Nature *383*, 407-413.

Choi, Y.J., Lee, D.H., Choi, M.G., Lee, S.J., Kim, S.K., Song, G.A., Rhee, P.L., Jung, H.Y., Kang, D.H., Lee, Y.C., *et al.* (2017). Evaluation of the Efficacy and Safety of DA-9601 versus Its New Formulation, DA-5204, in Patients with Gastritis: Phase III, Randomized, Double-Blind, Non-Inferiority Study. J Korean Med Sci *32*, 1807-1813.

Chung, H.A., Yamamoto, T.S., and Ueno, N. (2007). ANR5, an FGF target gene product, regulates gastrulation in Xenopus. Curr Biol *17*, 932-939.

Clyman, M.J. (1966). Electron microscopy of the human fallopian tube. Fertil Steril *17*, 281-301.

Cole, D.G., Diener, D.R., Himelblau, A.L., Beech, P.L., Fuster, J.C., and Rosenbaum, J.L. (1998). Chlamydomonas kinesin-II-dependent intraflagellar transport (IFT): IFT particles contain proteins required for ciliary assembly in Caenorhabditis elegans sensory neurons. J Cell Biol *141*, 993-1008.

Cong, L., Ran, F.A., Cox, D., Lin, S., Barretto, R., Habib, N., Hsu, P.D., Wu, X., Jiang, W., Marraffini, L.A., *et al.* (2013). Multiplex genome engineering using CRISPR/Cas systems. Science *339*, 819-823.

Cooper, L.A., Stringer, A.M., and Wade, J.T. (2018). Determining the Specificity of Cascade Binding, Interference, and Primed Adaptation In Vivo in the Escherichia coli Type I-E CRISPR-Cas System. mBio *9*, e02100-02117.

Cooper, M.S., and D'Amico, L.A. (1996). A cluster of noninvoluting endocytic cells at the margin of the zebrafish blastoderm marks the site of embryonic shield formation. Dev Biol *180*, 184-198.

Cornillie, F.J., Lauweryns, J.M., and Corbeel, L. (1984). Atypical bronchial cilia in children with recurrent respiratory tract infections. A comparative ultrastructural study. Pathol Res Pract *178*, 595-604.

Cox, D.B.T., Gootenberg, J.S., Abudayyeh, O.O., Franklin, B., Kellner, M.J., Joung, J., and Zhang, F. (2017). RNA editing with CRISPR-Cas13. Science *358*, 1019-1027.

Csörgő, B., León, L.M., Chau-Ly, I.J., Vasquez-Rifo, A., Berry, J.D., Mahendra, C., Crawford, E.D., Lewis, J.D., and Bondy-Denomy, J. (2019). A minimal CRISPR-Cas3 system for genome engineering. bioRxiv, 860999.

Cui, Y., Xu, J., Cheng, M., Liao, X., and Peng, S. (2018). Review of CRISPR/Cas9 sgRNA Design Tools. Interdiscip Sci *10*, 455-465.

Dahl, H.A. (1967). On the cilium cell relationship in the adenohypophysis of the mouse. Z Zellforsch Mikrosk Anat *83*, 169-177.

Damerla, R.R., Cui, C., Gabriel, G.C., Liu, X., Craige, B., Gibbs, B.C., Francis, R., Li, Y., Chatterjee, B., San Agustin, J.T.*, et al.* (2015). Novel Jbts17 mutant mouse model of Joubert syndrome with cilia transition zone defects and cerebellar and other ciliopathy related anomalies. Hum Mol Genet *24*, 3994-4005.

Daniel, J.G., and Panizzi, J.R. (2019). Spatiotemporal expression profile of embryonic and adult ankyrin repeat and EF-hand domain containing protein 1-encoding genes ankef1a and ankef1b in zebrafish. Gene Expr Patterns *34*, 119069.

David, L., Blum, S., Feldman, M.W., Lavi, U., and Hillel, J. (2003). Recent duplication of the common carp (Cyprinus carpio L.) genome as revealed by analyses of microsatellite loci. Mol Biol Evol *20*, 1425-1434.

Dawe, H.R., Farr, H., and Gull, K. (2007). Centriole/basal body morphogenesis and migration during ciliogenesis in animal cells. J Cell Sci *120*, 7-15.

Deng, W.L., Gao, M.L., Lei, X.L., Lv, J.N., Zhao, H., He, K.W., Xia, X.X., Li, L.Y., Chen, Y.C., Li, Y.P.*, et al.* (2018). Gene Correction Reverses Ciliopathy and Photoreceptor Loss in iPSC-Derived Retinal Organoids from Retinitis Pigmentosa Patients. Stem Cell Reports *10*, 1267-1281.

Deretic, D., Huber, L.A., Ransom, N., Mancini, M., Simons, K., and Papermaster, D.S. (1995). rab8 in retinal photoreceptors may participate in rhodopsin transport and in rod outer segment disk morphogenesis. J Cell Sci *108 (Pt 1)*, 215-224.

Diaz, M., Pecinkova, P., Nowicka, A., Baroux, C., Sakamoto, T., Gandha, P.Y., Jerabkova, H., Matsunaga, S., Grossniklaus, U., and Pecinka, A. (2019). The SMC5/6 Complex Subunit NSE4A Is Involved in DNA Damage Repair and Seed Development. Plant Cell *31*, 1579-1597.

Douguet, D., Patel, A., and Honore, E. (2019). Structure and function of polycystins: insights into polycystic kidney disease. Nat Rev Nephrol *15*, 412-422.

Doyon, Y., McCammon, J.M., Miller, J.C., Faraji, F., Ngo, C., Katibah, G.E., Amora, R., Hocking, T.D., Zhang, L., Rebar, E.J.*, et al.* (2008). Heritable targeted gene disruption in zebrafish using designed zinc-finger nucleases. Nat Biotechnol *26*, 702-708.

Drummond, I. (2009). Studying cilia in zebrafish. Methods Cell Biol *93*, 197-217.

Drummond, I.A., and Davidson, A.J. (2016). Zebrafish kidney development. Methods Cell Biol *134*, 391-429.

Duan, C., Wang, H., Chen, Y., Chu, P., Xing, T., Gao, C., Yue, Z., Zheng, J., Jin, M., Gu, W.*, et al.* (2018). Whole exome sequencing reveals novel somatic alterations in neuroblastoma patients with chemotherapy. Cancer cell international *18*, 21.

Dupont, M.A., Humbert, C., Huber, C., Siour, Q., Guerrera, I.C., Jung, V., Christensen, A., Pouliet, A., Garfa-Traore, M., Nitschke, P.*, et al.* (2019). Human IFT52 mutations uncover a novel role for the protein in microtubule dynamics and centrosome cohesion. Hum Mol Genet *28*, 2720-2737.

Dzeja, P., and Terzic, A. (2009). Adenylate kinase and AMP signaling networks: metabolic monitoring, signal communication and body energy sensing. Int J Mol Sci *10*, 1729-1772.

Elkon, R., Milon, B., Morrison, L., Shah, M., Vijayakumar, S., Racherla, M., Leitch, C.C., Silipino, L., Hadi, S., Weiss-Gayet, M., *et al.* (2015). RFX transcription factors are essential for hearing in mice. Nat Commun *6*, 8549.

Essner, J.J., Amack, J.D., Nyholm, M.K., Harris, E.B., and Yost, H.J. (2005). Kupffer's vesicle is a ciliated organ of asymmetry in the zebrafish embryo that initiates left-right development of the brain, heart and gut. Development *132*, 1247-1260.

Essner, J.J., Vogan, K.J., Wagner, M.K., Tabin, C.J., Yost, H.J., and Brueckner, M. (2002). Conserved function for embryonic nodal cilia. Nature *418*, 37-38.

Fagerberg, L., Hallstrom, B.M., Oksvold, P., Kampf, C., Djureinovic, D., Odeberg, J., Habuka, M., Tahmasebpoor, S., Danielsson, A., Edlund, K., *et al.* (2014). Analysis of the human tissue-specific expression by genome-wide integration of transcriptomics and antibody-based proteomics. Mol Cell Proteomics *13*, 397-406.

Federman, M., and Nichols, G., Jr. (1974). Bone cell cilia: vestigial or functional organelles? Calcif Tissue Res *17*, 81-85.

Felsenstein, J. (1985). Confidence-Limits on Phylogenies - an Approach Using the Bootstrap. Evolution *39*, 783-791.

Fliegauf, M., Benzing, T., and Omran, H. (2007). When cilia go bad: cilia defects and ciliopathies. Nat Rev Mol Cell Biol *8*, 880-893.

Flynt, A.S., Rao, M., and Patton, J.G. (2017). Blocking Zebrafish MicroRNAs with Morpholinos. Methods Mol Biol *1565*, 59-78.

Gagnon, J.A., Valen, E., Thyme, S.B., Huang, P., Akhmetova, L., Pauli, A., Montague, T.G., Zimmerman, S., Richter, C., and Schier, A.F. (2014). Efficient mutagenesis by Cas9 protein-mediated oligonucleotide insertion and large-scale assessment of single-guide RNAs. PLoS One *9*, e98186.

Gaj, T., Gersbach, C.A., and Barbas, C.F., 3rd (2013). ZFN, TALEN, and CRISPR/Cas-based methods for genome engineering. Trends Biotechnol *31*, 397-405.

Garant, P.R., Szabo, G., and Nalbandian, J. (1968). The fine structure of the mouse odontoblast. Arch Oral Biol *13*, 857-876.

Gavan, S.P., Thompson, A.J., and Payne, K. (2018). The economic case for precision medicine. Expert Rev Precis Med Drug Dev *3*, 1-9.

Geremek, M., Bruinenberg, M., Zietkiewicz, E., Pogorzelski, A., Witt, M., and Wijmenga, C. (2011). Gene expression studies in cells from primary ciliary dyskinesia patients identify 208 potential ciliary genes. Human genetics *129*, 283-293.

Giannakopoulos, X., Stagikas, D., Peschos, D., Batistatou, A., and Charalabopoulos, K. (2007). Implication of protocadherin-PC in the progression of the advanced prostate cancer. Exp Oncol *29*, 74-75.

Gibbons, I.R. (1981). Cilia and flagella of eukaryotes. J Cell Biol *91*, 107s-124s.

Gilbert, Luke A., Larson, Matthew H., Morsut, L., Liu, Z., Brar, Gloria A., Torres, Sandra E., Stern-Ginossar, N., Brandman, O., Whitehead, Evan H., Doudna, Jennifer A.*, et al.* (2013). CRISPR-Mediated Modular RNA-Guided Regulation of Transcription in Eukaryotes. Cell *154*, 442-451.

Goetz, S.C., and Anderson, K.V. (2010). The primary cilium: a signalling centre during vertebrate development. Nature Reviews Genetics *11*, 331.

Goldstein, S.F., Besse, C., and Schrevel, J. (1979). Structure and Physiology of a 6 + 0 Flagellum. Acta Protozool *18*, 135-135.

Gomez-Requeni, P., de Vareilles, M., Kousoulaki, K., Jordal, A.E., Conceicao, L.E., and Ronnestad, I. (2011). Whole body proteome response to a dietary lysine imbalance in zebrafish Danio rerio. Comparative biochemistry and physiology Part D, Genomics & proteomics *6*, 178-186.

Gong, Z.Y., and Brandhorst, B.P. (1988). Multiple levels of regulation of tubulin gene expression during sea urchin embryogenesis. Dev Biol *130*, 144-153.

Goutaki, M., Eich, M.O., Halbeisen, F.S., Barben, J., Casaulta, C., Clarenbach, C., Hafen, G., Latzin, P., Regamey, N., Lazor, R.*, et al.* (2019). The Swiss Primary Ciliary Dyskinesia registry: objectives, methods and first results. Swiss Med Wkly *149*.

Greenstone, M., Rutman, A., Dewar, A., Mackay, I., and Cole, P.J. (1988). Primary ciliary dyskinesia: cytological and clinical features. Q J Med *67*, 405-423.

Greiner, J.V., Bodley, H.D., Weidman, T.A., and Peace, D.G. (1983). Pericentriolar processes of photoreceptor cell basal bodies in the mammalian retina. Z Mikrosk Anat Forsch *97*, 309-318.

Grover, V.K., Valadez, J.G., Bowman, A.B., and Cooper, M.K. (2011). Lipid modifications of Sonic hedgehog ligand dictate cellular reception and signal response. PLoS One *6*, e21353.

Guirao, B., Meunier, A., Mortaud, S., Aguilar, A., Corsi, J.M., Strehl, L., Hirota, Y., Desoeuvre, A., Boutin, C., Han, Y.G.*, et al.* (2010). Coupling between hydrodynamic forces and planar cell polarity orients mammalian motile cilia. Nat Cell Biol *12*, 341-350.

Gur, M., Cohen, E.B., Genin, O., Fainsod, A., Perles, Z., and Cinnamon, Y. (2017). Roles of the cilium-associated gene CCDC11 in left-right patterning and in laterality disorders in humans. Int J Dev Biol *61*, 267-276.

Hackett, T.A., Guo, Y., Clause, A., Hackett, N.J., Garbett, K., Zhang, P., Polley, D.B., and Mirnics, K. (2015). Transcriptional maturation of the mouse auditory forebrain. BMC Genomics *16*, 606.

Hammerschmidt, M., Bitgood, M.J., and McMahon, A.P. (1996a). Protein kinase A is a common negative regulator of Hedgehog signaling in the vertebrate embryo. Genes Dev *10*, 647-658.

Hammerschmidt, M., Pelegri, F., Mullins, M.C., Kane, D.A., Brand, M., van Eeden, F.J., Furutani-Seiki, M., Granato, M., Haffter, P., Heisenberg, C.P.*, et al.* (1996b). Mutations affecting morphogenesis during gastrulation and tail formation in the zebrafish, Danio rerio. Development *123*, 143-151.

Han, Y.G., and Alvarez-Buylla, A. (2010). Role of primary cilia in brain development and cancer. Curr Opin Neurobiol *20*, 58-67.

Han, Y.G., Kim, H.J., Dlugosz, A.A., Ellison, D.W., Gilbertson, R.J., and Alvarez-Buylla, A. (2009). Dual and opposing roles of primary cilia in medulloblastoma development. Nat Med *15*, 1062-1065.

Hashimoto, M., Shinohara, K., Wang, J., Ikeuchi, S., Yoshiba, S., Meno, C., Nonaka, S., Takada, S., Hatta, K., Wynshaw-Boris, A.*, et al.* (2010). Planar polarization of node cells determines the rotational axis of node cilia. Nat Cell Biol *12*, 170-176.

Hasso-Agopsowicz, M., Scriba, T.J., Hanekom, W.A., Dockrell, H.M., and Smith, S.G. (2018). Differential DNA methylation of potassium channel KCa3.1 and immune signalling pathways is associated with infant immune responses following BCG vaccination. Sci Rep *8*, 13086.

Herzberg, O., Moult, J., and James, M.N. (1986). A model for the Ca2+-induced conformational transition of troponin C. A trigger for muscle contraction. J Biol Chem *261*, 2638-2644.

Hinds, J.W., and Hinds, P.L. (1979). Differentiation of photoreceptors and horizontal cells in the embryonic mouse retina: an electron microscopic, serial section analysis. J Comp Neurol *187*, 495-511.

Hinkel, I., Duluc, I., Martin, E., Guenot, D., Freund, J.N., and Gross, I. (2012). Cdx2 controls expression of the protocadherin Mucdhl, an inhibitor of growth and beta-catenin activity in colon cancer cells. Gastroenterology *142*, 875-885 e873.

Hochstrasser, M.L., Taylor, D.W., Bhat, P., Guegler, C.K., Sternberg, S.H., Nogales, E., and Doudna, J.A. (2014). CasA mediates Cas3-catalyzed target degradation during CRISPR RNA-guided interference. Proc Natl Acad Sci U S A *111*, 6618-6623.

Hoff, S., Epting, D., Falk, N., Schroda, S., Braun, D.A., Halbritter, J., Hildebrandt, F., Kramer-Zucker, A., Bergmann, C., Walz, G.*, et al.* (2018). The nucleoside-diphosphate kinase NME3 associates with nephronophthisis proteins and is required for ciliary function during renal development. J Biol Chem *293*, 15243-15255.

Hoh, R.A., Stowe, T.R., Turk, E., and Stearns, T. (2012). Transcriptional program of ciliated epithelial cells reveals new cilium and centrosome components and links to human disease. PLoS One *7*, e52166.

Holland, N.D. (1976). The fine structure of the embryo during the gastrula stage of Comanthus japonica (Echinodermata: Crinoidea). Tissue Cell *8*, 491-510.

Holwill, M.E. (1977). Some biophysical aspects of ciliary and flagellar motility. Adv Microb Physiol *16*, 1-48.

Horani, A., and Ferkol, T.W. (2018). Advances in the Genetics of Primary Ciliary Dyskinesia: Clinical Implications. Chest *154*, 645-652.

Horowitz, E., Zhang, Z., Jones, B.H., Moss, S.B., Ho, C., Wood, J.R., Wang, X., Sammel, M.D., and Strauss, J.F., 3rd (2005). Patterns of expression of sperm flagellar genes: early expression of genes encoding axonemal proteins during the spermatogenic cycle and shared features of promoters of genes encoding central apparatus proteins. Mol Hum Reprod *11*, 307-317.

Horvath, J., Fliegauf, M., Olbrich, H., Kispert, A., King, S.M., Mitchison, H., Zariwala, M.A., Knowles, M.R., Sudbrak, R., Fekete, G.*, et al.* (2005). Identification and analysis of axonemal dynein light chain 1 in primary ciliary dyskinesia patients. Am J Respir Cell Mol Biol *33*, 41-47.

Howe, K., Clark, M.D., Torroja, C.F., Torrance, J., Berthelot, C., Muffato, M., Collins, J.E., Humphray, S., McLaren, K., Matthews, L.*, et al.* (2013). The zebrafish reference genome sequence and its relationship to the human genome. Nature *496*, 498-503.

Hu, R., Huang, W., Liu, J., Jin, M., Wu, Y., Li, J., Wang, J., Yu, Z., Wang, H., and Cao, Y. (2019). Mutagenesis of putative ciliary genes with the CRISPR/Cas9 system in zebrafish identifies genes required for retinal development. Faseb J *33*, 5248-5256.

Huang, K., Diener, D.R., Mitchell, A., Pazour, G.J., Witman, G.B., and Rosenbaum, J.L. (2007). Function and dynamics of PKD2 in Chlamydomonas reinhardtii flagella. J Cell Biol *179*, 501-514.

Huang, P., and Schier, A.F. (2009). Dampened Hedgehog signaling but normal Wnt signaling in zebrafish without cilia. Development *136*, 3089-3098.

Huang, P., Zhu, Z., Lin, S., and Zhang, B. (2012). Reverse genetic approaches in zebrafish. J Genet Genomics *39*, 421-433.

Huangfu, D., Liu, A., Rakeman, A.S., Murcia, N.S., Niswander, L., and Anderson, K.V. (2003). Hedgehog signalling in the mouse requires intraflagellar transport proteins. Nature *426*, 83-87.

Hudspeth, A.J., and Corey, D.P. (1977). Sensitivity, polarity, and conductance change in the response of vertebrate hair cells to controlled mechanical stimuli. Proc Natl Acad Sci U S A *74*, 2407-2411.

Huvila, J., Laajala, T.D., Edqvist, P.H., Mardinoglu, A., Talve, L., Ponten, F., Grenman, S., Carpen, O., Aittokallio, T., and Auranen, A. (2018). Combined ASRGL1 and p53 immunohistochemistry as an independent predictor of survival in endometrioid endometrial carcinoma. Gynecol Oncol *149*, 173-180.

Hwang, W.Y., Fu, Y., Reyon, D., Maeder, M.L., Tsai, S.Q., Sander, J.D., Peterson, R.T., Yeh, J.R., and Joung, J.K. (2013). Efficient genome editing in zebrafish using a CRISPR-Cas system. Nat Biotechnol *31*, 227-229.

Ibraghimov-Beskrovnaya, O., Bukanov, N.O., Donohue, L.C., Dackowski, W.R., Klinger, K.W., and Landes, G.M. (2000). Strong homophilic interactions of the Ig-like domains of polycystin-1, the protein product of an autosomal dominant polycystic kidney disease gene, PKD1. Hum Mol Genet *9*, 1641-1649.

Ingham, P.W., Taylor, A.M., and Nakano, Y. (1991). Role of the Drosophila patched gene in positional signalling. Nature *353*, 184-187.

Ishikawa, T. (2015). Cryo-electron tomography of motile cilia and flagella. Cilia *4*, 3.

Ishikawa, T. (2017). Axoneme Structure from Motile Cilia. Cold Spring Harb Perspect Biol *9*.

Ishino, Y., Shinagawa, H., Makino, K., Amemura, M., and Nakata, A. (1987). Nucleotide sequence of the iap gene, responsible for alkaline phosphatase isozyme conversion in Escherichia coli, and identification of the gene product. J Bacteriol *169*, 5429-5433.

Jaeger, R.G., Fex, J., and Kachar, B. (1994). Structural basis for mechanical transduction in the frog vestibular sensory apparatus: II. The role of microtubules in the organization of the cuticular plate. Hear Res *77*, 207-215.

Jin, H.J., Jung, S., DebRoy, A.R., and Davuluri, R.V. (2016). Identification and validation of regulatory SNPs that modulate transcription factor chromatin binding and gene expression in prostate cancer. Oncotarget *7*, 54616-54626.

Jinek, M., Chylinski, K., Fonfara, I., Hauer, M., Doudna, J.A., and Charpentier, E. (2012). A programmable dual-RNA-guided DNA endonuclease in adaptive bacterial immunity. Science *337*, 816-821.

Jones, D.T., Taylor, W.R., and Thornton, J.M. (1992). The rapid generation of mutation data matrices from protein sequences. Comput Appl Biosci *8*, 275-282.

Kachi, S., Nishizawa, Y., Olshevskaya, E., Yamazaki, A., Miyake, Y., Wakabayashi, T., Dizhoor, A., and Usukura, J. (1999). Detailed localization of photoreceptor guanylate cyclase activating protein-1 and -2 in mammalian retinas using light and electron microscopy. Exp Eye Res *68*, 465-473.

Kalnins, V.I., and Porter, K.R. (1969). Centriole replication during ciliogenesis in the chick tracheal epithelium. Z Zellforsch Mikrosk Anat *100*, 1-30.

Karcher, C., Fischer, A., Schweickert, A., Bitzer, E., Horie, S., Witzgall, R., and Blum, M. (2005). Lack of a laterality phenotype in Pkd1 knock-out embryos correlates with absence of polycystin-1 in nodal cilia. Differentiation *73*, 425-432.

Kartagener, M. (1933). Zur pathogenese der bronchiektasien. Beiträge zur Klinik der Tuberkulose und spezifischen Tuberkulose-Forschung *84*, 73-85.

Kasahara, K., Aoki, H., Kiyono, T., Wang, S., Kagiwada, H., Yuge, M., Tanaka, T., Nishimura, Y., Mizoguchi, A., Goshima, N*., et al.* (2018). EGF receptor kinase suppresses ciliogenesis through activation of USP8 deubiquitinase. Nat Commun *9*, 758.

Kataoka, H., Bonnefin, P., Vieyra, D., Feng, X., Hara, Y., Miura, Y., Joh, T., Nakabayashi, H., Vaziri, H., Harris, C.C*., et al.* (2003). ING1 represses transcription by direct DNA binding and through effects on p53. Cancer Res *63*, 5785-5792.

Katrekar, D., Chen, G., Meluzzi, D., Ganesh, A., Worlikar, A., Shih, Y.R., Varghese, S., and Mali, P. (2019). In vivo RNA editing of point mutations via RNA-guided adenosine deaminases. Nat Methods *16*, 239-242.

Katz, M.J., and Lasek, R.J. (1980). Invited review: guidance cue patterns and cell migration in multicellular organisms. Cell Motil *1*, 141-157.

Katz, S.M., and Morgan, J.J. (1984). Cilia in the human kidney. Ultrastruct Pathol *6*, 285-294.

Kawakami, K., Shima, A., and Kawakami, N. (2000). Identification of a functional transposase of the Tol2 element, an Ac-like element from the Japanese medaka fish, and its transposition in the zebrafish germ lineage. Proc Natl Acad Sci U S A *97*, 11403-11408.

Kawakami, K., Takeda, H., Kawakami, N., Kobayashi, M., Matsuda, N., and Mishina, M. (2004). A transposon-mediated gene trap approach identifies developmentally regulated genes in zebrafish. Dev Cell *7*, 133-144.

Khan, S.Y., Vasanth, S., Kabir, F., Khan, A.O., Ma, Z.W., Riazuddin, S., Pourmand, N., Zaghloul, N.A., Hejtmancik, J.F., and Riazuddin, S.A. (2016). Functional Dissection

Shows FOXE3 Contributes to Peters Anomaly through the Transcriptional Regulation of an Autophagy Associated Co-Chaperone, DNAJB1. Invest Ophth Vis Sci *57*.

Khan, T.N., Khan, K., Sadeghpour, A., Reynolds, H., Perilla, Y., McDonald, M.T., Gallentine, W.B., Baig, S.M., Task Force for Neonatal, G., Davis, E.E.*, et al.* (2019). Mutations in NCAPG2 Cause a Severe Neurodevelopmental Syndrome that Expands the Phenotypic Spectrum of Condensinopathies. Am J Hum Genet *104*, 94-111.

Kim, J., Krishnaswami, S.R., and Gleeson, J.G. (2008). CEP290 interacts with the centriolar satellite component PCM-1 and is required for Rab8 localization to the primary cilium. Hum Mol Genet *17*, 3796-3805.

Kim, S.H., Yamamoto, A., Bouwmeester, T., Agius, E., and Robertis, E.M. (1998). The role of paraxial protocadherin in selective adhesion and cell movements of the mesoderm during Xenopus gastrulation. Development *125*, 4681-4690.

Kim, Y.J., and Kim, J. (2019). Therapeutic perspectives for structural and functional abnormalities of cilia. Cell Mol Life Sci *76*, 3695-3709.

Kim, Y.J., Kim, S., Jung, Y., Jung, E., Kwon, H.J., and Kim, J. (2018). Eupatilin rescues ciliary transition zone defects to ameliorate ciliopathy-related phenotypes. J Clin Invest *128*, 3642-3648.

Kimmel, C.B., Ballard, W.W., Kimmel, S.R., Ullmann, B., and Schilling, T.F. (1995). Stages of embryonic development of the zebrafish. Dev Dyn *203*, 253-310.

King, S.M., and Patel-King, R.S. (2015). The oligomeric outer dynein arm assembly factor CCDC103 is tightly integrated within the ciliary axoneme and exhibits periodic binding to microtubules. J Biol Chem *290*, 7388-7401.

King, S.M., and Patel-King, R.S. (2019). The outer dynein arm assembly factor CCDC103 forms molecular scaffolds through multiple self-interaction sites. Cytoskeleton (Hoboken).

Kinzler, K.W., Ruppert, J.M., Bigner, S.H., and Vogelstein, B. (1988). The GLI gene is a member of the Kruppel family of zinc finger proteins. Nature *332*, 371-374.

Kiselak, E.A., Shen, X., Song, J., Gude, D.R., Wang, J., Brody, S.L., Strauss, J.F., 3rd, and Zhang, Z. (2010). Transcriptional regulation of an axonemal central apparatus gene, sperm-associated antigen 6, by a SRY-related high mobility group transcription factor, S-SOX5. J Biol Chem *285*, 30496-30505.

Kohl, S., Coppieters, F., Meire, F., Schaich, S., Roosing, S., Brennenstuhl, C., Bolz, S., van Genderen, M.M., Riemslag, F.C., European Retinal Disease, C.*, et al.* (2012). A nonsense mutation in PDE6H causes autosomal-recessive incomplete achromatopsia. Am J Hum Genet *91*, 527-532.

Kramer-Zucker, A.G., Olale, F., Haycraft, C.J., Yoder, B.K., Schier, A.F., and Drummond, I.A. (2005). Cilia-driven fluid flow in the zebrafish pronephros, brain and Kupffer's vesicle is required for normal organogenesis. Development *132*, 1907-1921.

Kretsinger, R.H., and Nockolds, C.E. (1973). Carp muscle calcium-binding protein. II. Structure determination and general description. J Biol Chem *248*, 3313-3326.

Kretsinger, R.H., Rudnick, S.E., and Weissman, L.J. (1986). Crystal structure of calmodulin. J Inorg Biochem *28*, 289-302.

Kucenas, S., Takada, N., Park, H.C., Woodruff, E., Broadie, K., and Appel, B. (2008). CNS-derived glia ensheath peripheral nerves and mediate motor root development. Nat Neurosci *11*, 143-151.

Kuehni, C.E., Frischer, T., Strippoli, M.P., Maurer, E., Bush, A., Nielsen, K.G., Escribano, A., Lucas, J.S., Yiallouros, P., Omran, H.*, et al.* (2010). Factors influencing age at diagnosis of primary ciliary dyskinesia in European children. Eur Respir J *36*, 1248-1258.

Kumar, S., Stecher, G., Li, M., Knyaz, C., and Tamura, K. (2018). MEGA X: Molecular Evolutionary Genetics Analysis across Computing Platforms. Mol Biol Evol *35*, 1547-1549.

Lamar, E., Deblandre, G., Wettstein, D., Gawantka, V., Pollet, N., Niehrs, C., and Kintner, C. (2001). Nrarp is a novel intracellular component of the Notch signaling pathway. Genes Dev *15*, 1885-1899.

Lawrence, C. (2007). The husbandry of zebrafish (Danio rerio): A review. Aquaculture *269*, 1-20.

Leenay, R.T., Maksimchuk, K.R., Slotkowski, R.A., Agrawal, R.N., Gomaa, A.A., Briner, A.E., Barrangou, R., and Beisel, C.L. (2016). Identifying and Visualizing Functional PAM Diversity across CRISPR-Cas Systems. Mol Cell *62*, 137-147.

Lehman, J.M., Michaud, E.J., Schoeb, T.R., Aydin-Son, Y., Miller, M., and Yoder, B.K. (2008). The Oak Ridge Polycystic Kidney mouse: modeling ciliopathies of mice and men. Dev Dyn *237*, 1960-1971.

Leick, V., Koppelhus, U., and Rosenberg, J. (1994). Cilia-mediated oriented chemokinesis in Tetrahymena thermophila. J Eukaryot Microbiol *41*, 546-553.

Leigh, M.W., Pittman, J.E., Carson, J.L., Ferkol, T.W., Dell, S.D., Davis, S.D., Knowles, M.R., and Zariwala, M.A. (2009a). Clinical and genetic aspects of primary ciliary dyskinesia/Kartagener syndrome. Genet Med *11*, 473-487.

Leigh, M.W., Zariwala, M.A., and Knowles, M.R. (2009b). Primary ciliary dyskinesia: improving the diagnostic approach. Curr Opin Pediatr *21*, 320-325.

Lemullois, M., Boisvieux-Ulrich, E., Laine, M.C., Chailley, B., and Sandoz, D. (1988). Development and functions of the cytoskeleton during ciliogenesis in metazoa. Biol Cell *63*, 195-208.

Lewis, K.E., Concordet, J.P., and Ingham, P.W. (1999). Characterisation of a second patched gene in the zebrafish Danio rerio and the differential response of patched genes to Hedgehog signalling. Dev Biol *208*, 14-29.

Li, J., Gao, F., Zhao, Y., He, L., Huang, Y., Yang, X., Zhou, Y., Yu, L., Zhao, Q., and Dong, X. (2019). Zebrafish znfl1s regulate left-right asymmetry patterning through controlling the expression of fgfr1a. J Cell Physiol *234*, 1987-1995.

Li, Y., Zhang, H., Litingtung, Y., and Chiang, C. (2006). Cholesterol modification restricts the spread of Shh gradient in the limb bud. Proc Natl Acad Sci U S A *103*, 6548-6553.

Lin, C.Y., Tsai, M.Y., Liu, Y.H., Lu, Y.F., Chen, Y.C., Lai, Y.R., Liao, H.C., Lien, H.W., Yang, C.H., Huang, C.J.*, et al.* (2017). Klf8 regulates left-right asymmetric patterning through modulation of Kupffer's vesicle morphogenesis and spaw expression. J Biomed Sci *24*, 45.

Lin, S., Gaiano, N., Culp, P., Burns, J.C., Friedmann, T., Yee, J.K., and Hopkins, N. (1994). Integration and germ-line transmission of a pseudotyped retroviral vector in zebrafish. Science *265*, 666-669.

Lindstrand, A., Frangakis, S., Carvalho, C.M., Richardson, E.B., McFadden, K.A., Willer, J.R., Pehlivan, D., Liu, P., Pediaditakis, I.L., Sabo, A.*, et al.* (2016). Copy-Number Variation

Contributes to the Mutational Load of Bardet-Biedl Syndrome. Am J Hum Genet *99*, 318-336.

Liu, C., Cao, R., Xu, Y., Li, T., Li, F., Chen, S., Xu, R., and Sun, K. (2018). Rare copy number variants analysis identifies novel candidate genes in heterotaxy syndrome patients with congenital heart defects. Genome Med *10*, 40.

Liu, P., Luk, K., Shin, M., Idrizi, F., Kwok, S., Roscoe, B., Mintzer, E., Suresh, S., Morrison, K., Frazao, J.B*., et al.* (2019). Enhanced Cas12a editing in mammalian cells and zebrafish. Nucleic Acids Res *47*, 4169-4180.

Liu, Q., Tan, G., Levenkova, N., Li, T., Pugh, E.N., Jr., Rux, J.J., Speicher, D.W., and Pierce, E.A. (2007). The proteome of the mouse photoreceptor sensory cilium complex. Mol Cell Proteomics *6*, 1299-1317.

Liu, Y.P., Bosch, D.G., Siemiatkowska, A.M., Rendtorff, N.D., Boonstra, F.N., Moller, C., Tranebjaerg, L., Katsanis, N., and Cremers, F.P. (2017). Putative digenic inheritance of heterozygous RP1L1 and C2orf71 null mutations in syndromic retinal dystrophy. Ophthalmic Genet *38*, 127-132.

Livak, K.J., and Schmittgen, T.D. (2001). Analysis of relative gene expression data using real-time quantitative PCR and the 2(-Delta Delta C(T)) Method. Methods *25*, 402-408.

Lo, K.W., Kan, H.M., and Pfister, K.K. (2006). Identification of a novel region of the cytoplasmic Dynein intermediate chain important for dimerization in the absence of the light chains. J Biol Chem *281*, 9552-9559.

Lodh, S., Hostelley, T.L., Leitch, C.C., O'Hare, E.A., and Zaghloul, N.A. (2016). Differential effects on beta-cell mass by disruption of Bardet-Biedl syndrome or Alstrom syndrome genes. Hum Mol Genet *25*, 57-68.

Loges, N.T., Olbrich, H., Fenske, L., Mussaffi, H., Horvath, J., Fliegauf, M., Kuhl, H., Baktai, G., Peterffy, E., Chodhari, R., *et al.* (2008). DNAI2 mutations cause primary ciliary dyskinesia with defects in the outer dynein arm. Am J Hum Genet *83*, 547-558.

Long, L., Guo, H., Yao, D., Xiong, K., Li, Y., Liu, P., Zhu, Z., and Liu, D. (2015). Regulation of transcriptionally active genes via the catalytically inactive Cas9 in C. elegans and D. rerio. Cell Res *25*, 638-641.

Lu, H., Galeano, M.C.R., Ott, E., Kaeslin, G., Kausalya, P.J., Kramer, C., Ortiz-Bruchle, N., Hilger, N., Metzis, V., Hiersche, M., *et al.* (2017). Mutations in DZIP1L, which encodes a ciliary-transition-zone protein, cause autosomal recessive polycystic kidney disease. Nat Genet *49*, 1025-1034.

Lucas, J.S., Burgess, A., Mitchison, H.M., Moya, E., Williamson, M., Hogg, C., and National Pcd Service, U.K. (2014). Diagnosis and management of primary ciliary dyskinesia. Arch Dis Child *99*, 850-856.

Lv, X.F., Hong, H.Q., Liu, L., Cui, S.H., Ren, C.C., Li, H.Y., Zhang, X.A., Zhang, L.D., Wei, T.X., Liu, J.J., *et al.* (2018). RNAimediated downregulation of asparaginaselike protein 1 inhibits growth and promotes apoptosis of human cervical cancer line SiHa. Mol Med Rep *18*, 931-937.

Lynch, M. (2010). Rate, molecular spectrum, and consequences of human mutation. Proc Natl Acad Sci U S A *107*, 961-968.

Ma, D., and Liu, F. (2015). Genome Editing and Its Applications in Model Organisms. Genomics Proteomics Bioinformatics *13*, 336-344.

Ma, M., Gallagher, A.R., and Somlo, S. (2017). Ciliary Mechanisms of Cyst Formation in Polycystic Kidney Disease. Cold Spring Harb Perspect Biol *9*.

Ma, R., Li, W.P., Rundle, D., Kong, J., Akbarali, H.I., and Tsiokas, L. (2005). PKD2 functions as an epidermal growth factor-activated plasma membrane channel. Mol Cell Biol *25*, 8285-8298.

MacArthur, D.G., and Tyler-Smith, C. (2010). Loss-of-function variants in the genomes of healthy humans. Hum Mol Genet *19*, R125-130.

Macke, J.P., Davenport, C.M., Jacobson, S.G., Hennessey, J.C., Gonzalez-Fernandez, F., Conway, B.P., Heckenlively, J., Palmer, R., Maumenee, I.H., Sieving, P.*, et al.* (1993). Identification of novel rhodopsin mutations responsible for retinitis pigmentosa: implications for the structure and function of rhodopsin. Am J Hum Genet *53*, 80-89.

Mali, P., Yang, L., Esvelt, K.M., Aach, J., Guell, M., DiCarlo, J.E., Norville, J.E., and Church, G.M. (2013). RNA-guided human genome engineering via Cas9. Science *339*, 823-826.

Mao, S.F., Shah, A.S., Moninger, T.O., Ostedgaard, L.S., Lu, L., Tang, X.X., Thornell, I.M., Reznikov, L.R., Ernst, S.E., Karp, P.H.*, et al.* (2018). Motile cilia of human airway epithelia contain hedgehog signaling components that mediate noncanonical hedgehog signaling. P Natl Acad Sci USA *115*, 1370-1375.

McClintock, T.S., Glasser, C.E., Bose, S.C., and Bergman, D.A. (2008). Tissue expression patterns identify mouse cilia genes. Physiol Genomics *32*, 198-206.

McCurley, A.T., and Callard, G.V. (2008). Characterization of housekeeping genes in zebrafish: male-female differences and effects of tissue type, developmental stage and chemical treatment. BMC Mol Biol *9*, 102.

Medina, A., Swain, R.K., Kuerner, K.M., and Steinbeisser, H. (2004). Xenopus paraxial protocadherin has signaling functions and is involved in tissue separation. Embo J *23*, 3249-3258.

Melby, A.E., Warga, R.M., and Kimmel, C.B. (1996). Specification of cell fates at the dorsal margin of the zebrafish gastrula. Development *122*, 2225-2237.

Meng, X., Noyes, M.B., Zhu, L.J., Lawson, N.D., and Wolfe, S.A. (2008). Targeted gene inactivation in zebrafish using engineered zinc-finger nucleases. Nat Biotechnol *26*, 695-701.

Milton, A.S. (1959). The action of tubocurarine on ciliary movement. Br J Pharmacol Chemother *14*, 323-326.

Mojica, F.J., Diez-Villasenor, C., Garcia-Martinez, J., and Soria, E. (2005). Intervening sequences of regularly spaced prokaryotic repeats derive from foreign genetic elements. J Mol Evol *60*, 174-182.

Mojica, F.J., Ferrer, C., Juez, G., and Rodriguez-Valera, F. (1995). Long stretches of short tandem repeats are present in the largest replicons of the Archaea Haloferax mediterranei and Haloferax volcanii and could be involved in replicon partitioning. Mol Microbiol *17*, 85-93.

Moreno-Mateos, M.A., Vejnar, C.E., Beaudoin, J.D., Fernandez, J.P., Mis, E.K., Khokha, M.K., and Giraldez, A.J. (2015). CRISPRscan: designing highly efficient sgRNAs for CRISPR-Cas9 targeting in vivo. Nat Methods *12*, 982-988.

Morgan, D., Goodship, J., Essner, J.J., Vogan, K.J., Turnpenny, L., Yost, H.J., Tabin, C.J., and Strachan, T. (2002). The left-right determinant inversin has highly conserved ankyrin repeat and IQ domains and interacts with calmodulin. Human genetics *110*, 377-384.

Morisaka, H., Yoshimi, K., Okuzaki, Y., Gee, P., Kunihiro, Y., Sonpho, E., Xu, H., Sasakawa, N., Naito, Y., Nakada, S.*, et al.* (2019). CRISPR-Cas3 induces broad and unidirectional genome editing in human cells. Nat Commun *10*, 5302.

Moss, A.G., Sale, W.S., Fox, L.A., and Witman, G.B. (1992). The alpha subunit of sea urchin sperm outer arm dynein mediates structural and rigor binding to microtubules. J Cell Biol *118*, 1189-1200.

Motoyama, J., Milenkovic, L., Iwama, M., Shikata, Y., Scott, M.P., and Hui, C.C. (2003). Differential requirement for Gli2 and Gli3 in ventral neural cell fate specification. Dev Biol *259*, 150-161.

Munger, B.L. (1958). A light and electron microscopic study of cellular differentiation in the pancreatic islets of the mouse. Am J Anat *103*, 275-311.

Munro, N.C., Currie, D.C., Lindsay, K.S., Ryder, T.A., Rutman, A., Dewar, A., Greenstone, M.A., Hendry, W.F., and Cole, P.J. (1994). Fertility in men with primary ciliary dyskinesia presenting with respiratory infection. Thorax *49*, 684-687.

Nasevicius, A., and Ekker, S.C. (2000). Effective targeted gene 'knockdown' in zebrafish. Nat Genet *26*, 216-220.

Nesmith, J.E., Hostelley, T.L., Leitch, C.C., Matern, M.S., Sethna, S., McFarland, R., Lodh, S., Westlake, C.J., Hertzano, R., Ahmed, Z.M.*, et al.* (2019). Genomic knockout of alms1 in zebrafish recapitulates Alstrom syndrome and provides insight into metabolic phenotypes. Hum Mol Genet *28*, 2212-2223.

Ng, P.C., Levy, S., Huang, J., Stockwell, T.B., Walenz, B.P., Li, K., Axelrod, N., Busam, D.A., Strausberg, R.L., and Venter, J.C. (2008). Genetic variation in an individual human exome. PLoS Genet *4*, e1000160.

Nguyen, N.M., de Oliveira Andrade, F., Jin, L., Zhang, X., Macon, M., Cruz, M.I., Benitez, C., Wehrenberg, B., Yin, C., Wang, X.*, et al.* (2017). Maternal intake of high n-6 polyunsaturated fatty acid diet during pregnancy causes transgenerational increase in mammary cancer risk in mice. Breast Cancer Res *19*, 77.

Nieminen, J., St-Pierre, C., and Sato, S. (2005). Galectin-3 interacts with naive and primed neutrophils, inducing innate immune responses. J Leukoc Biol *78*, 1127-1135.

Nonaka, S., Tanaka, Y., Okada, Y., Takeda, S., Harada, A., Kanai, Y., Kido, M., and Hirokawa, N. (1998). Randomization of left-right asymmetry due to loss of nodal cilia generating leftward flow of extraembryonic fluid in mice lacking KIF3B motor protein. Cell *95*, 829-837.

Novas, R., Cardenas-Rodriguez, M., Lepanto, P., Fabregat, M., Rodao, M., Fariello, M.I., Ramos, M., Davison, C., Casanova, G., Alfaya, L*., et al.* (2018). Kinesin 1 regulates cilia length through an interaction with the Bardet-Biedl syndrome related protein CCDC28B. Sci Rep *8*, 3019.

Nusslein-Volhard, C., and Wieschaus, E. (1980). Mutations affecting segment number and polarity in Drosophila. Nature *287*, 795-801.

Nutt, S.L., Dingwell, K.S., Holt, C.E., and Amaya, E. (2001). Xenopus Sprouty2 inhibits FGF-mediated gastrulation movements but does not affect mesoderm induction and patterning. Gene Dev *15*, 1152-1166.

Okada, H., Fujioka, H., Tatsumi, N., Fujisawa, M., Gohji, K., Arakawa, S., Kato, H., Kobayashi, S., Isojima, S., and Kamidono, S. (1999). Assisted reproduction for infertile patients with 9 + 0 immotile spermatozoa associated with autosomal dominant polycystic kidney disease. Hum Reprod *14*, 110-113.

Okazaki, N., Takahashi, N., Kojima, S., Masuho, Y., and Koga, H. (2002). Protocadherin LKC, a new candidate for a tumor suppressor of colon and liver cancers, its association with contact inhibition of cell proliferation. Carcinogenesis *23*, 1139-1148.

Ose, R., Oharaa, O., and Nagase, T. (2012). Galectin-1 and Galectin-3 Mediate Protocadherin-24-Dependent Membrane Localization of beta-catenin in Colon Cancer Cell Line HCT116. Curr Chem Genomics *6*, 18-26.

Pampliega, O., Orhon, I., Patel, B., Sridhar, S., Diaz-Carretero, A., Beau, I., Codogno, P., Satir, B.H., Satir, P., and Cuervo, A.M. (2013). Functional interaction between autophagy and ciliogenesis. Nature *502*, 194-200.

Panizzi, J.R., Becker-Heck, A., Castleman, V.H., Al-Mutairi, D.A., Liu, Y., Loges, N.T., Pathak, N., Austin-Tse, C., Sheridan, E., Schmidts, M., *et al.* (2012). CCDC103 mutations cause primary ciliary dyskinesia by disrupting assembly of ciliary dynein arms. Nat Genet *44*, 714-719.

Papon, J.F., Coste, A., Roudot-Thoraval, F., Boucherat, M., Roger, G., Tamalet, A., Vojtek, A.M., Amselem, S., and Escudier, E. (2010). A 20-year experience of electron microscopy in the diagnosis of primary ciliary dyskinesia. Eur Respir J *35*, 1057-1063.

Patek, E., and Nilsson, L. (1973). Scanning electron microscopic observations on the ciliogenesis of the infundibulum of the human fetal and adult fallopian tube epithelium. Fertil Steril *24*, 819-831.

Pazour, G.J., Dickert, B.L., Vucica, Y., Seeley, E.S., Rosenbaum, J.L., Witman, G.B., and Cole, D.G. (2000). Chlamydomonas IFT88 and its mouse homologue, polycystic kidney disease gene tg737, are required for assembly of cilia and flagella. J Cell Biol *151*, 709-718.

Pazour, G.J., and Rosenbaum, J.L. (2002). Intraflagellar transport and cilia-dependent diseases. Trends Cell Biol *12*, 551-555.

Pelak, K., Shianna, K.V., Ge, D., Maia, J.M., Zhu, M., Smith, J.P., Cirulli, E.T., Fellay, J., Dickson, S.P., Gumbs, C.E., *et al.* (2010). The characterization of twenty sequenced human genomes. PLoS Genet *6*, e1001111.

Philipp, M., Fralish, G.B., Meloni, A.R., Chen, W., MacInnes, A.W., Barak, L.S., and Caron, M.G. (2008). Smoothened Signaling in Vertebrates Is Facilitated by a G Protein-coupled Receptor Kinase. Molecular Biology of the Cell *19*, 5478-5489.

Popper, H., and Jakse, R. (1982). [Diagnosis and pathogenetic aspects of the Kartagener syndrome based on nasal mucosa biopsies]. Wien Klin Wochenschr *94*, 370-372.

Popper, H., Jakse, R., and Loidolt, D. (1985). Problems in the differential diagnosis of Kartagener's syndrome and ATP-ase deficiency. Pathol Res Pract *180*, 481-485.

Pourcel, C., Salvignol, G., and Vergnaud, G. (2005). CRISPR elements in Yersinia pestis acquire new repeats by preferential uptake of bacteriophage DNA, and provide additional tools for evolutionary studies. Microbiology *151*, 653-663.

Praetorius, H.A., Praetorius, J., Nielsen, S., Frokiaer, J., and Spring, K.R. (2004). β1-Integrins in the primary cilium of MDCK cells potentiate fibronectin-induced Ca2+ signaling. American Journal of Physiology-Renal Physiology *287*, F969-F978.

Praetorius, H.A., and Spring, K.R. (2005). A physiological view of the primary cilium. Annu Rev Physiol *67*, 515-529.

Prensier, G., Vivier, E., Goldstein, S., and Schrevel, J. (1980). Motile flagellum with a "3 + 0" ultrastructure. Science *207*, 1493-1494.

Prykhozhij, S.V., Caceres, L., and Berman, J.N. (2017). New Developments in CRISPR/Cas-based Functional Genomics and their Implications for Research Using Zebrafish. Curr Gene Ther *17*, 286-300.

Pulz, L.H., Barra, C.N., Alexandre, P.A., Huete, G.C., Cadrobbi, K.G., Nishiya, A.T., de Freitas, S.H., Fukumasu, H., and Strefezzi, R.F. (2019). Identification of two molecular subtypes in canine mast cell tumours through gene expression profiling. PLoS One *14*, e0217343.

Pusapati, G.V., Kong, J.H., Patel, B.B., Krishnan, A., Sagner, A., Kinnebrew, M., Briscoe, J., Aravind, L., and Rohatgi, R. (2018). CRISPR Screens Uncover Genes that Regulate Target Cell Sensitivity to the Morphogen Sonic Hedgehog. Dev Cell *44*, 113-129 e118.

Qi, L.S., Larson, M.H., Gilbert, L.A., Doudna, J.A., Weissman, J.S., Arkin, A.P., and Lim, W.A. (2013). Repurposing CRISPR as an RNA-guided platform for sequence-specific control of gene expression. Cell *152*, 1173-1183.

Qin, H., Rosenbaum, J.L., and Barr, M.M. (2001). An autosomal recessive polycystic kidney disease gene homolog is involved in intraflagellar transport in C. elegans ciliated sensory neurons. Curr Biol *11*, 457-461.

Qu, S., Niswender, K.D., Ji, Q., van der Meer, R., Keeney, D., Magnuson, M.A., and Wisdom, R. (1997). Polydactyly and ectopic ZPA formation in Alx-4 mutant mice. Development *124*, 3999-4008.

Raftopoulou, M., and Hall, A. (2004). Cell migration: Rho GTPases lead the way. Dev Biol *265*, 23-32.

Randolph, J.F., and Castleman, W.L. (1984). Immotile cilia syndrome in two Old English Sheepdog litter-mates. Journal of Small Animal Practice *25*, 679-686.

Rawlins, E.L., and Hogan, B.L. (2008). Ciliated epithelial cell lifespan in the mouse trachea and lung. Am J Physiol Lung Cell Mol Physiol *295*, L231-234.

Rebagliati, M.R., Toyama, R., Fricke, C., Haffter, P., and Dawid, I.B. (1998). Zebrafish nodal-related genes are implicated in axial patterning and establishing left-right asymmetry. Dev Biol *199*, 261-272.

Reiter, J.F., and Leroux, M.R. (2017). Genes and molecular pathways underpinning ciliopathies. Nat Rev Mol Cell Biol *18*, 533-547.

Ringo, D.L. (1967). Flagellar motion and fine structure of the flagellar apparatus in Chlamydomonas. J Cell Biol *33*, 543-571.

Robert, A., Margall-Ducos, G., Guidotti, J.E., Bregerie, O., Celati, C., Brechot, C., and Desdouets, C. (2007). The intraflagellar transport component IFT88/polaris is a centrosomal protein regulating G1-S transition in non-ciliated cells. J Cell Sci *120*, 628-637.

Roberts, A.J., Numata, N., Walker, M.L., Kato, Y.S., Malkova, B., Kon, T., Ohkura, R., Arisaka, F., Knight, P.J., Sutoh, K*., et al.* (2009). AAA+ Ring and linker swing mechanism in the dynein motor. Cell *136*, 485-495.

Rohatgi, R., Milenkovic, L., and Scott, M.P. (2007). Patched1 Regulates Hedgehog Signaling at the Primary Cilium. Science *317*, 372-376.

Rosenbaum, J.L., and Witman, G.B. (2002). Intraflagellar transport. Nat Rev Mol Cell Biol *3*, 813-825.

Ross, A.J., Dailey, L.A., Brighton, L.E., and Devlin, R.B. (2007). Transcriptional profiling of mucociliary differentiation in human airway epithelial cells. Am J Respir Cell Mol Biol *37*, 169-185.

Roy, A., Kucukural, A., and Zhang, Y. (2010). I-TASSER: a unified platform for automated protein structure and function prediction. Nat Protoc *5*, 725-738.

Ruan, G.X., Barry, E., Yu, D., Lukason, M., Cheng, S.H., and Scaria, A. (2017). CRISPR/Cas9-Mediated Genome Editing as a Therapeutic Approach for Leber Congenital Amaurosis 10. Mol Ther *25*, 331-341.

Ruat, M., Hoch, L., Faure, H., and Rognan, D. (2014). Targeting of Smoothened for therapeutic gain. Trends in pharmacological sciences *35*, 237-246.

Ruiz-Gomez, A., Molnar, C., Holguin, H., Mayor, F., Jr., and de Celis, J.F. (2007). The cell biology of Smo signalling and its relationships with GPCRs. Biochim Biophys Acta *1768*, 901-912.

Ryoo, S.B., Oh, H.K., Yu, S.A., Moon, S.H., Choe, E.K., Oh, T.Y., and Park, K.J. (2014). The effects of eupatilin (stillen(R)) on motility of human lower gastrointestinal tracts. Korean J Physiol Pharmacol *18*, 383-390.

Saitou, N., and Nei, M. (1987). The neighbor-joining method: a new method for reconstructing phylogenetic trees. Mol Biol Evol *4*, 406-425.

Sale, W.S., and Satir, P. (1977). Direction of active sliding of microtubules in Tetrahymena cilia. Proc Natl Acad Sci U S A *74*, 2045-2049.

Sampangi, R., Chaudhuri, Z., Menon, V., and Saxena, R. (2005). Cone-rod dystrophy and acquired dissociated vertical nystagmus. J Pediatr Ophthalmol Strabismus *42*, 114-116.

San Agustin, J.T., Pazour, G.J., and Witman, G.B. (2015). Intraflagellar transport is essential for mammalian spermiogenesis but is absent in mature sperm. Mol Biol Cell *26*, 4358-4372.

Satir, P. (1963). Studies on Cilia. The Fixation of the Metachronal Wave. J Cell Biol *18*, 345-365.

Satir, P. (1965). Structure and Function in Cilia and Flagella. In Structure and Function in Cilia and Flagella / Trichocystes, Corps Trichocystoïdes, Cnidocystes et Colloblastes, P. Satir, and R. Hovasse, eds. (Vienna: Springer Vienna), pp. 1-52.

Satir, P. (1980). Structural basis of ciliary movement. Environ Health Perspect *35*, 77-82.

Sedykh, I., Yoon, B., Roberson, L., Moskvin, O., Dewey, C.N., and Grinblat, Y. (2017). Zebrafish zic2 controls formation of periocular neural crest and choroid fissure morphogenesis. Dev Biol *429*, 92-104.

Sedzinski, J., Hannezo, E., Tu, F., Biro, M., and Wallingford, J.B. (2017). RhoA regulates actin network dynamics during apical surface emergence in multiciliated epithelial cells. J Cell Sci *130*, 420-428.

Seol, S.Y., Kim, M.H., Ryu, J.S., Choi, M.G., Shin, D.W., and Ahn, B.O. (2004). DA-9601 for erosive gastritis: results of a double-blind placebo-controlled phase III clinical trial. World J Gastroenterol *10*, 2379-2382.

Sha, Y.W., Ding, L., and Li, P. (2014). Management of primary ciliary dyskinesia/Kartagener's syndrome in infertile male patients and current progress in defining the underlying genetic mechanism. Asian J Androl *16*, 101-106.

Shah, A.S., Ben-Shahar, Y., Moninger, T.O., Kline, J.N., and Welsh, M.J. (2009). Motile cilia of human airway epithelia are chemosensory. Science *325*, 1131-1134.

Shahid, U., and Singh, P. (2018). Emerging Picture of Deuterosome-Dependent Centriole Amplification in MCCs. Cells *7*.

Shapiro, A.J., Davis, S.D., Polineni, D., Manion, M., Rosenfeld, M., Dell, S.D., Chilvers, M.A., Ferkol, T.W., Zariwala, M.A., Sagel, S.D., *et al.* (2018). Diagnosis of Primary Ciliary

Dyskinesia. An Official American Thoracic Society Clinical Practice Guideline. Am J Respir Crit Care Med *197*, e24-e39.

Sharma, K.R., Heckler, K., Stoll, S.J., Hillebrands, J.L., Kynast, K., Herpel, E., Porubsky, S., Elger, M., Hadaschik, B., Bieback, K.*, et al.* (2016). ELMO1 protects renal structure and ultrafiltration in kidney development and under diabetic conditions. Sci Rep *6*, 37172.

Shibuya, T., and Takagi, S.F. (1963). Electrical Response and Growth of Olfactory Cilia of the Olfactory Epithelium of the Newt in Water and on Land. J Gen Physiol *47*, 71-82.

Shimizu, T., Yabe, T., Muraoka, O., Yonemura, S., Aramaki, S., Hatta, K., Bae, Y.K., Nojima, H., and Hibi, M. (2005). E-cadherin is required for gastrulation cell movements in zebrafish. Mech Dev *122*, 747-763.

Shishodia, G., Koul, S., and Koul, H.K. (2019). Protocadherin 7 is overexpressed in castration resistant prostate cancer and promotes aberrant MEK and AKT signaling. Prostate *79*, 1739-1751.

Siewert, A. (1904). Ueber einen Fall van Bronchiectasie bei einem patienten mito Situs inversus viscerum. Berlin Klin Wochen schr *6*, 139-141.

Smith, J.L., Osborn, J.C., and Stanisstreet, M. (1976). Scanning electron microscopy of lithium-induced exogastrulae of Xenopus laevis. J Embryol Exp Morphol *36*, 513-522.

Sohocki, M.M., Daiger, S.P., Bowne, S.J., Rodriquez, J.A., Northrup, H., Heckenlively, J.R., Birch, D.G., Mintz-Hittner, H., Ruiz, R.S., Lewis, R.A.*, et al.* (2001). Prevalence of mutations causing retinitis pigmentosa and other inherited retinopathies. Hum Mutat *17*, 42-51.

Solnica-Krezel, L., Stemple, D.L., Mountcastle-Shah, E., Rangini, Z., Neuhauss, S.C., Malicki, J., Schier, A.F., Stainier, D.Y., Zwartkruis, F., Abdelilah, S.*, et al.* (1996). Mutations affecting cell fates and cellular rearrangements during gastrulation in zebrafish. Development *123*, 67-80.

Somlo, S., and Ehrlich, B. (2001). Human disease: Calcium signaling in polycystic kidney disease. Current Biology *11*, R356-R360.

Sorokin, S.P. (1968). Reconstructions of centriole formation and ciliogenesis in mammalian lungs. J Cell Sci *3*, 207-230.

Sreenivasan, R., Cai, M., Bartfai, R., Wang, X., Christoffels, A., and Orban, L. (2008). Transcriptomic analyses reveal novel genes with sexually dimorphic expression in the zebrafish gonad and brain. PLoS One *3*, e1791.

Stainier, D.Y.R., Raz, E., Lawson, N.D., Ekker, S.C., Burdine, R.D., Eisen, J.S., Ingham, P.W., Schulte-Merker, S., Yelon, D., Weinstein, B.M.*, et al.* (2017). Guidelines for morpholino use in zebrafish. PLoS Genet *13*, e1007000.

Stawicki, T.M., Hernandez, L., Esterberg, R., Linbo, T., Owens, K.N., Shah, A.N., Thapa, N., Roberts, B., Moens, C.B., Rubel, E.W.*, et al.* (2016). Cilia-Associated Genes Play Differing Roles in Aminoglycoside-Induced Hair Cell Death in Zebrafish. G3-Genes Genom Genet *6*, 2225-2235.

Stayner, C., Brooke, D.G., Bates, M., and Eccles, M.R. (2019). Targeted Therapies for Autosomal Dominant Polycystic Kidney Disease. Curr Med Chem *26*, 3081-3102.

Steinman, R.M. (1968). An electron microscopic study of ciliogenesis in developing epidermis and trachea in the embryo of Xenopus laevis. Am J Anat *122*, 19-55.

Steinman, R.M. (1970). Inhibitory effects of colchicine on ciliogenesis in ectoderm of Xenopus laevis. J Ultrastruct Res *30*, 423-440.

Stephens, R.E. (1999). Turnover of tubulin in ciliary outer doublet microtubules. Cell Struct Funct *24*, 413-418.

Stojanovic, A., and Hwa, J. (2002). Rhodopsin and retinitis pigmentosa: shedding light on structure and function. Receptors and Channels *8*, 33-50.

Sung, C.H., Davenport, C.M., Hennessey, J.C., Maumenee, I.H., Jacobson, S.G., Heckenlively, J.R., Nowakowski, R., Fishman, G., Gouras, P., and Nathans, J. (1991). Rhodopsin mutations in autosomal dominant retinitis pigmentosa. Proc Natl Acad Sci U S A *88*, 6481-6485.

Symoens, S., Barnes, A.M., Gistelinck, C., Malfait, F., Guillemyn, B., Steyaert, W., Syx, D., D'Hondt, S., Biervliet, M., De Backer, J.*, et al.* (2015). Genetic Defects in TAPT1 Disrupt Ciliogenesis and Cause a Complex Lethal Osteochondrodysplasia. Am J Hum Genet *97*, 521-534.

Tadesse, A., Alemu, H., Silamsaw, M., and Gebrewold, Y. (2018). Kartagener's syndrome: a case report. Journal of Medical Case Reports *12*, 5.

Tan, P.L., Barr, T., Inglis, P.N., Mitsuma, N., Huang, S.M., Garcia-Gonzalez, M.A., Bradley, B.A., Coforio, S., Albrecht, P.J., Watnick, T.*, et al.* (2007). Loss of Bardet Biedl syndrome proteins causes defects in peripheral sensory innervation and function. Proc Natl Acad Sci U S A *104*, 17524-17529.

Tang, Q., Iyer, S., Lobbardi, R., Moore, J.C., Chen, H., Lareau, C., Hebert, C., Shaw, M.L., Neftel, C., Suva, M.L.*, et al.* (2017). Dissecting hematopoietic and renal cell heterogeneity in adult zebrafish at single-cell resolution using RNA sequencing. J Exp Med *214*, 2875-2887.

Tang, R., Dodd, A., Lai, D., McNabb, W.C., and Love, D.R. (2007). Validation of zebrafish (Danio rerio) reference genes for quantitative real-time RT-PCR normalization. Acta Biochim Biophys Sin (Shanghai) *39*, 384-390.

Tang, Z., Lin, M.G., Stowe, T.R., Chen, S., Zhu, M., Stearns, T., Franco, B., and Zhong, Q. (2013). Autophagy promotes primary ciliogenesis by removing OFD1 from centriolar satellites. Nature *502*, 254-257.

Taylor, M.D., Zhang, X., Liu, L., Hui, C.C., Mainprize, T.G., Scherer, S.W., Wainwright, B., Hogg, D., and Rutka, J.T. (2004). Failure of a medulloblastoma-derived mutant of SUFU to suppress WNT signaling. Oncogene *23*, 4577-4583.

Thisse, B., Heyer, V., Lux, A., Alunni, V., Degrave, A., Seiliez, I., Kirchner, J., Parkhill, J.P., and Thisse, C. (2004). Spatial and temporal expression of the zebrafish genome by large-scale in situ hybridization screening. Methods Cell Biol *77*, 505-519.

Thisse, C., and Thisse, B. (2005). High Throughput Expression Analysis of ZF-Models Consortium Clones. ZFIN Direct Data Submission.

Thisse, C., and Thisse, B. (2008). High-resolution in situ hybridization to whole-mount zebrafish embryos. Nat Protoc *3*, 59-69.

Tsai, I.C., Adams, K.A., Tzeng, J.A., Shennib, O., Tan, P.L., and Katsanis, N. (2019). Genome-wide suppressor screen identifies USP35/USP38 as therapeutic candidates for ciliopathies. Jci Insight *4*.

Tsang, S.H., and Sharma, T. (2018). Rod Monochromatism (Achromatopsia). Adv Exp Med Biol *1085*, 119-123.

Udvadia, A.J. (2008). 3.6 kb genomic sequence from Takifugu capable of promoting axon growth-associated gene expression in developing and regenerating zebrafish neurons. Gene Expr Patterns *8*, 382-388.

Untergasser, A., Cutcutache, I., Koressaar, T., Ye, J., Faircloth, B.C., Remm, M., and Rozen, S.G. (2012a). Primer3--new capabilities and interfaces. Nucleic Acids Res *40*, e115.

Untergasser, A., Cutcutache, I., Koressaar, T., Ye, J., Faircloth, B.C., Remm, M., and Rozen, S.G. (2012b). Primer3-new capabilities and interfaces. Nucleic Acids Research *40*.

Valerius, N.H., Knudsen, B.B., and Pedersen, M. (1983). Defective neutrophil motility in patients with primary ciliary dyskinesia. Eur J Clin Invest *13*, 489-494.

Vandenbrouck, Y., Lane, L., Carapito, C., Duek, P., Rondel, K., Bruley, C., Macron, C., Gonzalez de Peredo, A., Couté, Y., Chaoui, K*., et al.* (2016). Looking for Missing Proteins in the Proteome of Human Spermatozoa: An Update. Journal of Proteome Research *15*, 3998-4019.

Vejnar, C.E., Moreno-Mateos, M.A., Cifuentes, D., Bazzini, A.A., and Giraldez, A.J. (2016a). Optimization Strategies for the CRISPR-Cas9 Genome-Editing System. Cold Spring Harb Protoc *2016*.

Vejnar, C.E., Moreno-Mateos, M.A., Cifuentes, D., Bazzini, A.A., and Giraldez, A.J. (2016b). Optimized CRISPR-Cas9 System for Genome Editing in Zebrafish. Cold Spring Harb Protoc *2016*.

Villefranc, J.A., Amigo, J., and Lawson, N.D. (2007). Gateway compatible vectors for analysis of gene function in the zebrafish. Dev Dyn *236*, 3077-3087.

Vokes, S.A., Ji, H., Wong, W.H., and McMahon, A.P. (2008). A genome-scale analysis of the cis-regulatory circuitry underlying sonic hedgehog-mediated patterning of the mammalian limb. Genes Dev *22*, 2651-2663.

Wald, G., Durell, J., and St George, C.C. (1950). The light reaction in the bleaching of rhodopsin. Science *111*, 179-181.

Warga, R.M., and Nusslein-Volhard, C. (1999). Origin and development of the zebrafish endoderm. Development *126*, 827-838.

Waters, A.M., and Beales, P.L. (2011). Ciliopathies: an expanding disease spectrum. Pediatr Nephrol *26*, 1039-1056.

Weidinger, G., Wolke, U., Koprunner, M., Klinger, M., and Raz, E. (1999). Identification of tissues and patterning events required for distinct steps in early migration of zebrafish primordial germ cells. Development *126*, 5295-5307.

Whittaker, M., and Milligan, R.A. (1997). Conformational changes due to calcium-induced calmodulin dissociation in brush border myosin I-decorated F-actin revealed by cryoelectron microscopy and image analysis. J Mol Biol *269*, 548-557.

WHO (2019). Genes and human diseases. https://wwwwhoint/genomics/public/geneticdiseases/en/index2html.

Wierson, W.A., Simone, B.W., WareJoncas, Z., Mann, C., Welker, J.M., Kar, B., Emch, M.J., Friedberg, I., Gendron, W.A.C., Barry, M.A.*, et al.* (2019). Expanding the CRISPR Toolbox with ErCas12a in Zebrafish and Human Cells. Crispr J *2*, 417-433.

Wong, S.Y., Seol, A.D., So, P.L., Ermilov, A.N., Bichakjian, C.K., Epstein, E.H., Dlugosz, A.A., and Reiter, J.F. (2009a). Primary cilia can both mediate and suppress Hedgehog pathway-dependent tumorigenesis. Nature Medicine *15*, 1055-U1109.

Wong, S.Y., Seol, A.D., So, P.L., Ermilov, A.N., Bichakjian, C.K., Epstein, E.H., Jr., Dlugosz, A.A., and Reiter, J.F. (2009b). Primary cilia can both mediate and suppress Hedgehog pathway-dependent tumorigenesis. Nat Med *15*, 1055-1061.

Worthington, W.C., Jr., and Cathcart, R.S., 3rd (1963). Ependymal cilia: distribution and activity in the adult human brain. Science *139*, 221-222.

Wunnenberg-Stapleton, K., Blitz, I.L., Hashimoto, C., and Cho, K.W. (1999). Involvement of the small GTPases XRhoA and XRnd1 in cell adhesion and head formation in early Xenopus development. Development *126*, 5339-5351.

Xu, W., Jin, M., Hu, R., Wang, H., Zhang, F., Yuan, S., and Cao, Y. (2017). The Joubert Syndrome Protein Inpp5e Controls Ciliogenesis by Regulating Phosphoinositides at the Apical Membrane. J Am Soc Nephrol *28*, 118-129.

Xue, C., and Mei, C.L. (2019). Polycystic Kidney Disease and Renal Fibrosis. Adv Exp Med Biol *1165*, 81-100.

Yam, P.T., Langlois, S.D., Morin, S., and Charron, F. (2009). Sonic hedgehog guides axons through a noncanonical, Src-family-kinase-dependent signaling pathway. Neuron *62*, 349-362.

Yamamoto, A., Amacher, S.L., Kim, S.H., Geissert, D., Kimmel, C.B., and De Robertis, E.M. (1998). Zebrafish paraxial protocadherin is a downstream target of spadetail involved in morphogenesis of gastrula mesoderm. Development *125*, 3389-3397.

Yamauchi, H., Miyakawa, N., Miyake, A., and Itoh, N. (2009). Fgf4 is required for left-right patterning of visceral organs in zebrafish. Dev Biol *332*, 177-185.

Yang, J., Yan, R., Roy, A., Xu, D., Poisson, J., and Zhang, Y. (2015). The I-TASSER Suite: protein structure and function prediction. Nat Methods *12*, 7-8.

Yang, J., and Zhang, Y. (2015). Protein Structure and Function Prediction Using I-TASSER. Curr Protoc Bioinformatics *52*, 5 8 1-5 8 15.

Yin, L., Maddison, L.A., Li, M., Kara, N., LaFave, M.C., Varshney, G.K., Burgess, S.M., Patton, J.G., and Chen, W. (2015). Multiplex Conditional Mutagenesis Using Transgenic Expression of Cas9 and sgRNAs. Genetics *200*, 431-441.

Yu, Y., Fuscoe, J.C., Zhao, C., Guo, C., Jia, M., Qing, T., Bannon, D.I., Lancashire, L., Bao, W., Du, T.*, et al.* (2014). A rat RNA-Seq transcriptomic BodyMap across 11 organs and 4 developmental stages. Nat Commun *5*, 3230.

Zariwala, M.A., Knowles, M.R., and Leigh, M.W. (1993). Primary Ciliary Dyskinesia. In GeneReviews((R)), M.P. Adam, H.H. Ardinger, R.A. Pagon, S.E. Wallace, L.J.H. Bean, K. Stephens, and A. Amemiya, eds. (Seattle (WA)).

Zayats, V., Samad, A., Minofar, B., Roelofs, K.E., Stockner, T., and Ettrich, R. (2013). Regulation of the transient receptor potential channel TRPA1 by its N-terminal ankyrin repeat domain. J Mol Model *19*, 4689-4700.

Zhang, Y., Liu, H., Li, W., Zhang, Z., Shang, X., Zhang, D., Li, Y., Zhang, S., Liu, J., Hess, R.A.*, et al.* (2017). Intraflagellar transporter protein (IFT27), an IFT25 binding partner, is essential for male fertility and spermiogenesis in mice. Dev Biol *432*, 125-139.

Zhu, L., Chen, L., Yan, L., Perkins, B.D., Li, S., Li, B., Xu, H.A., and Li, X.J. (2019). Mutant Ahi1 Affects Retinal Axon Projection in Zebrafish via Toxic Gain of Function. Front Cell Neurosci *13*, 81.